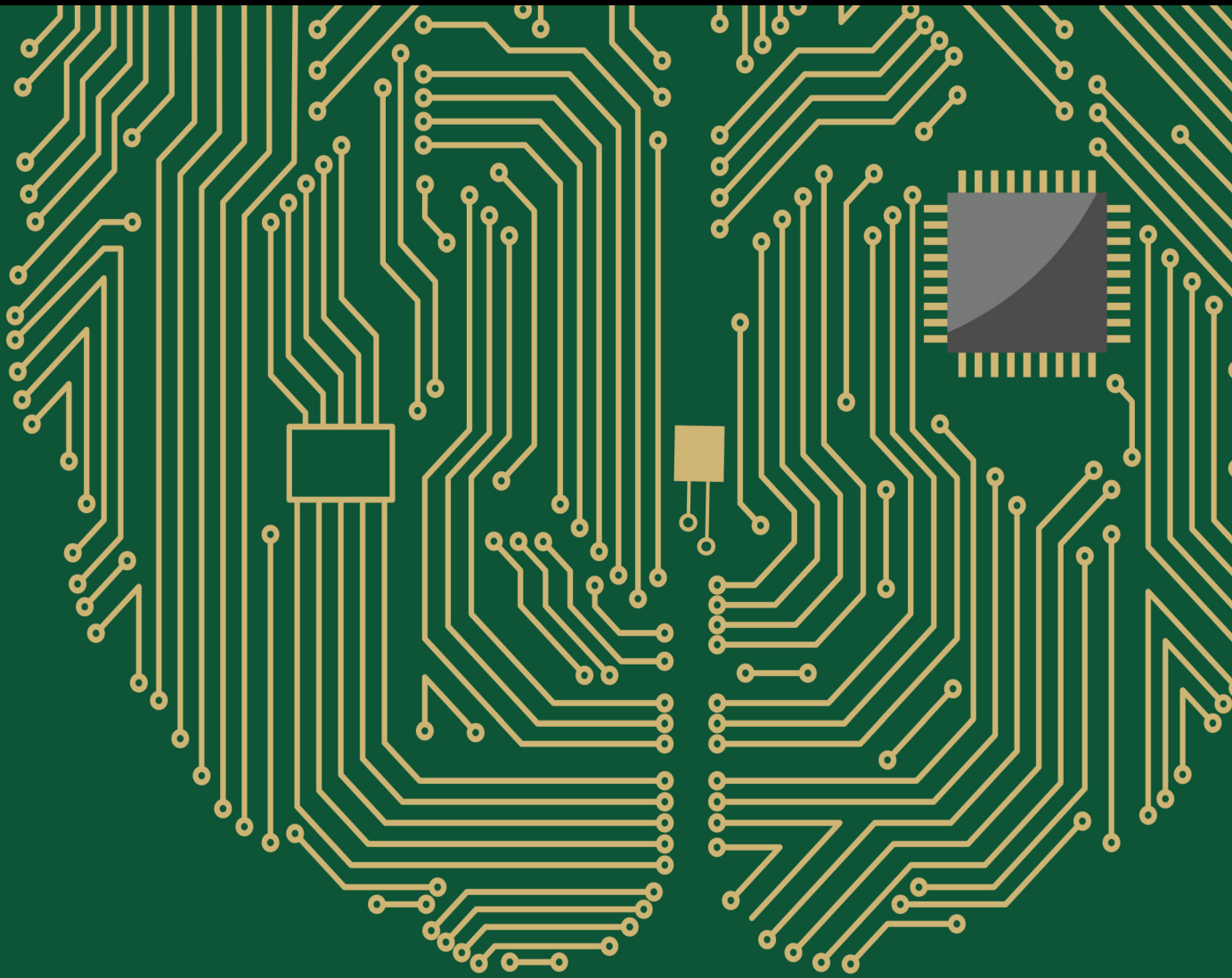


Multimedia Computing with Explainable Artificial Intelligence for Telehealth

Lead Guest Editor: Ashish Khanna

Guest Editors: Joel J. P. C. Rodrigues and Utku Kose





Multimedia Computing with Explainable Artificial Intelligence for Telehealth

Computational Intelligence and Neuroscience

**Multimedia Computing with
Explainable Artificial Intelligence for
Telehealth**

Lead Guest Editor: Ashish Khanna

Guest Editors: Joel J. P. C. Rodrigues and Utku Kose



Copyright © 2023 Hindawi Limited. All rights reserved.

This is a special issue published in "Computational Intelligence and Neuroscience." All articles are open access articles distributed under the Creative Commons Attribution License, which permits unrestricted use, distribution, and reproduction in any medium, provided the original work is properly cited.

Chief Editor

Andrzej Cichocki, Poland

Associate Editors

Arnaud Delorme, France
Cheng-Jian Lin , Taiwan
Saeid Sanei, United Kingdom

Academic Editors

Mohamed Abd Elaziz , Egypt
Tariq Ahanger , Saudi Arabia
Muhammad Ahmad, Pakistan
Ricardo Aler , Spain
Nouman Ali, Pakistan
Pietro Aricò , Italy
Lerina Aversano , Italy
Ümit Ağbulut , Turkey
Najib Ben Aoun , Saudi Arabia
Surbhi Bhatia , Saudi Arabia
Daniele Bibbo , Italy
Vince D. Calhoun , USA
Francesco Camastra, Italy
Zhicheng Cao, China
Hubert Cecotti , USA
Jyotir Moy Chatterjee , Nepal
Rupesh Chikara, USA
Marta Cimitile, Italy
Silvia Conforto , Italy
Paolo Crippa , Italy
Christian W. Dawson, United Kingdom
Carmen De Maio , Italy
Thomas DeMarse , USA
Maria Jose Del Jesus, Spain
Arnaud Delorme , France
Anastasios D. Doulamis, Greece
António Dourado , Portugal
Sheng Du , China
Said El Kafhali , Morocco
Mohammad Reza Feizi Derakhshi , Iran
Quanxi Feng, China
Zhong-kai Feng, China
Steven L. Fernandes, USA
Agostino Forestiero , Italy
Piotr Franaszczuk , USA
Thippa Reddy Gadekallu , India
Paolo Gastaldo , Italy
Samanwoy Ghosh-Dastidar, USA

Manuel Graña , Spain
Alberto Guillén , Spain
Gaurav Gupta, India
Rodolfo E. Haber , Spain
Usman Habib , Pakistan
Anandakumar Haldorai , India
José Alfredo Hernández-Pérez , Mexico
Luis Javier Herrera , Spain
Alexander Hošovský , Slovakia
Etienne Hugues, USA
Nadeem Iqbal , Pakistan
Sajad Jafari, Iran
Abdul Rehman Javed , Pakistan
Jing Jin , China
Li Jin, United Kingdom
Kanak Kalita, India
Ryotaro Kamimura , Japan
Pasi A. Karjalainen , Finland
Anitha Karthikeyan, Saint Vincent and the
Grenadines
Elpida Keravnou , Cyprus
Asif Irshad Khan , Saudi Arabia
Muhammad Adnan Khan , Republic of
Korea
Abbas Khosravi, Australia
Tai-hoon Kim, Republic of Korea
Li-Wei Ko , Taiwan
Raşit Köker , Turkey
Deepika Koundal , India
Sunil Kumar , India
Fabio La Foresta, Italy
Kuruva Lakshmana , India
Maciej Lawrynczuk , Poland
Jianli Liu , China
Giosuè Lo Bosco , Italy
Andrea Loddo , Italy
Kezhi Mao, Singapore
Paolo Massobrio , Italy
Gerard McKee, Nigeria
Mohit Mittal , France
Paulo Moura Oliveira , Portugal
Debajyoti Mukhopadhyay , India
Xin Ning , China
Nasimul Noman , Australia
Fivos Panetsos , Spain

Evgeniya Pankratova , Russia
Rocío Pérez de Prado , Spain
Francesco Pistolesi , Italy
Alessandro Sebastian Podda , Italy
David M Powers, Australia
Radu-Emil Precup, Romania
Lorenzo Putzu, Italy
S P Raja, India
Dr.Anand Singh Rajawat , India
Simone Ranaldi , Italy
Upaka Rathnayake, Sri Lanka
Navid Razmjooy, Iran
Carlo Ricciardi, Italy
Jatinderkumar R. Saini , India
Sandhya Samarasinghe , New Zealand
Friedhelm Schwenker, Germany
Mijanur Rahaman Seikh, India
Tapan Senapati , China
Mohammed Shuaib , Malaysia
Kamran Siddique , USA
Gaurav Singal, India
Akansha Singh , India
Chiranjibi Sitaula , Australia
Neelakandan Subramani, India
Le Sun, China
Rawia Tahrir , Iraq
Binhua Tang , China
Carlos M. Travieso-González , Spain
Vinh Truong Hoang , Vietnam
Fath U Min Ullah , Republic of Korea
Pablo Varona , Spain
Roberto A. Vazquez , Mexico
Mario Versaci, Italy
Gennaro Vessio , Italy
Ivan Volosyak , Germany
Leyi Wei , China
Jianghui Wen, China
Lingwei Xu , China
Cornelio Yáñez-Márquez, Mexico
Zaher Mundher Yaseen, Iraq
Yugen Yi , China
Qiangqiang Yuan , China
Miaolei Zhou , China
Michal Zochowski, USA
Rodolfo Zunino, Italy

Contents

Retracted: Diagnosis of Breast Cancer Using Computational Intelligence Models and IoT Applications

Computational Intelligence and Neuroscience


Retraction (1 page), Article ID 9871426, Volume 2023 (2023)

Retracted: Factors Analysis of the Compliance Rate of Hypertension Detection Control and Self-Assessment Control in Community Outpatient Clinics

Computational Intelligence and Neuroscience


Retraction (1 page), Article ID 9860750, Volume 2023 (2023)

Face Recognition Method under Adaptive Image Matching and Dictionary Learning Algorithm

Xue Lv, Mingxia Su, and Zekun Wang 

Research Article (8 pages), Article ID 8225630, Volume 2023 (2023)

Artificial Intelligence Based Study Association between p53 Gene Polymorphism and Endometriosis: A Systematic Review and Meta-analysis

Xia Ma, Xiaoxiao Jin, Xiujuan Shao, Wanjing Hu, Haihong Jin, and Yiqun Wang 


Review Article (8 pages), Article ID 8568820, Volume 2022 (2022)

[Retracted] Diagnosis of Breast Cancer Using Computational Intelligence Models and IoT Applications

Mohammed Alghamdi , Mohammed Maray , and Malik Bader Alazzam 

Research Article (7 pages), Article ID 2143510, Volume 2022 (2022)

Recurrence Rate and Exploration of Clinical Factors after Pituitary Adenoma Surgery: A Systematic Review and Meta-Analysis based on Computer Artificial Intelligence System

Xianghe Zhang, Fan Yang, and Nianchen Han 


Review Article (10 pages), Article ID 6002672, Volume 2022 (2022)

A Method for Extracting Building Information from Remote Sensing Images Based on Deep Learning

Lianying Li , Xi Chen , and Lianchao Li 

Research Article (10 pages), Article ID 9968665, Volume 2022 (2022)

[Retracted] Factors Analysis of the Compliance Rate of Hypertension Detection Control and Self-Assessment Control in Community Outpatient Clinics

Zhigao Chen and Rui Xiong 

Research Article (9 pages), Article ID 9432202, Volume 2022 (2022)

Observation on the Clinical Efficacy of Traditional Chinese Medicine Non-Drug Therapy in the Treatment of Insomnia: A Systematic Review and Meta-Analysis Based on Computer Artificial Intelligence System

Jingqing Zhuang , Jian Wu, Liang Fan, and Chongnan Liang 

Review Article (11 pages), Article ID 1081713, Volume 2022 (2022)

Artificial Intelligence Algorithm-Based Feature Extraction of Computed Tomography Images and Analysis of Benign and Malignant Pulmonary Nodules

Yuantong Gao , Yuyang Chen, Yuegui Jiang, Yongchou Li, Xia Zhang, Min Luo, Xiaoyang Wang, and Yang Li

Research Article (9 pages), Article ID 5762623, Volume 2022 (2022)

Retraction

Retracted: Diagnosis of Breast Cancer Using Computational Intelligence Models and IoT Applications

Computational Intelligence and Neuroscience

Received 31 October 2023; Accepted 31 October 2023; Published 1 November 2023

Copyright © 2023 Computational Intelligence and Neuroscience. This is an open access article distributed under the Creative Commons Attribution License, which permits unrestricted use, distribution, and reproduction in any medium, provided the original work is properly cited.

This article has been retracted by Hindawi following an investigation undertaken by the publisher [1]. This investigation has uncovered evidence of one or more of the following indicators of systematic manipulation of the publication process:

- (1) Discrepancies in scope
- (2) Discrepancies in the description of the research reported
- (3) Discrepancies between the availability of data and the research described
- (4) Inappropriate citations
- (5) Incoherent, meaningless and/or irrelevant content included in the article
- (6) Peer-review manipulation

The presence of these indicators undermines our confidence in the integrity of the article's content and we cannot, therefore, vouch for its reliability. Please note that this notice is intended solely to alert readers that the content of this article is unreliable. We have not investigated whether authors were aware of or involved in the systematic manipulation of the publication process.

Wiley and Hindawi regrets that the usual quality checks did not identify these issues before publication and have since put additional measures in place to safeguard research integrity.

We wish to credit our own Research Integrity and Research Publishing teams and anonymous and named external researchers and research integrity experts for contributing to this investigation.

The corresponding author, as the representative of all authors, has been given the opportunity to register their agreement or disagreement to this retraction. We have kept a record of any response received.

References

- [1] M. Alghamdi, M. Maray, and M. B. Alazzam, "Diagnosis of Breast Cancer Using Computational Intelligence Models and IoT Applications," *Computational Intelligence and Neuroscience*, vol. 2022, Article ID 2143510, 7 pages, 2022.

Retraction

Retracted: Factors Analysis of the Compliance Rate of Hypertension Detection Control and Self-Assessment Control in Community Outpatient Clinics

Computational Intelligence and Neuroscience

Received 17 October 2023; Accepted 17 October 2023; Published 18 October 2023

Copyright © 2023 Computational Intelligence and Neuroscience. This is an open access article distributed under the Creative Commons Attribution License, which permits unrestricted use, distribution, and reproduction in any medium, provided the original work is properly cited.

This article has been retracted by Hindawi following an investigation undertaken by the publisher [1]. This investigation has uncovered evidence of one or more of the following indicators of systematic manipulation of the publication process:

- (1) Discrepancies in scope
- (2) Discrepancies in the description of the research reported
- (3) Discrepancies between the availability of data and the research described
- (4) Inappropriate citations
- (5) Incoherent, meaningless and/or irrelevant content included in the article
- (6) Peer-review manipulation

The presence of these indicators undermines our confidence in the integrity of the article's content and we cannot, therefore, vouch for its reliability. Please note that this notice is intended solely to alert readers that the content of this article is unreliable. We have not investigated whether authors were aware of or involved in the systematic manipulation of the publication process.

Wiley and Hindawi regrets that the usual quality checks did not identify these issues before publication and have since put additional measures in place to safeguard research integrity.

We wish to credit our own Research Integrity and Research Publishing teams and anonymous and named external researchers and research integrity experts for contributing to this investigation.


The corresponding author, as the representative of all authors, has been given the opportunity to register their agreement or disagreement to this retraction. We have kept a record of any response received.

References

- [1] Z. Chen and R. Xiong, "Factors Analysis of the Compliance Rate of Hypertension Detection Control and Self-Assessment Control in Community Outpatient Clinics," *Computational Intelligence and Neuroscience*, vol. 2022, Article ID 9432202, 9 pages, 2022.

Research Article

Face Recognition Method under Adaptive Image Matching and Dictionary Learning Algorithm

Xue Lv, Mingxia Su, and Zekun Wang 

Wuhan Huaxia University of Technology, Wuhan 430223, China

Correspondence should be addressed to Zekun Wang; 2019050375@stu.cdut.edu.cn

Received 9 July 2022; Revised 2 September 2022; Accepted 8 September 2022; Published 21 February 2023

Academic Editor: Ashish Khanna

Copyright © 2023 Xue Lv et al. This is an open access article distributed under the Creative Commons Attribution License, which permits unrestricted use, distribution, and reproduction in any medium, provided the original work is properly cited.

In this research, a robust face recognition method based on adaptive image matching and a dictionary learning algorithm was proposed. A Fisher discriminant constraint was introduced into the dictionary learning algorithm program so that the dictionary had certain category discrimination ability. The purpose was to use this technology to reduce the influence of pollution, absence, and other factors on face recognition and improve the recognition rate. The optimization method was used to solve the loop iteration to obtain the expected specific dictionary, and the selected specific dictionary was used as the representation dictionary in adaptive sparse representation. In addition, if a specific dictionary was placed in a seed space of the original training data, the mapping matrix can be used to represent the mapping relationship between the specific dictionary and the original training sample, and the test sample could be corrected according to the mapping matrix to remove the contamination in the test sample. Moreover, the feature face method and dimension reduction method were used to process the specific dictionary and the corrected test sample, and the dimensions were reduced to 25, 50, 75, 100, 125, and 150, respectively. In this research, the recognition rate of the algorithm in 50 dimensions was lower than that of the discriminatory low-rank representation method (DLRR), and the recognition rate in other dimensions was the highest. The adaptive image matching classifier was used for classification and recognition. The experimental results showed that the proposed algorithm had a good recognition rate and good robustness against noise, pollution, and occlusion. Health condition prediction based on face recognition technology has the advantages of being noninvasive and convenient operation.

1. Introduction

With the continuous development of social informatization, information security has gradually been widely considered by national security, public security, banking systems, e-commerce, and other fields with a high demand for information security. In recent years, the field of identity recognition technology has gradually become a popular subject at home and abroad [1, 2]. Traditional identification technology is mainly based on personal documents or passwords, which cause many inconveniences to the public because it is inconvenient to carry or forget them easily. Therefore, it is urgent to explore a fast, safe, and effective identification technology [3–5].

The face recognition method has very important academic research value and wide application prospects. In

recent years, the International Conference on Computer Vision and Pattern Recognition and other top conferences in the field of computer vision will contain many excellent papers related to face recognition methods. Many research institutions promote the development of face recognition methods through research and communication [6–8]. To date, research on face recognition technology has gained rich experience, but it is still limited in practical applications. For example, the face acquisition process may be affected by light intensity and the posture and expression of the recognized person, and the recognition is not robust. In addition, due to the occlusion of glasses, scarves, and other objects, the recognition image is incomplete, and the recognition accuracy is reduced [7–10]. Therefore, it is urgent to seek a more accurate, faster, and more robust face recognition technology.

Phillips et al. [11] took the lead in applying it to face recognition research, and put forward sparse representation-based classification (SRC), which constructs a dictionary matrix from registered sample sets and calculates the sparse representation coefficient of the sample to be detected relative to the dictionary matrix by minimizing L1 norm. Finally, the reconstruction errors are calculated according to the sparse coefficients corresponding to each class, and the classification results are obtained. On this basis, Han et al. [12] proposed a face recognition algorithm based on kernel sparse representation to map the nonlinear separable samples into the high-dimensional feature space so that the test samples can be better represented linearly by the training sample set.

This study was developed to explore the face recognition technology model based on adaptive sparse representation based on the extraction form of biometric features for face recognition. An adaptive innovative image matching and dictionary learning algorithm for robust face recognition methods is proposed, and the Fisher discriminant constraint dictionary learning algorithm program is introduced so that the dictionary can have a certain class identification capability. It aims to use the technology to reduce the influence of factors such as pollution and missing faces on face recognition and improve the recognition rate.

2. Methods

2.1. Face Recognition Based on Adaptive Sparse Representation. The face recognition technology of adaptive sparse representation is constructed on the basis of compressed sensing theory. All the collected face images of each person can be constructed into independent subspaces in the image space. It is assumed that the training samples of the same class are distributed in the same subspace; then, the samples of the same class can be represented by dictionary atoms of the same class. If massive training samples are collected to form a complete dictionary, a linear combination of training samples can be used to represent any one of the face images.

The self-sparse representation coefficient of the test sample is obtained from a given dictionary. It is assumed that there are d faces; then, dictionary B is expressed as follows:

$$B = [B_1, B_2, B_3, \dots, B_d]. \quad (1)$$

B is a dictionary matrix composed of training samples, and B_i represents a subset of i .

The test image Y is based on the dictionary B , and the sparse coding coefficient is obtained as follows:

$$\hat{k} = \arg \min_{\beta} \{ \|Y - Bk\|_2^2 + \delta \|k\|_p \}, p = 1. \quad (2)$$

Reconstruction errors are calculated by sparse coefficients and classified as follows:

$$\text{identity}(Y) = \arg \min_i \{c_i\}. \quad (3)$$

The above equation satisfies $c_i = \|Y - B_i \hat{\beta}_i\|_2$, $\hat{\beta} = [\hat{\beta}_1, \hat{\beta}_2, \hat{\beta}_3, \dots, \hat{\beta}_d]$, and $\hat{\beta}_i$ represents the coding coefficient of category i .

2.2. Dictionary Learning Algorithm Based on the Fisher Discriminant Constraint. Although face recognition technology can still obtain a satisfactory recognition effect under the condition of a small amount of noise pollution in the test image, it will still affect the performance of the face recognition method when the number of training samples is very small. Face recognition technology can directly construct a dictionary learning matrix after subsampling of training samples [13]. Due to the influence of interference information, the dictionary may lose considerable classification information hidden in the training samples and cannot represent the test samples completely and effectively. Therefore, a dictionary learning algorithm based on the Fisher criterion was adopted in this study to obtain the best dictionary matrix of classification ability and representation ability through training samples. In this study, the collected face images are preprocessed, and then the pixel values are rearranged. Principal component analysis (PCA) dimension reduction is adopted as the feature vector of the face, and the dictionary learning algorithm with the Fisher discriminant constraint is used to train the sample set to obtain the dictionary.

The training sets are expressed as follows:

$$\begin{aligned} B &= [B_1, B_2, B_3, \dots, B_d] \\ M &= [M_1, M_2, M_3, \dots, M_d]. \end{aligned} \quad (4)$$

The sparse coefficient of the training sample is expressed as follows:

$$N = [N_1, N_2, N_3, \dots, N_d]. \quad (5)$$

In the above equation, B_i represents the subset whose category is i , M_i represents the corresponding dictionary matrix of class i , and N_i represents the sparse coefficient of B_i . The dictionary learning is transformed into an objective function.

$$T_{(M,N)} = \arg \min_{M,N} \{r(B, M, N) + \delta_1 \|N\|_1 + \delta_2 f(N)\}. \quad (6)$$

In the above equation, $r(B, M, N)$ represents the fidelity term of dictionary expression ability, $\|N\|_1$ represents sparse constraint, $f(N)$ represents the fidelity term of dictionary resolution, and δ_1 and δ_2 are fix quantifications.

It is assumed that the coding coefficient of training sample B_i relative to dictionary M is as follows:

$$M_i = [N_i^1, N_i^2, N_i^3, \dots, N_i^d]. \quad (7)$$

In the above equation, N_i^j represents the corresponding coding coefficient of the j class. The training sample can be well expressed linearly by the dictionary, that is, $B_i \approx MN_i$. At the same time, the sample B_i can be expressed by M_i but cannot be expressed by M_j . As a result, there is the following equation.

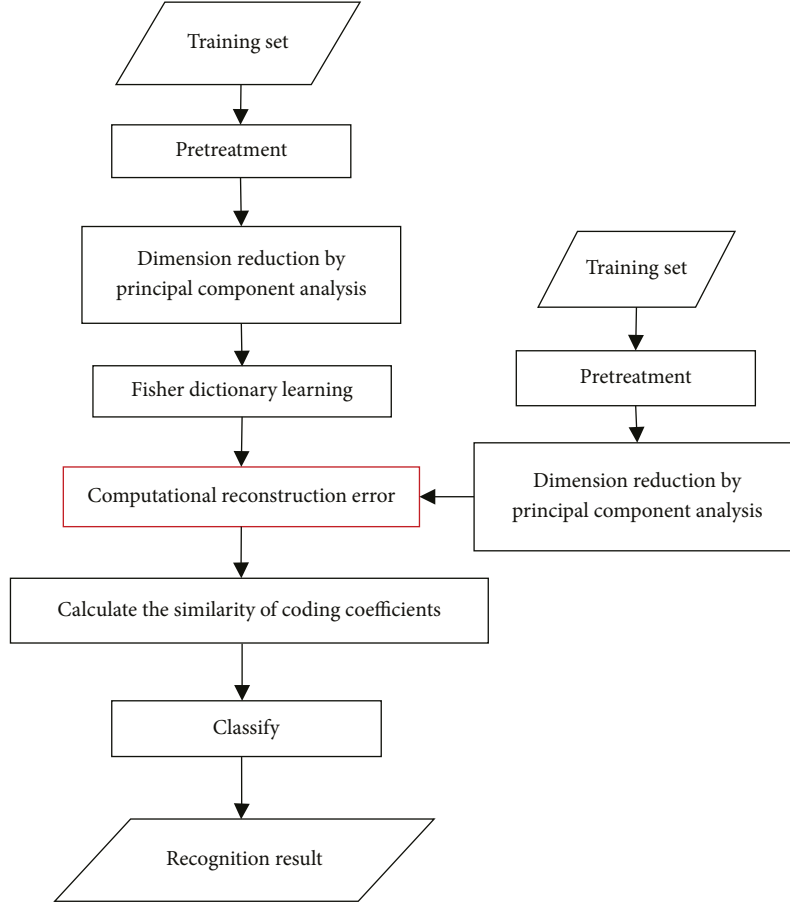


FIGURE 1: Flow chart of face recognition.

$$r(B, M, N) = \sum_{i=1}^d r(B_i, M, N_i) = \sum_{i=1}^d \left[\|B_i - MN_i\|_F^2 + \|B_i - MN_i^j\|_F^2 + \|M_j N_i^j\|_F^2 \right]. \quad (8)$$

To ensure the classification ability of dictionary M on training samples in A , the Fisher discriminant constraint can be used to minimize the in-class error $S_I(N)$ and maximize the cumulative error $S_b(N)$ of decoding coefficient N of sample set B .

$$S_I(N) = \sum_{i=1}^d n_i (p_i - p)(p_i - p)^T, \quad (9)$$

$$S_b(N) = \sum_{i=1}^d \sum_{x_i} (x_k - p_i)(x_k - p_i)^T,$$

In the above equation, p_i and p represent the mean values of the encoding coefficient matrices N_i and N , respectively. Intuitively, $f(N)$ is defined as follows:

$$f(N) = \text{tr}(S_I(N_i)) - \text{tr}(S_b(N)). \quad (10)$$

However, this function is unstable, so an additional elastic term is needed, optimized as follows:

$$f(N) = \text{tr}(S_I(N_i)) - \text{tr}(S_b(N)) + \lambda \|N\|_F^2. \quad (11)$$

In the above equation, $r(B, M, N)$ can ensure that the training set is represented by a linear combination of the dictionary basis vectors of the class so that dictionary M can show the best ability for any sample in the training sample set, $f(N)$ can ensure the minimum intraclass error value and the maximum interclass error value in the training sample coding coefficient so that dictionary M can obtain the optimal classification ability.

2.3. Low-Rank Matrix Recovery. In face recognition sample collection, training samples may be contaminated and missing, which directly affects the final effect of face recognition technology. Partial matrix restoration is applied to the algorithm to obtain a better recognition effect, and a low-rank matrix is widely used. The low-rank matrix considers that if only a small part of dictionary M is polluted, it can be decomposed into the sum of the low-rank matrix and sparse error matrix to realize the recovery of dictionary M .

$$M = L + E. \quad (12)$$

In the above equation, L is a low-rank matrix, and E is a coefficient error matrix. The robust principal component analysis (RPCA) method is used to recover the low-rank

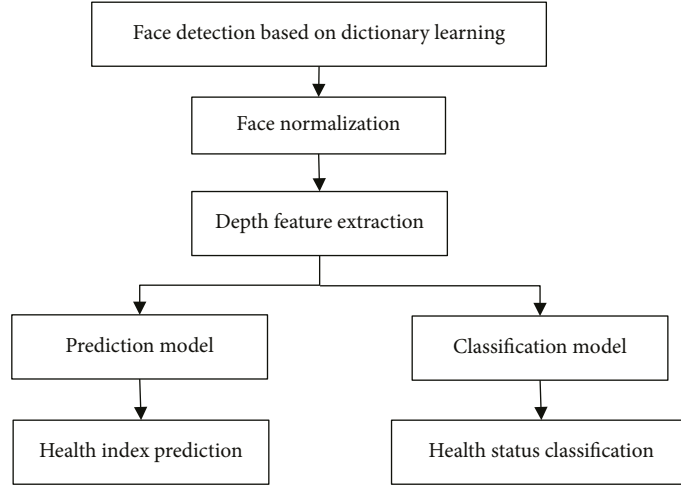


FIGURE 2: Health condition based on the dictionary learning algorithm.

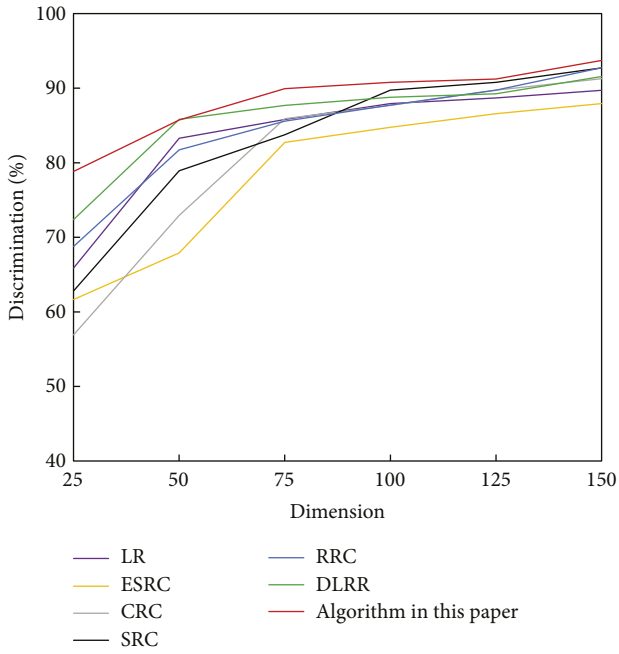


FIGURE 3: Recognition rates of unoccluded training samples in the AR face database.

matrix L even if dictionary M is highly polluted, where the sparse error matrix E is considered to be arbitrarily sparse. The RPCA model is as follows:

$$\begin{aligned} \min_{L,E} \text{rank}(L) + \xi \|E\|_0, \\ \text{s.t. } M = L + E. \end{aligned} \quad (13)$$

In the above equation, ξ represents the regularization parameter. On the basis of the RPCA model, the following model is proposed.

$$\begin{aligned} \min_{Z,E} \|E\|_* + \xi \|E\|_\lambda, \\ \text{s.t. } M = AZ + E. \end{aligned} \quad (14)$$

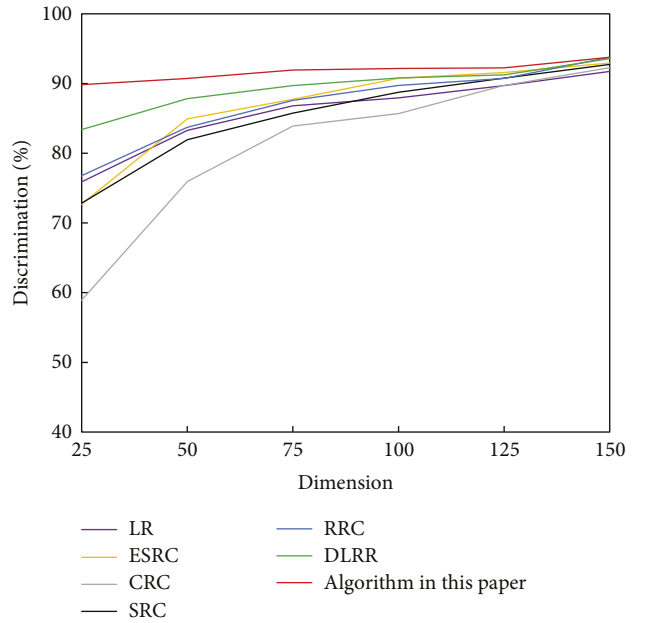


FIGURE 4: Recognition rate of Extended Yale B face database.

In the above equation, $\|\cdot\|_\lambda$ represents different regularization strategies for different degrees of pollution, and A represents a given dictionary.

2.4. Classification Method Based on Gaussian Mixture Sparse Representation. According to the face recognition algorithm of self-sparse representation, the similarity between each test input image and the training image can be represented by the reconstruction error of the corresponding category of face. It is assumed that the coding coefficient matrix of the class i training sample is $G_i = [G_i^1, G_i^2, G_i^3, \dots, G_i^d]$. After calculation, the following equation is obtained as follows:

$$h_i = \gamma \|\hat{\theta} - z_i\|_2^2 + \frac{\|Y - M_i \hat{\theta}_i\|_2^2}{\|\hat{\theta}_i\|_2^2}, \quad (15)$$

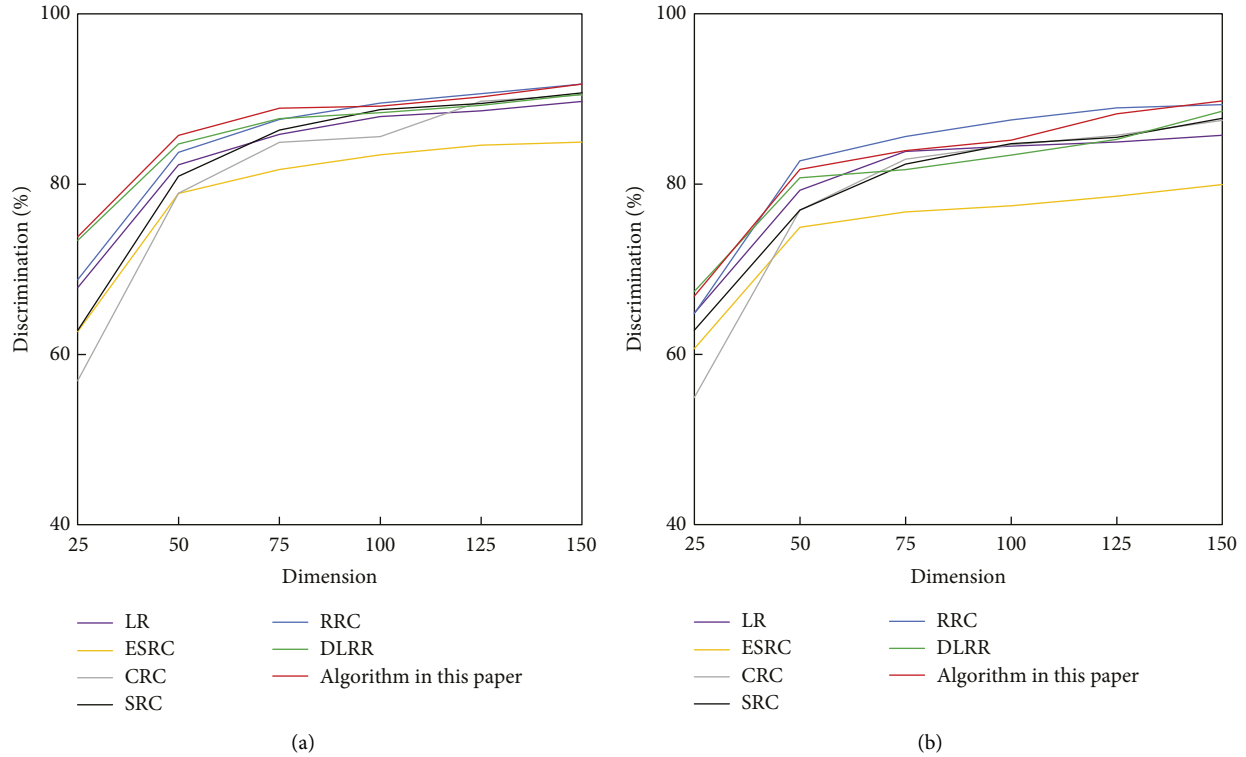


FIGURE 5: Recognition rate of the AR face database with pixel contamination. (a) Recognition rate of 10% added pixel pollution; (b) recognition rate of 20% added pixel pollution.

The above equation satisfies $z_i = 1/p \sum G_i^j$, which is the mean value of the coding coefficient of the class i sample. $i = \arg \min \{h_i\}$ is used to calculate the category of test samples. The face recognition process in this study is shown in Figure 1.

2.5. The Realization Process of Health Condition Prediction Technology Based on Face Recognition. There are two most commonly used methods to collect face images for health prediction. One is the traditional method based on geometric extraction, and the other is the widely used method based on a dictionary learning algorithm. The process of health prediction based on the dictionary learning algorithm is shown in Figure 2.

2.6. Experimental Database and Experimental Environment. To verify the effectiveness and robustness of the proposed algorithm, many experiments were carried out in the Active Record (AR) face database [14] and the Extended Yale B face database [15], and relevant experimental data were obtained. The Extended Yale B face database included full-face images of 36 people with different expressions and occluders under 52 different lighting conditions, some of which are damaged. A total of 2,356 intact face images were selected as test samples. The AR face database included more than 4,000 images of 74 men and 58 women with different expressions, lighting, and shading. The unoccluded subset of 100 classes is selected as test samples. Some classical algorithms are selected for comparison, including sparse representation-

based classification (SRC) [16], cyclic redundancy check (CRC) [17], regularized robust coding for face recognition (RRC) [18], low-rank matrix recovery with structural incoherence (LR) [19], extended sparse representation-based classification (ESRC) [20], and discriminative low-rank representation method (DLRR) [21]. All experiments are carried out on a computer with an Intel(R), Xeon(R), CPU E5-2630 processor, 64G memory, and MATLAB version R2014b [22].

3. Results

3.1. Test Results on the AR Database. The AR face database is composed of 128 people with more than 3,500 frontal face images. This experiment used one of the subdatabases, including 74 males and 58 females under different illumination, expression, and more than 4,000 pictures. Everyone contains 13 images, including seven sharp images without sunscreen, three images of the sunglasses, and three images of the scarves. Of these, 100 class subsets without sunscreen are selected as test samples.

In this experiment, 4 images without occlusion in the first subset of each person are selected as training samples, and 4 images without occlusion in the second subset of each person are selected as test samples. In the PCA dimension reduction process, the dimensions are reduced to 25, 50, 75, 100, 125, and 150. The parameters in dictionary decomposition are $\tau = 0.01, \lambda = 1.4, \delta = 0.8v, \eta = 1.2v$. The experimental results are shown in Figure 3. According to Figure 3, the algorithm proposed in this study has the highest

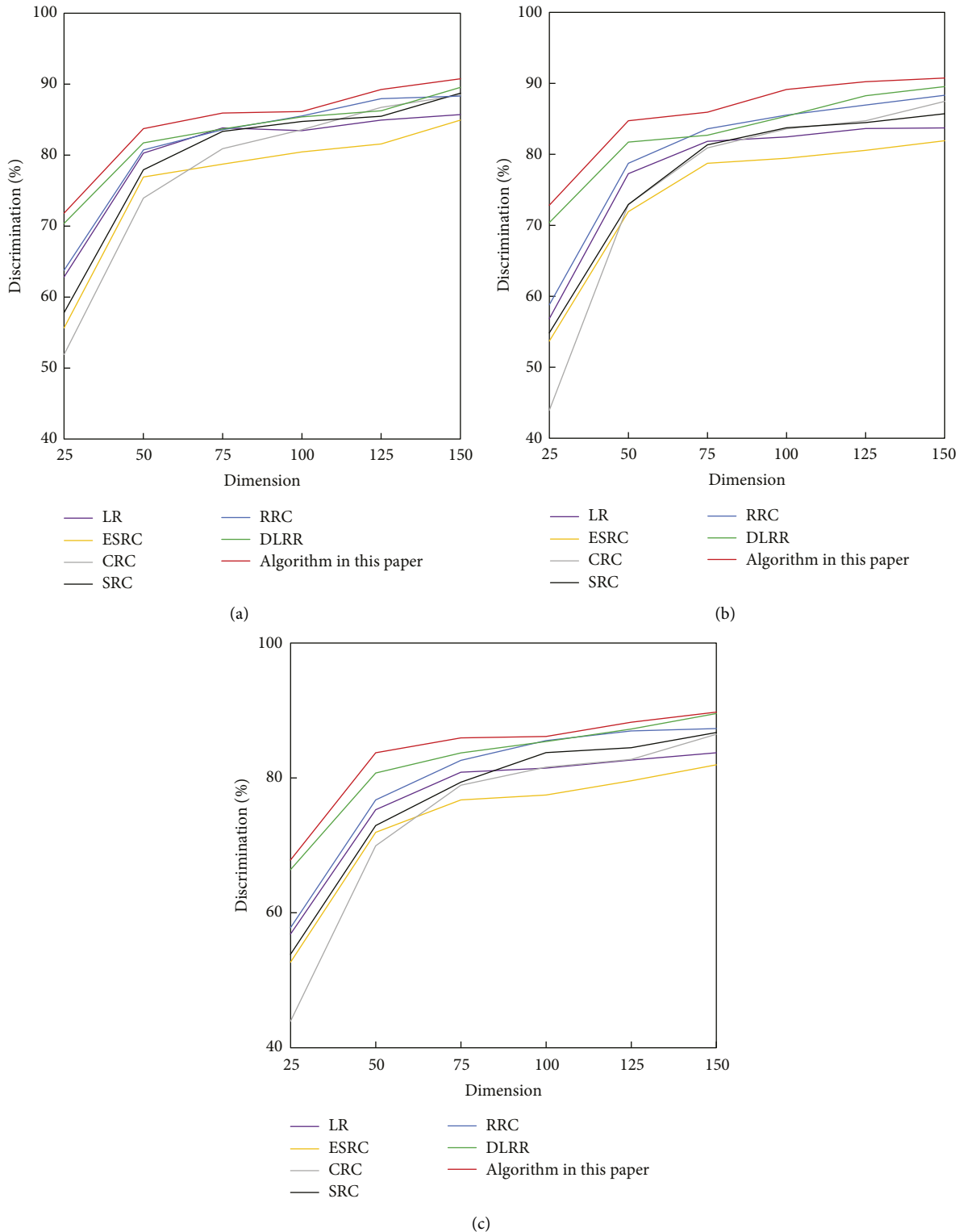


FIGURE 6: Recognition rate of the AR face database containing real occlusion. (a) Recognition rate with sunglasses occlusion; (b) recognition rate with scarf occlusion; (c) recognition rate with sunglasses and scarf occlusion.

recognition rate in all dimensions except in dimension 50, which is lower than that of DLRR. Because the face images of both training samples and test samples are nonoccluded, the superiority of the proposed algorithm cannot be fully reflected. However, according to the data

results, it is found that the proposed algorithm has a high recognition rate.

3.2. Test Results on the Extended Yale B Database. Some images in the Extended Yale B face database are corrupted.

Among them, 2,356 complete face images were selected as test samples. Figure 4 shows some samples using the Extended Yale B face database. Using the feature face method, the dimensions are reduced to 25, 50, 75, 100, 125, and 150. The parameters in dictionary decomposition are $\tau = 0.01, \lambda = 1.2, \delta = 0.8v, \eta = 1.2v$. In this research, some classical algorithms, SRC, CRC, RRC, LR, ESRC, DLRR, and DLRR are selected for comparison. The average recognition rate calculated after 10 runs is shown in Figure 4. In the Extended Yale B face database, the recognition rate of the algorithm presented in this study is close to that of RRC and DLRR and higher than that of other types of algorithms in other dimensions except the 150-dimension.

3.3. Dirty Face Recognition Experiments. In this experiment, two kinds of artificial pollution methods are used: pixel pollution and pixel block pollution. Some training samples without occlusion in the AR face database are selected and applied to the experiment of artificially adding pixel pollution. Four images without occlusion in the first subset of each person are used as training samples, and four images without occlusion in the second subset are used as test samples. In this experiment, some samples with 10% or 20% artificial pixel pollution are considered. In the acute dimension reduction treatment with the feature face method, the dimensions are reduced to 25, 50, 75, 100, 125, and 150. The parameters during dictionary decomposition are set to $\tau = 0.01, \lambda = 1.1, \delta = 0.8v, \eta = 1.2v$. After the experiment is run 15 times, the average value is calculated and are shown in Figures 5(a) and 5(b).

3.4. Experiments with Real Shielding. To verify the effectiveness and robustness of the proposed algorithm, the AR face database is selected for the experiment when the sample contains real occlusion. According to the characteristics of AR face database images, three experiments are set up, and the dimensions are reduced to 25, 50, 75, 100, 125, and 150 in the dimension reduction process using the feature face method. When the sample images are blocked by sunglasses, 4 unblocked images in the first subset of each person and 1 random image with blocked sunglasses are selected for the training sample, and 4 unblocked images in the second subset and the remaining images blocked by sunglasses are selected for the test sample. The parameters during dictionary decomposition are set to $\tau = 0.01, \lambda = 1.6, \delta = 0.8v, \eta = 1.2v$. The sample images are covered by scarves. The training sample selects 4 images without occlusion and 1 random image with scarf occlusion in the first subset of each person. The test sample selects 4 images without occlusion in the second subset, and the remaining images are covered by scarves. The parameters during dictionary decomposition are set to $\tau = 0.01, \lambda = 1.2, \delta = 0.8v, \eta = 1.2v$. The sample image contained sunglasses and scarf occlusion. The training sample selects 4 images without occlusion from the first subset of each person and randomly selects one image with sunglasses occlusion and one image with scarf occlusion. The test sample selects all the remaining images. The parameters during dictionary decomposition are set to

$\tau = 0.01, \lambda = 1.7, \delta = 0.8v, \eta = 1.2v$. From Figure 6, compared with other algorithms, the proposed algorithm has a better recognition effect, which reflects the effectiveness and robustness of the proposed algorithm for the existence of real occlusions in the samples.

4. Conclusions

To solve the problems of noise, pollution, occlusion, and poor performance of the self-sparse representation classifier in training samples, this experiment is developed to study a face recognition algorithm based on adaptive sparse representation combined with dictionary learning. It is designed to improve the recognition rate of face recognition technology and the robustness to noise, pollution, and occlusion, which has achieved good results. A dictionary decomposition model is constructed based on dictionary learning theory, and the biometric features of original face images are extracted for classification to avoid the influence of pollution. The desired class-specific dictionary is obtained by iterative optimization, and the dictionary is used as the dictionary in the adaptive sparse representation classifier. Finally, using the feature face method, dimension reduction is performed on the training samples and test samples of face images without occlusion and with contamination. An adaptive sparse representation classifier is used for recognition and classification, and experiments are designed on two public face databases. The good recognition rate of the proposed algorithm is verified, which means that the proposed algorithm has good robustness to noise, pollution, and occlusion. Health condition prediction based on face recognition technology has the advantages of being noninvasive and convenient operation.

In this experiment, learning dictionary decomposition is used to extract the feature information from the original face image, and this feature information is classified to avoid the interference of other adverse factors. The mapping matrix is used to represent the correlation between the original information and feature information. The training samples are corrected by the mapping matrix, and good experimental results are achieved.

Due to the limitations of researchers' own research and understanding, there is still much work to be done in the future. The difficulty of face image recognition with occlusion and pollution is still relatively large, and the recognition rate needs to be improved. Research on face recognition technology is becoming increasingly mature, but in practical applications, especially in the field of high demand for identity security, face recognition technology as a special authentication method still needs to be further strengthened.

Data Availability

The data used to support the findings of this study are available from the corresponding author upon request.

Conflicts of Interest

The authors declare that they have no conflicts of interest.

References

- [1] S. A. F. Manssor, S. Sun, and M. A. M. Elhassan, "Real-time human recognition at night via integrated face and gait recognition technologies," *Sensors*, vol. 21, no. 13, p. 4323, 2021.
- [2] M. Kosinski, "Facial recognition technology can expose political orientation from naturalistic facial images," *Scientific Reports*, vol. 11, no. 1, p. 100, 2021.
- [3] N. K. Jaafa, B. Mokaya, S. M. Savai, A. Yeung, A. M. Siika, and M. Were, "Implementation of fingerprint technology for unique patient matching and identification at an HIV care and treatment facility in western Kenya: cross-sectional study," *Journal of Medical Internet Research*, vol. 23, no. 12, p. e28958, Article ID e28958, 2021.
- [4] N. Takamiya, T. Maekawa, T. Yamasaki et al., "Different hemispheric specialization for face/word recognition: a high-density ERP study with hemifield visual stimulation," *Brain Behav*, vol. 10, no. 6, p. e01649, Article ID e01649, 2020.
- [5] H. Zhao, A. Paxton, V. Sarkar et al., "Prevention of radiation therapy treatment deviations by a novel combined biometric, radiofrequency identification, and surface imaging system," *Practical Radiation Oncology*, vol. 11, no. 2, pp. e229–e235, 2021.
- [6] M. Hu, Y. Zhong, S. Xie, H. Lv, and Z. Lv, "Fuzzy system based medical image processing for brain disease prediction," *Frontiers in Neuroscience*, vol. 15, p. 714318, Article ID 714318, 2021.
- [7] A. Ghazarian, J. Zheng, H. El-Askary, H. Chu, G. Fu, and C. Rakovski, "Increased risks of Re-identification for patients posed by deep learning-based ECG identification algorithms," in *Proceedings of the Annual International Conference of the IEEE Engineering in Medicine and Biology Society. IEEE Engineering in Medicine and Biology Society. Annual International Conference*, pp. 1969–1975, Beijing China, November 2021.
- [8] Z. Wan, Y. Dong, Z. Yu, H. Lv, and Z. Lv, "Semi-supervised support vector machine for digital twins based brain image fusion," *Frontiers in Neuroscience*, vol. 15, p. 705323, Article ID 705323, 2021.
- [9] Z. Lv, L. Qiao, Q. Wang, and F. Piccialli, "Advanced machine-learning methods for brain-computer interfacing," *IEEE/ACM Transactions on Computational Biology and Bioinformatics*, vol. 18, no. 5, pp. 1688–1698, 2021.
- [10] X. Zhou, Y. Li, and W. Liang, "CNN-RNN based intelligent recommendation for online medical pre-diagnosis support," *IEEE/ACM Transactions on Computational Biology and Bioinformatics*, vol. 18, no. 3, pp. 912–921, 2021.
- [11] P. J. Phillips, A. N. Yates, Y. Hu et al., "Face recognition accuracy of forensic examiners, superrecognizers, and face recognition algorithms," *Proceedings of the National Academy of Sciences of the United States of America*, vol. 115, no. 24, pp. 6171–6176, 2018.
- [12] M. Han, F. Zhang, N. Ning, J. Zhou, A. Shanthini, and G. N. Vivekananda, "FPLP3D: security robot for face recognition in the workplace environment using face pose detection assisted controlled FACE++ tool position: a three-dimensional robot," *Work*, vol. 68, no. 3, pp. 881–890, 2021.
- [13] G. Kostka, L. Steinacker, and M. Meckel, "Between security and convenience: facial recognition technology in the eyes of citizens in China, Germany, the United Kingdom, and the United States," *Public Understanding of Science*, vol. 30, no. 6, pp. 671–690, 2021.
- [14] S. Yi, Z. He, X. Y. Jing, Y. Li, Y. M. Cheung, and F. Nie, "Adaptive weighted sparse principal component analysis for robust unsupervised feature selection," *IEEE Transactions on Neural Networks and Learning Systems*, vol. 31, no. 6, pp. 2153–2163, 2020.
- [15] J. Zeng, X. Zhao, J. Gan, C. Mai, Y. Zhai, and F. Wang, "Deep convolutional neural network used in single sample per person face recognition," *Computational Intelligence and Neuroscience*, vol. 2018, pp. 1–11, Article ID 3803627, 2018.
- [16] W. Deng, J. Hu, and J. Guo, "Face recognition via collaborative representation: its discriminant nature and superposed representation," *IEEE Transactions on Pattern Analysis and Machine Intelligence*, vol. 40, no. 10, pp. 2513–2521, 2018.
- [17] M. Meng, X. Yin, Q. She, Y. Gao, W. Kong, and Z. Luo, "Sparse representation-based classification with two-dimensional dictionary optimization for motor imagery EEG pattern recognition," *Journal of Neuroscience Methods*, vol. 361, p. 361, 202.
- [18] S. M. Noor and E. B. John, "Resource shared galois field computation for energy efficient AES/CRC in IoT applications," *IEEE Trans Sustain Comput*, vol. 4, no. 4, pp. 340–348, 2019.
- [19] H. Yang, C. Gong, K. Huang, K. Song, and Z. Yin, "Weighted feature histogram of multi-scale local patch using multi-bit binary descriptor for face recognition," *IEEE Transactions on Image Processing*, vol. 30, pp. 3858–3871, 2021.
- [20] G. Ongie, S. Biswas, and M. Jacob, "Convex recovery of continuous domain piecewise constant images from non-uniform Fourier samples," *IEEE Transactions on Signal Processing*, vol. 66, no. 1, pp. 236–250, 2018.
- [21] G. Zhang, H. Sun, F. Porikli, Y. Liu, and Q. Sun, "Optimal couple projections for domain adaptive sparse representation-based classification," *IEEE Transactions on Image Processing*, vol. 26, no. 12, pp. 5922–5935, 2017.
- [22] A. Li, X. Liu, Y. Wang et al., "Subspace structural constraint-based discriminative feature learning via nonnegative low rank representation," *PLoS One*, vol. 14, no. 5, p. e0215450, Article ID e0215450, 2019.

Review Article

Artificial Intelligence Based Study Association between p53 Gene Polymorphism and Endometriosis: A Systematic Review and Meta-analysis

Xia Ma,¹ Xiaoxiao Jin,¹ Xiujuan Shao,¹ Wanjing Hu,² Haihong Jin,³ and Yiqun Wang³ 

¹Department of Obstetrics and Gynecology, Taizhou Hospital, Taizhou 317000, Zhejiang, China

²Department of Obstetrics and Gynecology, Taizhou Women and Children's Hospital, Taizhou 318000, Zhejiang, China

³Department of Obstetrics, Taizhou Hospital, Taizhou 317000, Zhejiang, China

Correspondence should be addressed to Yiqun Wang; wangyiqun_4@163.com

Received 22 September 2022; Revised 4 October 2022; Accepted 6 October 2022; Published 18 November 2022

Academic Editor: Ashish Khanna

Copyright © 2022 Xia Ma et al. This is an open access article distributed under the Creative Commons Attribution License, which permits unrestricted use, distribution, and reproduction in any medium, provided the original work is properly cited.

Background. The P53 gene is critical to the onset and progression of cancers. Currently, relevant study findings indicate that the p53 gene may have a strong association with the risk of endometriosis, but these findings have not been united. To gather more statistically meaningful clinical data, we used meta-analysis to examine the relationship between the rs1042522 single nucleotide polymorphism of the tumor suppressor gene p53 and the incidence of endometriosis. **Methods.** Through a comprehensive literature survey of PubMed, MEDLINE, EMBASE, Springer, and Web of Science literature databases, we obtained a clinical control case study on the relationship between p53 gene polymorphism and the prevalence of female endometriosis and finally traced the relevant references included. The quality of the literature included in this study was evaluated, and Revman5.3 was used to complete the meta-analysis. **Results.** This research includes eight publications. The total number of cases in the study group was 1551, whereas the total number of cases in the control group was 1440. The findings of the sensitivity analyses of each omitted piece of the literature revealed no significant difference. The results of the meta-analysis showed that there were significant differences in the GG gene frequency (OR = 0.56, 95%CI (0.38, 0.92), $P = 0.003$), allele G (OR = 2.46, 95%CI (1.41, 4.29), $P = 0.002$), and allele C (OR = 0.62, 95%CI (0.46, 0.84), $P = 0.002$) between the study group and the control group ($P < 0.01$), but there was no significant difference in the GC gene frequency (OR = 1.17, 95%CI (1.01, 1.36), $P = 0.03$), and the CC gene frequency (OR = 1.25, 95%CI (0.85, 1.82), $P = 0.26$) ($P > 0.01$). **Conclusion.** Our study results show that there is a significant correlation between the single nucleotide of the p53 gene and the incidence rate of female endometriosis, in which the decrease of the GG gene frequency and the increase of allele C are likely to increase the risk of such diseases.

1. Introduction

Endometriosis refers to a series of clinical symptoms caused by the presence of endometrial glands and stroma outside the uterine cavity. Although this kind of disease is usually benign, its incidence rate in the global female population is quite high, up to 10%–15%, and according to the relevant epidemiological survey results, this kind of disease is increasing year by year [1–3]. Although the clinical symptoms of endometriosis are benign, if we do not pay attention and get targeted treatment, it is likely to have invasion and pathological metastasis and eventually lead to more serious

diseases [4–6]. Therefore, some clinicians and experts believe that endometriosis is a kind of tumor disease that is closely related to polygenic genetic factors [7–9]. Among them, the p53 gene is a kind of pathogenic gene that is strongly linked to tumor incidence, and its unique single nucleotide polymorphism is linked to the prevalence of female endometriosis. [10, 11] (see Figure 1). Therefore, many doctors and researchers have carried out clinical research on the problem and made research progress to varying degrees [12, 13]. However, there is no unified conclusion about the real intrinsic role of the p53 gene SNP and endometriosis. To better evaluate the relationship between the two, this study selected

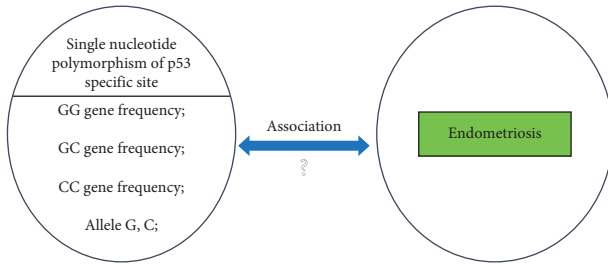


FIGURE 1: Possible association between a p53-specific single nucleotide polymorphism and endometriosis.

for meta-analysis the internationally published clinical control case studies on p53 gene polymorphism and female endometriosis prevalence from 2001 to 2022 and systematically evaluated the relationship between p53 gene polymorphism and endometriosis prevalence, in order to provide more evidence-based medical data for revealing the internal relationship between gene polymorphism and endometriosis prevalence. The report is as follows.

2. Materials and Methods

2.1. Data Sources and Literature Search Methods. PubMed, MEDLINE, EMBASE, Springer, and Web of Science literature databases were comprehensively searched through Computer artificial intelligence systems to obtain highly relevant literature related to this study. The language of literature retrieval is limited to English, and the retrieval period of literature is from 2001 to 2022. The strategies of literature retrieval are fast retrieval of English words and combinatorial retrieval of literature keywords. The key words were “endometriosis,” “rs1045552,” “p53 gene,” “SNP polymorphism,” “genetic variation analysis,” and “control test.” We can trace the complete text of the database by freely combining these keywords simultaneously, paired with manual retrieval to get further relevant reference material. The retrieval time is April 30, 2022.

2.2. Inclusion Criteria. ① The included literature is the international published literature about the relationship between p53 gene polymorphism and female endometriosis incidence rate; ② the purpose and statistical methods of each study in the literature are highly similar; ③ the subjects were all patients with endometriosis confirmed by clinical diagnosis; ④ the genotype frequency distribution of patients in the control group conformed to Hardy–Weinberg law; ⑤ the study included the main outcome indicators set out in this paper, and the data used for analysis were complete.

2.3. Exclusion Criteria. ① The literature does not provide specific research methods or complete data; ② the experimental group was nonendometriosis patients with other related diseases; ③ the genotype frequency distribution of patients in the control group did not meet Hardy–Weinberg law; ④ for the repeatedly published research content, only one piece of literature was introduced into this study.

2.4. Selection of Literature. Two studiers independently finished the screening of the literature. First, all literature titles and abstracts were independently read and analysed by these 2 studiers. The unfit for paper and report were then eliminated, and the fit for paper and report were collected and systematically reviewed by these two researchers. Following that, two researchers undertook cross-checking in order to exclude the questioned literature. Finally, a third studier was added to help in arbitration. In this literature, the NUI questionnaire assessed general health, mental health symptomatology, use of alcohol, nicotine 23, cannabis, and other substances, including the nonmedical use of prescription substances; migraines and headaches; inattention 24; and baldness.

2.5. Data Extraction. Two studiers were assigned to independently and professionally extract the relevant data from this study. The data information mainly includes the following: the first author of the literature, the year of publication, the number of patients in the study group and the control group, and the age, gender, and physical condition of the patients included in this study. In this study, all data are independently analyzed and compared by two researchers. When there are significant disparities in the study data, a third-party research team will be assembled to undertake another round of systematic examination.

2.6. Literature Quality Assessment. For this study, the recommended criteria for evaluating genotype frequency and gene-disease association research were adopted [14]. First, two researchers were arranged to read and analyze independently according to the criteria for inclusion and exclusion of literature, and then representative literature was selected and timely literature was proposed with insufficient data sample size, poor quality, and high repetition. Finally, cross-check the literature; if there are differences again, arrange an on-site discussion or enlist a third party to determine whether to include them in this study. In this study, the Ottawa News Broadcasting Scale (NOS scoring method) was used to comprehensively evaluate the quality of each document. The higher the score of a document, the better the quality of the document and the more representative it is.

2.7. Statistical Analysis. Revman5.3 data meta-analysis software. First, the statistical heterogeneity of the literature included in this research was examined. When there is no statistical heterogeneity among the research findings ($P > 0.1$, $I^2 > 50\%$), the fixed effects model is used for analysis; when there is statistical heterogeneity among the research results ($P > 0.1$, $I^2 > 50\%$), first examine whether the data included in the study is accurate. The full text of the literature is then carefully read to objectively evaluate and judge whether there is obvious clinical research heterogeneity or methodological heterogeneity in the literature; if there is a large heterogeneity, the random effects model is used to consolidate and analyze the data. The OR value and 95% CI

were used as endometriosis incidence rate analysis markers in this research.

3. Results

3.1. Literature Search Method and Screening Process. In this study, a total of 489 pieces of literature were obtained after preliminary screening. After reading the title, abstract, and full-text content of the literature, the literature that obviously did not meet the inclusion criteria, such as summary literature, case reports, and repetitive literature, was excluded. Finally, 8 pieces of literature with high quality and important representative significance were included, as shown in Figure 2. At the same time, the excluded literature and the main reasons for excluding this literature are listed in Table 1.

3.2. Literature Quality Evaluation. According to the retrieval scheme and document retrieval process described in 1.1 above, 8 articles were finally included in our study [17]. These articles included 2991 female patients with endometriosis, including 1551 patients in the experimental group and 1440 patients in the control group. There was no statistical significance in the age, weight, sex ratio, and family genetic history of female endometriosis patients. The NOS scoring standard was used to evaluate the treatment of the literature included in this study. This literature met the NOS scoring standard [12]. The evaluation results are shown in Table 2.

3.3. Meta-Analysis Results

3.3.1. GG Genotype Frequency. Eight pieces of literature [18–25] reported the relationship between the single nucleotide polymorphism GG genotype frequency at the rs1042522 site of the p53 gene and female endometriosis, including 1551 patients with female endometriosis and 1440 patients with nonendometriosis. There was heterogeneity in the literature ($I^2 = 79\%$, $P < 0.0001$). The random effect model analysis showed that the GG genotype frequency of endometriosis patients in the experimental group was significantly lower than that in the control group, with a significant difference (OR = 0.56, 95%CI (0.38, 0.92), $P = 0.003$) (see Figure 3).

3.3.2. GC Genotype Frequency. Eight pieces of literature [18–25] reported the relationship between the GC genotype frequency of a single nucleotide polymorphism at the rs1042522 site of the p53 gene and female endometriosis, including 1551 patients with female endometriosis and 1440 patients with nonendometriosis. There was no significant heterogeneity in the literature ($I^2 = 31\%$, $P = 0.18$). Fixed effect model analysis showed that there was no significant difference in the frequency of GC genotypes in the experimental group of endometriosis patients (OR = 1.17, 95%CI (1.01, 1.36), $P = 0.03$) (see Figure 4).

3.3.3. CC Genotype Frequency. Eight pieces of literature [18–25] reported the relationship between the CC genotype frequency of the single nucleotide polymorphism at the rs1042522 of the p53 gene and female endometriosis, including 1551 patients with female endometriosis and 1440 patients with nonendometriosis. There was heterogeneity in the literature ($I^2 = 63\%$, $P = 0.009$). The random effect model analysis showed that there was no significant difference in the CC genotype frequency between the experimental group and the control group (OR = 1.25, 95%CI (0.85, 1.82), $P = 0.26$) (see Figure 5).

3.3.4. Allele G. Six pieces of literature [19–25] reported the relationship between the single nucleotide polymorphic allele G at the rs1042522 locus of the p53 gene and female endometriosis, including 1472 patients with female endometriosis and 1357 patients with nonendometriosis. There was heterogeneity in the literature ($I^2 = 91\%$, $P < 0.00001$). The random effect model analysis showed that there was a significant difference in allele G between the experimental group and the control group, with a statistical significance (OR = 2.46, 95% CI (1.41, 4.29), $P = 0.002$) (see Figure 6).

3.3.5. Allele C. Six pieces of literature [19–25] reported the relationship between the single nucleotide polymorphism allele C at the rs1042522 locus of the p53 gene and female endometriosis, including 1472 patients with female endometriosis and 1357 patients with nonendometriosis. There was heterogeneity in the literature ($I^2 = 67\%$, $P = 0.01$). The random effect model analysis showed that there was a significant difference in allele C between the experimental group and the control group, with a statistical significance (OR = 0.62, 95%CI (0.46, 0.84), $P = 0.002$) (see Figure 7).

3.3.6. Analysis of Publication Bias. No publication bias analysis was performed because there were few articles in this study.

4. Discussion

Endometriosis is the most common and frequently occurring gynecological disease among women in the reproductive period. Clinically, such diseases mainly include dysmenorrhea, chronic intermittent pelvic pain, infertility, and other symptoms. At present, there is no completely effective treatment [26, 27]. Although most of these diseases have benign clinical manifestations, they are highly invasive and recurrent due to their wide range of incidence and diverse clinical pathological features [28, 29]. This has not only greatly affected the physical and mental health of women but also greatly reduced their quality of life. As a result, it is critical for these patients to uncover the molecular pathogenic process of this illness after doing more in-depth clinical research and thoroughly reviewing current research data. It may not only enhance the prognosis of female patients but also their overall quality of life. Endometriosis affects approximately 10% (190 million) of women and girls

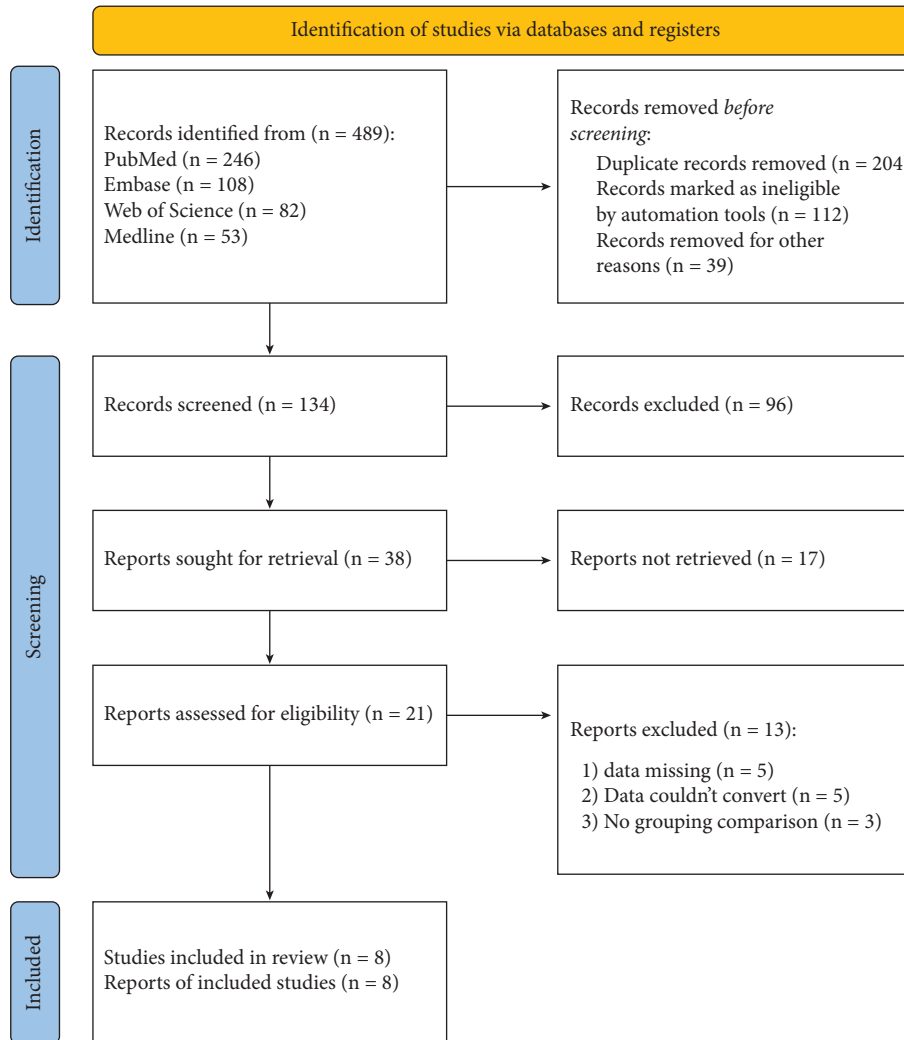


FIGURE 2: Flow chart of literature screening included in this study.

TABLE 1: Excluded literature and the main reasons for exclusion (not all).

Serial number	Author	Date of publication	Reason for exclusion
1	Hsieh and Lin [15]	2006	Data cannot be effectively transformed
2	Ying et al [16]	2011	Limited data

TABLE 2: Basic characteristics of included literature.

Serial number	Author	Study location	Date of publication	Total cases
1	Dastjerdi et al [18]	Isfahan, Iran	(2013)	180
2	Ammendol et al [19]	Rome, Italy	(2008)	376
3	Vietri et al [20]	Naples, Italy	(2007)	192
4	Gallegos-Arreola et al. [21]	Guadalajara, México	(2012)	386
5	Lattuada et al. [22]	Milano, Italy	(2004)	303

of reproductive age worldwide. Early diagnosis and effective treatment of endometriosis are important, but in many cases (including in low- and middle-income countries), access to early diagnosis and effective treatment is difficult. More research and increased awareness are therefore needed

worldwide to achieve effective prevention, early diagnosis, and better management of this disease.

In recent years, great progress has been made in the study of the pathogenesis of female endometriosis, but there is no unified conclusion on its essential pathogenesis. Many

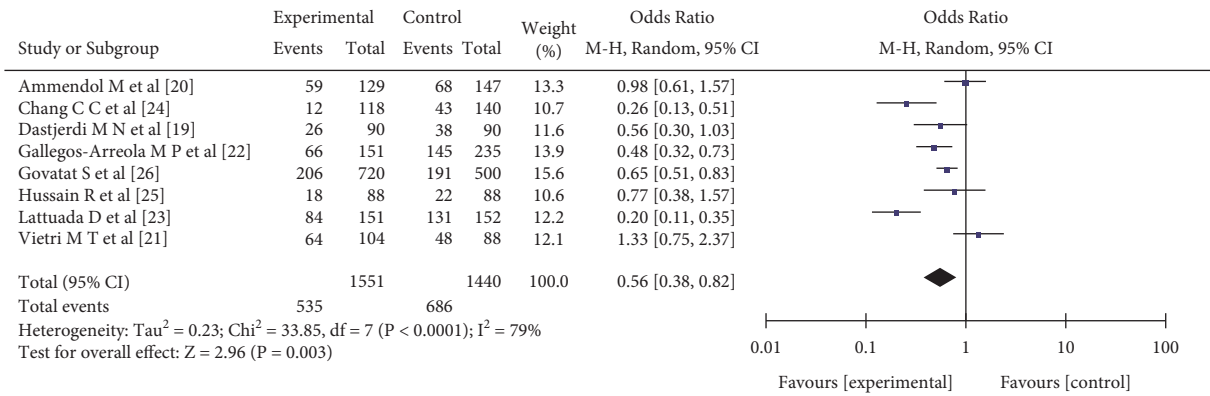


FIGURE 3: The correlation between the GG genotype frequency and female endometriosis incidence rate.

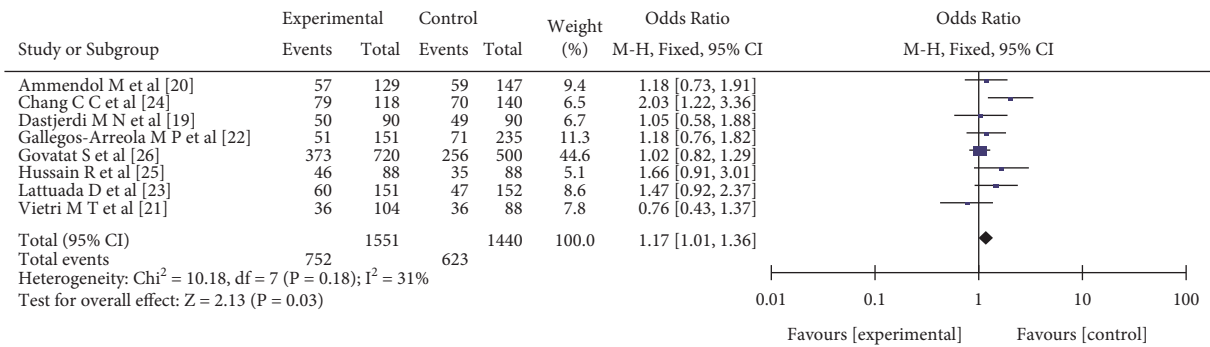


FIGURE 4: The correlation between the GC genotype frequency and female endometriosis incidence rate.

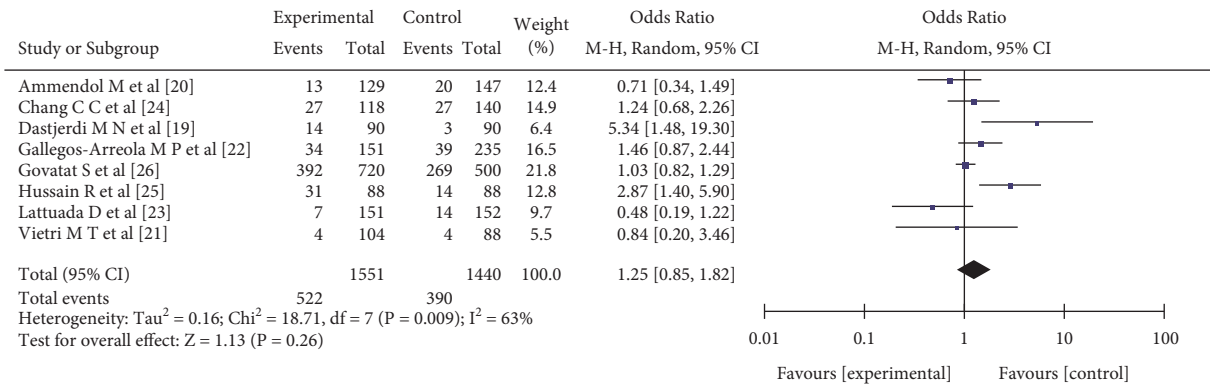


FIGURE 5: The correlation between the CC genotype frequency and female endometriosis incidence rate.

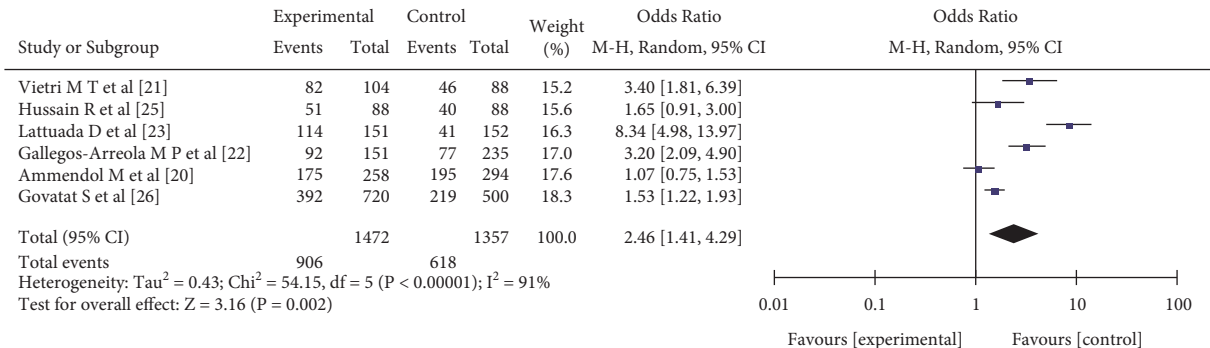


FIGURE 6: The correlation between allele G and female endometriosis incidence rate.

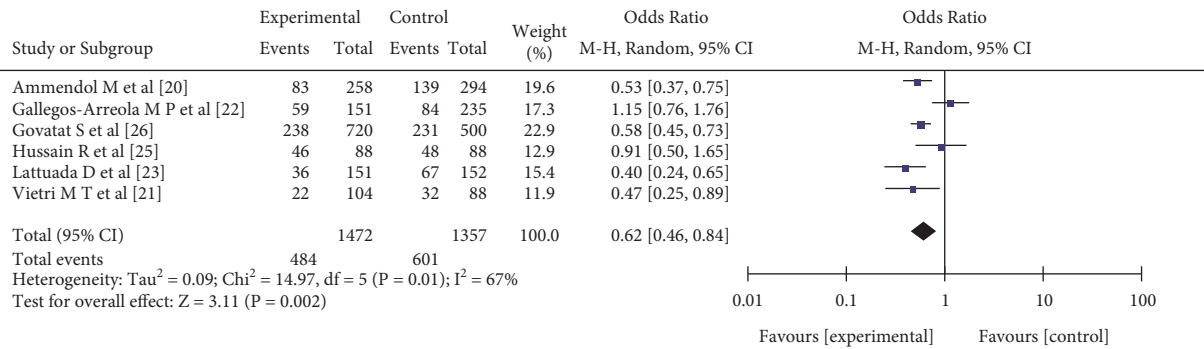


FIGURE 7: The correlation between allele C and female endometriosis incidence rate.

clinicians and experts generally believe that endometriosis is a kind of disease affected by a variety of environmental and genetic factors, such as tumor-related genes, environmental detoxification genes, immune-related genes, and hormone level-regulating genes, of which tumor-related genes are the most representative factors [30, 31]. Among tumor-related genes, the p53 gene, which functions as a tumor suppressor, is not only one of the most often altered genes in human malignant tumors but it is also linked to more than half of all human malignancies. Under normal physiological settings, this gene is not required for the human body. When human DNA is damaged or abnormally proliferated, the p53 gene is overexpressed. [32]. In recent years, many clinicians and scholars at home and abroad have carried out in-depth research on the relationship between the single nucleotide polymorphism of the rs1042522 and the incidence rate of endometriosis, and they have achieved significant research results [33, 34]. However, due to the difference in the genetic background among different races, their conclusions are inconsistent. For example, the research results of MP Gallegos Arreola et al. [21] suggest that the polymorphism of the rs1042522 single nucleotide at the special site of the p53 gene is closely related to the occurrence of endometriosis, while the research results of Shinya Omori et al. show that the polymorphism of rs1042522 single nucleotide at the special site of the p53 gene is not significantly related to the occurrence of endometriosis.

Endometriosis has significant social, public health, and economic implications. The intense pain, fatigue, depression, anxiety, and infertility associated with the disease reduce the quality of life. Endometriosis causes intolerable pain for some patients, preventing them from going to work or school. In this context, treating endometriosis could reduce school absences or improve the labour capacity of individuals. Dyspareunia due to endometriosis can result in the interruption or escape of sexual intercourse, thus affecting the sexual health of patients and/or their partners. Treatment of endometriosis will help patients enjoy their human rights to access the highest standards of sexual and reproductive hygiene, quality of life, and overall well-being, thereby empowering them. As a consequence, it is of tremendous value and therapeutic relevance to thoroughly examine all of the data using meta-analysis for these current study findings and the most recent studies.

In this study, after the selection and repeated demonstration of research topics and further condensing keywords, 8 highly representative pieces of research literature were effectively obtained. In the literature, various researchers have concentrated on reporting the relationship between the GG genotype frequency, the GC genotype frequency, the CC genotype frequency, allele G, and allele C in the single nucleotide polymorphisms at special sites of the p53 gene and endometriosis. Through further statistics and meta-analysis of these literature results, we found that there were significant differences between the study group and the control group in the GG gene frequency, allele G, and allele C of the special site rs1042522 of the tumor suppressor gene p53 ($P < 0.01$), but there were no significant differences in the GC gene frequency and the CC gene frequency between them ($P > 0.01$). As a consequence of our findings, there is a strong link between the single nucleotide polymorphism rs1042522 at the particular location of the p53 gene and endometriosis, with a drop in the GG gene frequency and an increase in allele C likely increasing the risk of this illness. On the other hand, for commonly used antibiotics, such as amoxicillin [35], ornidazole [36], etc., the efficacy of some natural drugs for this disease is also of concern [37].

5. Summary

In this systematic review and meta-analysis about the association between p53 gene polymorphism and endometriosis, a total of 8 pieces of literature were included. The results of our study show that the single nucleotide polymorphism of rs1042522 at the special site of the p53 gene is highly correlated with endometriosis. As a result, in future clinical research, doctors will be able to effectively combine these data to carry out more extensive and in-depth joint analysis, revealing the pathogenesis of such diseases and doing a good job at prevention in advance, eventually controlling the clinical malignant rate of endometriosis.

Data Availability

The data used in this study are available from the author upon request.

Conflicts of Interest

The authors declare that there no conflicts of interest.

Acknowledgments

This study was supported by the project “To investigate the role and mechanism of Oxyberberine in the prevention and treatment of endometriosis based on the regulation of PINK1/Parkin autophagy pathway by P53” and grants from the Health Bureau of Zhejiang Province No. 2023KY1314.

References

- [1] F. Parazzini, G. Esposito, L. Tozzi, S. Noli, and S. Bianchi, “Epidemiology of endometriosis and its comorbidities,” *European Journal of Obstetrics & Gynecology and Reproductive Biology*, vol. 209, pp. 3–7, 2017.
- [2] P. R. Koninckx, A. Ussia, L. Adamyan et al., “The epidemiology of endometriosis is poorly known as the pathophysiology and diagnosis are unclear,” *Best Practice & Research Clinical Obstetrics & Gynaecology*, vol. 71, pp. 14–26, 2021.
- [3] A. N. Peiris, E. Chaljub, and D. Medlock, “Endometriosis,” *JAMA*, vol. 320, no. 24, p. 2608, 2018.
- [4] F. Guidozzi, “Endometriosis-associated cancer,” *Climacteric*, vol. 24, no. 6, pp. 587–592, 2021.
- [5] U. Leone Roberti Maggiore, S. Ferrero, A. Bergamini et al., “A systematic review on endometriosis during pregnancy: diagnosis, misdiagnosis, complications and outcomes,” *Human Reproduction Update*, vol. 22, no. 1, pp. 70–103, 2016.
- [6] F. Sorrentino, M. De Padova, M. Falagario et al., “Endometriosis and adverse pregnancy outcome,” *Minerva Obstet Gynecol*, vol. 74, no. 1, pp. 31–44, 2022.
- [7] P. Vercellini, P. Viganò, E. Somigliana, and L. Fedele, “Endometriosis: pathogenesis and treatment,” *Nature Reviews Endocrinology*, vol. 10, no. 5, pp. 261–275, 2014.
- [8] L. Méar, M. Herr, A. Fauconnier, C. Pineau, and F. Vialard, “Polymorphisms and endometriosis: a systematic review and meta-analyses,” *Human Reproduction Update*, vol. 26, no. 1, pp. 73–103, 2020.
- [9] S. Gupta 1, J. M. Goldberg, and N. Aziz, “Pathogenic mechanisms in endometriosis-associated infertility [J],” *Fertility and Sterility*, vol. 90, no. 2, pp. 247–257, 2008.
- [10] J. Pollacco, K. Sacco, M. Portelli, P. Schembri-Wismayer, and J. Calleja-Agius, “Molecular links between endometriosis and cancer,” *Gynecological Endocrinology*, vol. 28, no. 8, pp. 577–581, 2012.
- [11] R. Sáinz de la Cuesta, M. Izquierdo, M. Canamero, J. J. Granizo, and F. Manzarbeitia, “Increased prevalence of p53 overexpression from typical endometriosis to atypical endometriosis and ovarian cancer associated with endometriosis,” *European Journal of Obstetrics & Gynecology and Reproductive Biology*, vol. 113, no. 1, pp. 87–93, 2004.
- [12] Y. Huang, L. Zong, J. Lin et al., “Association of P53 gene polymorphisms with susceptibility to endometriosis,” *Zhonghua Yi Xue Yi Chuan Xue Za Zhi*, vol. 30, no. 3, pp. 335–339, 2013.
- [13] K. S. F. Silva and K. K. V. O. Moura, “Genetic polymorphisms in patients with endometriosis: an analytical study in Goiânia (Central West of Brazil),” *Genetics and Molecular Research*, vol. 15, no. 2, 2016.
- [14] D. Luo and L. Zhong, “Combination of methotrexate and mifepristone versus methotrexate alone for patients with ectopic pregnancy: a systematic review,” *Med J Chin PLA*, vol. 36, no. 2, pp. 184–187, 2011.
- [15] Y.-Y. Hsieh and C.-S. Lin, “P53 codon 11, 72, and 248 gene polymorphisms in endometriosis,” *International Journal of Biological Sciences*, vol. 2, no. 4, pp. 188–193, 2006.
- [16] T. H Ying, C.-J. Tseng, S. J Tsai et al., “Association of p53 and CDKN1A genotypes with endometriosis,” *Anticancer Research*, vol. 31, no. 12, pp. 4301–4306, 2011.
- [17] S. Omori, S. Yoshida, S. H. Kennedy et al., “Polymorphism at codon 72 of the p53 gene is not associated with endometriosis in a Japanese population,” *Journal of the Society for Gynecologic Investigation*, vol. 11, no. 4, pp. 232–236, 2004.
- [18] M. Nikbakht Dastjerdi, R. Aboutorabi, and B. Eslami Farsani, “Association of TP53 gene codon 72 polymorphism with endometriosis risk in Isfahan,” *Iranian Journal of Reproductive Medicine*, vol. 11, no. 6, pp. 473–478, 2013.
- [19] M. Ammendola, F. Gloria-Bottini, F. Sesti, E. Piccione, and E. Bottini, “Association of p53 codon 72 polymorphism with endometriosis,” *Fertility and Sterility*, vol. 90, no. 2, pp. 406–408, 2008.
- [20] M. T. Vietri, A. M. Molinari, I. Iannella et al., “Arg72Pro p53 polymorphism in Italian women: no association with endometriosis,” *Fertility and Sterility*, vol. 88, no. 5, pp. 1468–1469, 2007.
- [21] M. Gallegos-Arreola, L. Figuera-Villanueva, A. M. Puebla-Pérez, H. Montoya-Fuentes, A. Suarez-Rincon, and G. Zuniga Gonzalez, “Association of TP53 gene codon 72 polymorphism with endometriosis in Mexican women,” *Genetics and Molecular Research*, vol. 11, no. 2, pp. 1401–1408, 2012.
- [22] D. Lattuada, P. Viganò, E. Somigliana, and A. Abbiati, “Analysis of the codon 72 polymorphism of the TP53 gene in patients with endometriosis,” *Molecular Human Reproduction*, vol. 10, no. 9, pp. 651–654, 2004.
- [23] C.-C. Chang, Y.-Y. Hsieh, F. J. Tsai, H. D. Tsai, C. C. Lin, and C. H. Tsai, “The proline form of p53 codon 72 polymorphism is associated with endometriosis,” *Fertility and Sterility*, vol. 77, no. 1, pp. 43–45, 2002.
- [24] R. Hussain, S. Khaliq, S. M. Raza, S. Khaliq, and K. P. Lone, “Association of TP53 codon 72 polymorphism in women suffering from endometriosis from Lahore, Pakistan,” *Journal of Pakistan Medical Association*, vol. 68, no. 2, pp. 224–230, 2018.
- [25] S. Govatati, B. Chakravarty, M. Deenadayal et al., “p53 and risk of endometriosis in Indian women,” *Genetic Testing and Molecular Biomarkers*, vol. 16, no. 8, pp. 865–873, 2012.
- [26] T. Falcone and R. Flyckt, “Clinical management of endometriosis,” *Obstetrics & Gynecology*, vol. 131, no. 3, pp. 557–571, 2018.
- [27] C. Chapron, L. Marcellin, B. Borghese, and P. Santulli, “Rethinking mechanisms, diagnosis and management of endometriosis,” *Nature Reviews Endocrinology*, vol. 15, no. 11, pp. 666–682, 2019.
- [28] A. Zakhari, E. Delpero, S. McKeown, G. Tomlinson, O. Bougie, and A. Murji, “Endometriosis recurrence following post-operative hormonal suppression: a systematic review and meta-analysis,” *Human Reproduction Update*, vol. 27, no. 1, pp. 96–107, 2021.
- [29] A. Zakhari, D. Edwards, M. Ryu, J. J. Matelski, O. Bougie, and A. Murji, “Dienogest and the risk of endometriosis recurrence following surgery: a systematic review and meta-analysis,” *Journal of Minimally Invasive Gynecology*, vol. 27, no. 7, pp. 1503–1510, 2020.

- [30] V. Baranov, O. Malysheva, and M. Yarmolinskaya, "Pathogenomics of endometriosis development," *International Journal of Molecular Sciences*, vol. 19, no. 7, p. 1852, 2018.
- [31] J. Meola, R. Ferriani, J. Rosa-e-Silva, and D Dentillo, "Common dysregulated genes in endometriosis and malignancies," *Revista Brasileira de Ginecologia e Obstetrícia*, vol. 38, no. 05, pp. 253–262, 2016.
- [32] X. Cheng, F. He, P. Sun, and Q. Chen, "Identification of unknown acid-resistant genes of oral microbiotas in patients with dental caries using metagenomics analysis," *AMB Express*, vol. 11, no. 1, pp. 39–10, 2021.
- [33] H. Falconer, T. D'Hooghe, and G. Fried, "Endometriosis and genetic polymorphisms," *Obstetrical and Gynecological Survey*, vol. 62, no. 9, pp. 616–628, 2007.
- [34] C. Baflligil, D. J. Thompson, A. Lophatananon et al., "Association between genetic polymorphisms and endometrial cancer risk: a systematic review," *Journal of Medical Genetics*, vol. 57, no. 9, pp. 591–600, 2020.
- [35] X. Cheng, F. Huang, K. Zhang, X. Yuan, and C. Song, "Effects of none-steroidal anti-inflammatory and antibiotic drugs on the oral immune system and oral microbial composition in rats," *Biochemical and Biophysical Research Communications*, vol. 507, no. 1-4, pp. 420–425, 2018.
- [36] X. Cheng, F. He, M. Si, P. Sun, and Q. Chen, "Effects of antibiotic use on saliva antibody content and oral microbiota in sprague dawley rats," *Frontiers in Cellular and Infection Microbiology*, vol. 12, Article ID 721691, 2022.
- [37] X. Cheng, Q. Chen, and P. Sun, "Natural phytochemicals that affect autophagy in the treatment of oral diseases and infections: a review," *Frontiers in Pharmacology*, vol. 13, Article ID 970596, 2022.

Retraction

Retracted: Diagnosis of Breast Cancer Using Computational Intelligence Models and IoT Applications

Computational Intelligence and Neuroscience

Received 31 October 2023; Accepted 31 October 2023; Published 1 November 2023

Copyright © 2023 Computational Intelligence and Neuroscience. This is an open access article distributed under the Creative Commons Attribution License, which permits unrestricted use, distribution, and reproduction in any medium, provided the original work is properly cited.

This article has been retracted by Hindawi following an investigation undertaken by the publisher [1]. This investigation has uncovered evidence of one or more of the following indicators of systematic manipulation of the publication process:

- (1) Discrepancies in scope
- (2) Discrepancies in the description of the research reported
- (3) Discrepancies between the availability of data and the research described
- (4) Inappropriate citations
- (5) Incoherent, meaningless and/or irrelevant content included in the article
- (6) Peer-review manipulation

The presence of these indicators undermines our confidence in the integrity of the article's content and we cannot, therefore, vouch for its reliability. Please note that this notice is intended solely to alert readers that the content of this article is unreliable. We have not investigated whether authors were aware of or involved in the systematic manipulation of the publication process.

Wiley and Hindawi regrets that the usual quality checks did not identify these issues before publication and have since put additional measures in place to safeguard research integrity.

We wish to credit our own Research Integrity and Research Publishing teams and anonymous and named external researchers and research integrity experts for contributing to this investigation.

The corresponding author, as the representative of all authors, has been given the opportunity to register their agreement or disagreement to this retraction. We have kept a record of any response received.

References

- [1] M. Alghamdi, M. Maray, and M. B. Alazzam, "Diagnosis of Breast Cancer Using Computational Intelligence Models and IoT Applications," *Computational Intelligence and Neuroscience*, vol. 2022, Article ID 2143510, 7 pages, 2022.

Research Article

Diagnosis of Breast Cancer Using Computational Intelligence Models and IoT Applications

Mohammed Alghamdi ^{1,2} Mohammed Maray ¹ and Malik Bader Alazzam ^{3,4}

¹College of Computer Science, King Khalid University, Abha 62529, Saudi Arabia

²University of Jeddah, Jeddah, Saudi Arabia

³Information Technology College, Ajloun National University, Ajloun, Jordan

⁴The University of Mashreq, Research Center, Baghdad, Iraq

Correspondence should be addressed to Malik Bader Alazzam; malikbader2@gmail.com

Received 3 September 2022; Revised 27 September 2022; Accepted 5 October 2022; Published 14 October 2022

Academic Editor: Ashish Khanna

Copyright © 2022 Mohammed Alghamdi et al. This is an open access article distributed under the Creative Commons Attribution License, which permits unrestricted use, distribution, and reproduction in any medium, provided the original work is properly cited.

The use of computer-aided diagnostic (CAD) models has been proposed to aid in the detection and classification of breast cancer. In this work, we evaluated the performance of multilayer perceptron neural network and nonlinear support vector machine models to classify breast cancer nodules. From the contour of 569 samples, ten morphological features were used as input to the classifiers. The average results obtained in the set of 50 simulations performed show that the proposed models showed good performance (all exceeded 90.0%) in terms of accuracy in the test set. The nonlinear support vector machine algorithm stands out when compared to the proposed multilayer perceptron neural network algorithm, with 99% accuracy and a 2% false-negative rate. The neural network model presented lower performance than the nonlinear support vector machine classifier. With the application of the proposed models, the average results obtained are promising in the classification of breast cancer.

1. Introduction

Cancer has become one of the most frequent diseases in the world, accounting for 15 percent of the almost 56 million deaths, with more than 14 million new cases annually [1]. In Iraq, estimates for 2018 point to more than 600,000 new cancer cases, where breast cancer is the one with the highest incidence, after nonmelanoma skin and prostate cancer [2, 3]. Since the beginning of research on breast cancer, the best way to cure the disease is early detection. Mammography is one of the best techniques for screening breast cancer currently available, capable of recording images of the breast in order to diagnose the presence or absence of structures that may indicate the disease. With this type of exam, the tumor can be detected before it becomes palpable. However, the evaluation of the mammography exam and the diagnosis, performed by a radiologist, requires a lot of skill, but there are limitations in the primary prediction of breast cancer. Studies have revealed that 10% to 30% of women

who have had breast cancer have negative results when undergoing mammography, which leads to the belief that there was a misinterpretation of the exams. Distortions in the interpretation and classification of lesions by specialists imply a greater number of unnecessary biopsies, that is, between 65% and 85% of breast biopsies are performed in benign lesions. As a result, there is a reduction in the cost-effectiveness of the tests and, in the worst case, the non-detection of the disease, characterizing a false-negative diagnosis. This neoplasm has attracted greater attention in public health and the scientific community, where researchers are using computational intelligence techniques to develop computer diagnostic support systems (CAD), aiming to increase the detection rate of breast cancer [4]. Among these techniques, Artificial Neural Networks (ANNs) [5, 6] and Support Vector Machines (SVMs) [7], because they are robust in a noisy dataset. Despite the good results obtained with ANNs, their results are stochastic and strongly depend on the order of presentation of objects and

the initial weights assigned to their connections. Therefore, it is recommended to run it several times for different configurations of the data and initial values of weights, obtaining an average of performance the Nonlinear Layers (NLPs) and Support Vector Machine (SVM) in a set of 50 simulations in the classification of breast malignancy, obtained from mammographic findings.

2. Theoretical Framework

Artificial Neural Networks (ANNs) are parallel and distributed systems made up of simple units (neurons or nodes), which calculate certain mathematical functions (mainly nonlinear) and have the capacity for generalization, self-organization, and temporal processing. Similarly to the nervous system of a human being, neurons are arranged in one or more layers and interconnected by numerous connections, usually unidirectional, called synapses [8, 9]. These connections are associated with values, called synaptic weights, responsible for weighing the inputs of each neuron as a way of storing knowledge of a particular model. Artificial neurons, also known as nodes, or processing units, are used in neural networks to facilitate learning. Figure 1 shows a representation of the nonlinear model of an artificial neuron.

An ANN has the characteristic of learning through examples and extracting knowledge from a given data set. Knowledge is acquired from the process by which the free hyperparameters of a neural network are adjusted through a continuous form of stimulation by the external environment, aiming to minimize the value of an error function. This process is defined as learning, which can be classified as supervised or unsupervised. Within the supervised learning context, we present the available inputs and the desired output to the network, and the algorithm works to adjust the synapse weights by calculating the difference between the desired output value $y_{di}(t)$ and the value predicted by the ANN $y_{pi}(t)$, at instant t thus producing an error $\delta(t)$ in the following equation:

$$\delta(t) = y_{di}(t) - y_{pi}(t). \quad (1)$$

The generic way to adjust the weights, by error correction, is presented in the following equation:

$$w_{ij}(t+1) = w_{ij}(t) + \eta e_i(t)x_j(t), \quad (2)$$

where η is the learning rate and $x_i(t)$ the input to neuron i at time t .

In unsupervised learning, the desired output values y are not known. Therefore, learning occurs through the identification of patterns in the inputs. The choice of an ANN architecture is related to the types of problems to be addressed and is defined by 4 main hyperparameters: number of network layers, number of neurons in each layer, type of connection between neurons, and the network topology. Regarding the number of layers, there are single-layer networks, which have only one node between the input and output layers of the network, being restricted to solving linearly separable problems.

Multilayer neural networks have more than one neuron between an input and an output of the network. Among the multilayer networks, we have the Multilayer Perceptions (MLP) type, which has one or more layers of intermediate or hidden neurons and is considered a universal approximator. According to the universal approximation theorem, any continuous function can be uniformly approximated by a network with at least one layer of hidden neurons and a sigmoid activation function [9]. Let $\varphi(\cdot)$ be a continuous, bounded, and monotonously function I_{mo} and a unitary hypercube $0,1]^{mo}$ of dimension mo . The space of continuous functions on I_{mo} is represented by $C(I_{mo})$. Then, given any function $f \in C(I_{mo})$ and $\varepsilon > 0$, there is an integer M and sets of real constants α_i , b_i and w_{ij} , where $i = 1, \dots, m$ and $j = 1, \dots, mo$ such that we can define:

$$F(x_1, \dots, x_{mo}) = \sum_{i=1}^m \alpha_i \varphi \left(\sum_{j=1}^{mo} w_{ij} x_j + b_i \right). \quad (3)$$

An approximation to the function $f(\cdot)$ is shown in 2.3,

$$|F(x_1, \dots, x_{mo}) - f(x_1, \dots, x_{mo})| < \varepsilon. \quad (4)$$

For (x_1, \dots, x_{mo}) everything in the input space.

So the universal approximation theorem is directly applicable to multilayer perceptrons. Figure 2 represents an MLP network with three inputs, two intermediate layers with four neurons, and an output layer with one neuron, producing single output information [10].

MLP networks have been successfully applied to solve several problems, through their training in a supervised way using the error backpropagation algorithm, which has two distinct phases. In the first phase, the functional signal propagates (feedforward) keeping the weights fixed to generate an output value from the inputs supplied to the network. In the second phase, the outputs are compared with the desired values, generating an error signal that propagates from the output to the input, adjusting the weights to minimize the error [11, 12]. Thus, the way to calculate the error depends on the layer in which the neuron is located, as shown in the following equation:

$$\delta_l = \left\{ f'_{a_l} e_l f'_a \sum w_{lk} \delta_k \text{ if } n_l \in C_{sai} \text{ } n_l \in C_{int}, \right. \quad (5)$$

where n_l is the l^{th} neuron, C_{sai} represents the output layer, C_{int} represents an intermediate layer, is the partial derivative of the neuron's activation function, and e_l is the squared error made by the output neuron when its response is compared to the desired, which is defined by the following equation:

$$e = \frac{1}{2} \sum_{q=1}^k (y_q - \hat{y}_q)^2, \quad (6)$$

where \hat{y}_q is the output produced by the neuron and y_q is the desired output.

The partial derivative defines the adjustment of the weights, using the gradient descent of the activation function. This derivative evaluates the contribution of each weight in the network error to the classification of a given

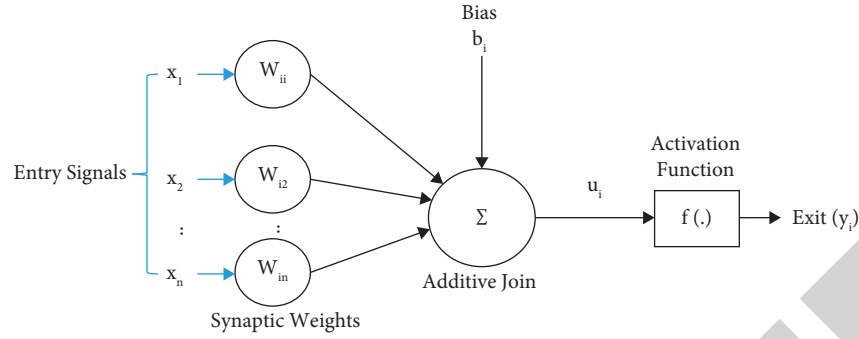


FIGURE 1: Nonlinear neuron model [9].

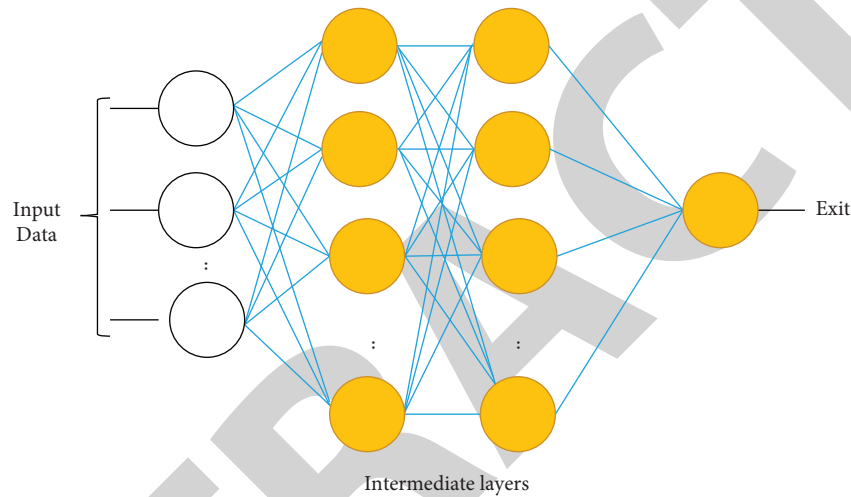


FIGURE 2: Graphical representation and an MLP network, with two intermediate layers.

object. If the derivative for a given weight is positive, the weight is causing the difference between the network output and the desired output to increase. Therefore, its magnitude must be reduced in order to decrease the error. Otherwise, the weight will contribute to the network output being closer to the desired one.

The Support Vector Machine (SVM) is a set of supervised learning methods used for data classification and regression based on statistical learning theory. Algorithms have qualities that allow them to generalise to previously unexplored data sets. Creating a border between two classes permits the prediction of labels from one or more feature vectors [13]. Using a hyperplane as a decision boundary, all data points near each class are placed as close to the boundary as possible. Support vectors are the names given to the closest points in space. Consider a training dataset that is labelled like this:

$$(x_1, y_1), \dots, (x_n, y_n), x_i \in R^d \text{ and } y_i \in (-1, +1), \quad (7)$$

where x_i is a representation of the feature vector and y_i , Negative or Positive Class Label of a Training Set It is thus possible to define the ideal hyperplane:

$$wx^t + b = 0, \quad (8)$$

where w , x , and b represent the input and trend, respectively (or bias). All elements of the training set must meet the following inequalities:

$$\begin{aligned} wx_i^t + b &\geq 1, & \text{if } y_i = 1, \\ wx_i^t + b &\leq -1, & \text{if } y_i = -1. \end{aligned} \quad (9)$$

In order to train an SVM model, the goal is to discover the w and b that maximise the margin $1/\|w\|^2$ in the hyperplane.

Thus, for a linearly separable dataset, SVMs are able to categorize two classes through an optimal hyperplane, obtaining a good generalization in its classification. However, for binary classification, where the data are not linearly separable in the original space, it is necessary to reference it in a new space of greater dimension, called feature space. For this, the use of nonlinear Support Vector Machines (nonlinear-SVMs) is necessary.

This type of approach is called nonlinear support vector machines (SVMs-nonlinear), and it is used to classify data represented in multidimensional feature space by the kernel function. SVMs use the kernel function to transform non-linearly separable data into linearly separable data in a higher-dimensional space. These functions convert the dataset into the feature space's original input space, i.e., a K

kernel takes two input space points x_i and x_j and returns the feature space's dot product. Kernels are incorporated into the SVMs classifier through the following equation:

$$f(x) = \text{sgn} \left(\sum_{i=1}^{n_{SV}} \alpha_i y_i K(\vec{x}_i, \vec{x}) + b \right), \quad (10)$$

where K denotes the kernel function, which receives as input the support vector i and the sample values to be classified, α_i the Lagrange multipliers and b the intercept value.

Methods based on kernel theory have provoked a real revolution in the algorithms of statistical learning theory, supervised and unsupervised, by enabling the creation of nonlinear versions of classical linear algorithms. Among the set of algorithms found in the literature that use kernel function, the support vector machine algorithm proposed by Vapnik 20 for binary classification is the most prominent. SVMs have kernel functions that characterize their pattern recognition mode, with polynomial, Gaussian, and sigmoidal being the most used (Table 1).

The degree (δ) can be defined during training in the polynomial function. In the Gaussian function that corresponds to an infinite-dimensional feature space, its use allows SVMs to present a radial basis function (RBF) neural network characteristics. The sigmoidal function allows behavior similar to that of an MLP neural network. SVMs use a decision function to distinguish between two groups of data (hyperplane). We refer to the points taken from the training data as support vectors (SVs). Unlike classic pattern recognition methods, SVMs focus on reducing structural risk rather than empirical risk.

3. Materials and Methods

The Wisconsin Diagnostic Breast Cancer public database 21 provided the data for this investigation, which included 569 records from women with probable breast cancer. Mean values of radius, texture, perimeter, and area are included in the data analysis, the number of concave points in the contour, and the fractal dimension of the lesion's contour. The methodology aims to compare the computational models structured in Neural Network MLP and Support Vector Machines (SVMs-nonlinear), in the classification of malignancy, referring to the morphological characteristics of the contour of the lesion found in mammographic findings (Figure 3).

To evaluate the performance of the models proposed in this study, the total accuracy or precision (ACC) and the error rate of the false-negative class (EFN) were used. Defined, respectively, by the following equation:

$$\text{Accuracy (ACC)} = \frac{VP + VN}{n}, \quad (11)$$

$$\text{False - negative class (EFN)} = \frac{FN + VN}{VP + FN},$$

where V P are positive-label samples (+1) predicted to be positive, V N are negative-label samples (-1) predicted to be negative, F N are positive-label samples (+1) predicted to be

TABLE 1: Mathematical equations regarding the most used kernel functions.

	Function ($k(x_i, x_j)$)	Parameters
Kernel type	$(\delta(x_i, x_j))^d$	δ, d, k
Polynomial	$e^{(-\sigma \ x_i, x_j\ ^2)}$	σ
Sigmoidal	$\tanh(\delta(x_i, x_j) + k)$	δ, k

negative, and n is the total number of samples. For each model, 50 simulations were performed to obtain a better generalization in the results obtained.

The computational models were implemented using the R software and the Kernlab13 and Neuralnet6 packages, respectively, in the SVMs-nonlinear model and in the MLP neural network model. The list of hyperparameters used in the RN-MLP and SVMs-nonlinear models is summarized in Tables 2 and 3, respectively. The hyperparameters used in the classification were obtained empirically.

4. Results and Discussions

The computational models proposed in this work were evaluated by incorporating attributes referring to the radius, texture, perimeter, area, smoothness, compactness, concavity, several concave points in the contour, symmetry, and fractal dimension of the lesion from the data set of patients with mammary microcalcification. The average results obtained in the 50 simulations with the application of the models are represented in Tables 4 and 5.

The RN-MLP model, in its best simulation, obtained an accuracy of over 94%, with a false negative value of 2%. Indicating an accuracy of 98% in terms of sensitivity in the test set. Regarding the error in false-negative detection, the model obtained an average value of less than 10% in the set of 50 simulations performed.

According to the analysis of the results presented in Table 5, it is possible to verify the promising performance of the SVM-nonlinear structured model. In its best simulation, an accuracy above 98% and a false negative error rate of less than 2% (1.96%) were obtained. Regarding the leave-one-out (CVE) cross-validation error, we can verify that it obtained an amplitude between the maximum and minimum value obtained of 4% in the 50 simulations performed. The average results obtained by the RN-MLP and SVM-nonlinear models, in the categorization of malignancy in the set of simulations performed, is represented in Table 6.

To select the best and worst simulation, the value of the false-negative error obtained by the models was used, since this hyperparameter is of paramount importance in categorising malignancy. Applying the test of comparison of means with p -value ≈ 0.05 , it is possible to verify the existence of a statistically significant difference between the results, referring to the accuracy between the models used in the study. Indicating that for the ACC hyperparameter the SVM-nonlinear model has better performance when compared to the RN-MLP model.

Although the SVM-nonlinear model presents a mean value of the false-negative error lower than that obtained by

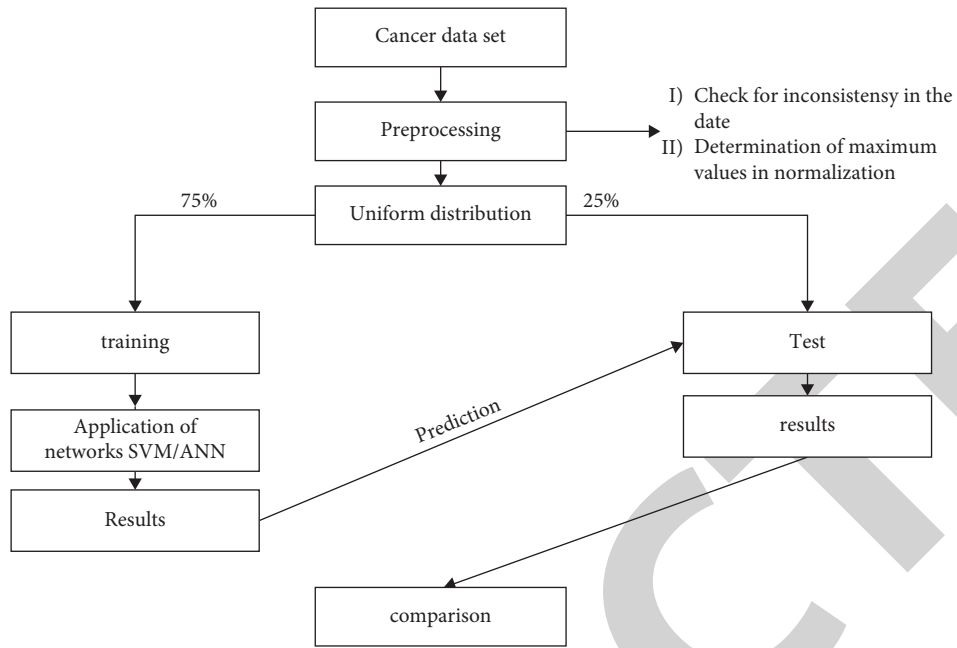


FIGURE 3: Flowchart of the proposed model.

TABLE 2: Parameters used in the RN-MLP model.

Parameters	Value
Number of simulations	50
Maximum number of seasons	100000
Activation function	Logistics
Training algorithm	Backpropagation
Metric used in training error	SSE
No. of hidden layers	2
Number of neurons in the first hidden layer	7
Number of neurons in the second hidden layer	4
Initialization of weights	Randomly with values [0, 1]
Stop criterion	0.001

TABLE 3: Parameters used in the SVM-nonlinear model.

Parameters	Value
Classifier type	C-SVM
Kernel function	RBF
Kernel function variance (s)	0.5
C Regularization parameter	1
Stop criterion	0.001

TABLE 4: Average performance of the RN-MLP model in categorising malignancy in the set of 50 simulations.

	SSE training error	ACC (%)	EFN (%)
Average ± SD	0.558 ± 0.50	92.58 ± 2.03	9.38 ± 4.39
Average ± irq	0.507 ± 0.94	92.25 ± 3.52	9.49 ± 6.64
Maximum-minimum	1.849-0.022	94.37-89.44	22.22-2.00
Best simulation	0.022	94.37	2

the RN-MLP model, there was no statistically significant difference at the level of 95% (p -value ≈ 0.05) among the results obtained by the models. In the 50 (fifty) simulations carried out in the test set, the SVM-nonlinear model obtained a simulation with a value of 100% of sensitivity, that is, 0% in the determination of the false negative error rate. This fact was not verified in the RN-MLP model, where a maximum value of 98% was obtained.

It is important to emphasize that the accuracy obtained by the models, in the classification of breast

microcalcification, is close to the values obtained in the literature using techniques based on computational intelligence. Comparing the results obtained by [7], who used the L2-SVM model, in the WDBC classification (ACC $\approx 96.09\%$ and EFN $\approx 2.47\%$), it can be verified that the model SVM-nonlinear proposed in this study, presented values in terms of accuracy (ACC $\approx 98.59\%$) and the value of the false negative error rate (EFN $\approx 1.97\%$) higher.

TABLE 5: Average performance of the SVM-nonlinear model in the categorization of malignancy in the set of 50 simulations.

	Error			
	Training error	CVE (%)	ACC (%)	EFN (%)
Average \pm SD	3.42 \pm 0.53	5.36 \pm 0.70	95.8 \pm 2.03	9.01 \pm 4.46
Average \pm irq	3.42 \pm 0.70	5.43 \pm 0.94	95.8 \pm 2.64	8.34 \pm 5.2
Maximum-minimum	4.46-2.22	7.249-3.259	98.59-90.84	21.16-0.01
Best simulation	3.52	5.61	98.59	1.97

TABLE 6: Average performance of the models proposed in the study, in the set of 50 simulations.

	SVM-non-linear		RN-MLP	
	ACC (%)	EFN (%)	ACC (%)	EFN (%)
Average \pm SD	95.01 \pm 1.66	9.01 \pm 4.62	92.59 \pm 2.07	9.39 \pm 4.39
Bad simulation	91.56	21.09	90.86	22.23
Best simulation	98.59	1.97	94.36	2.01

5. Conclusion

The high rate of incidence and deaths caused by breast cancer, currently in Iraq and the world, justify the development of scientific research aimed at strategies to aid in the early detection of the disease, a determining factor for the success of the treatment. In this work, we proposed using computational models structured in RN-MLP and nonlinear SVM to categorize malignancy in mammographic findings. The incorporation of information regarding the morphological characteristics of the contour of the breast lesion, contributed to the performance of the proposed models regarding the determination of the false-negative rate. Therefore, this metric is of paramount importance for health professionals, especially in detecting breast lump malignancy. Despite the results obtained, with the application of the neural network models of multilayer perceptrons and nonlinear support vector machine, the classification of mammary microcalcifications has presented promising results. It is perceived the need to deepen the study. To this end, we intend to develop a hybrid model structured in the future using genetic algorithms and a convolutional neural network to evaluate the performance in the classification of breast lesions and the optimization of the model's hyperparameters.

Data Availability

The data used to support the findings of this study are included within the article.

Conflicts of Interest

The authors declare that they have no conflicts of interest.

Acknowledgments

The authors extended their appreciation to the Deanship of Scientific Research at King Khalid University for funding this work through the General Research Project under Grant no. GRP.1/241/43. Received by Mohammed Alghamdi. <https://www.kku.edu.sa>.

References

- [1] R. A. Majid, H. A. Hassan, D. N. Muhealdeem, H. Mohammed, and M. D. Hughson, "Breast cancer in Iraq is associated with a unimodally distributed predominance of luminal type B over luminal type A surrogates from young to old age," *BMC Women's Health*, vol. 17, no. 1, p. 27, 2017.
- [2] A. O. J. Al-Isawi and J. Arkan, "Breast cancer in western Iraq: clinicopathological single institution study," *Advances in Breast Cancer Research*, vol. 5, no. 2, pp. 83–89, 2016.
- [3] R. M. Rangayyan, F. J. Ayres, and J. Leo Desautels, "A review of computer-aided diagnosis of breast cancer: toward the detection of subtle signs," *Journal of the Franklin Institute*, vol. 344, no. 3-4, pp. 312–348, 2007.
- [4] M. B. Alazzam, A. T. Al-Radaideh, N. Binsaif, A. S. AlGhamdi, and M. A. Rahman, "Advanced deep learning human herpes virus 6 (HHV-6) molecular detection in understanding human infertility," *Computational Intelligence and Neuroscience*, vol. 2022, Article ID 1422963, pp. 1-5, 2022.
- [5] M. H. U. Sharif, "Breast cancer detection using artificial neural networks," *International Journal for Research in Applied Science and Engineering Technology*, vol. 9, no. 10, pp. 1121–1126, 2021.
- [6] Y. I. Rejani and S. Thamarai, "Early detection of breast cancer using SVM classifier technique," *International Journal on Computer Science and Engineering*, vol. 1, no. 3, 2009.
- [7] M. Bader Alazzam, H. Mansour, M. M. Hammam et al., "Machine learning of medical applications involving complicated proteins and genetic measurements," *Computational Intelligence and Neuroscience*, vol. 2021, Article ID 1094054, pp. 1-6, 2021.
- [8] T. Ayer, O. Alagoz, J. Chhatwal et al., "Breast cancer risk estimation with artificial neural networks revisited," *Cancer*, vol. 116, no. 14, pp. 3310–3321, 2010.
- [9] J. Geng, S. Li, Y. Zhang, Z. Liu, and Z. Cheng, "LIFH: learning interactive features from HTTP payload using image reconstruction," in *Proceedings of the ICC 2021 IEEE International Conference on Communications*, pp. 1–6, Montreal, QC, Canada, June 2021.
- [10] M. B. Alazzam, A. T. Al-Radaideh, R. A. Alhamarnah, F. Alassery, F. Hajje, and A. Halasa, "A survey research on the willingness of gynecologists to employ mobile health applications," *Computational Intelligence and Neuroscience*, vol. 2021, Article ID 1220374, pp. 1-7, 2021.

Review Article

Recurrence Rate and Exploration of Clinical Factors after Pituitary Adenoma Surgery: A Systematic Review and Meta-Analysis based on Computer Artificial Intelligence System

Xianghe Zhang, Fan Yang, and Nianchen Han 

Department of Neurosurgery, The First Hospital of China Medical University, Shenyang, Liaoning 110001, China

Correspondence should be addressed to Nianchen Han; niabchen4906@163.com

Received 8 September 2022; Accepted 24 September 2022; Published 14 October 2022

Academic Editor: Ashish Khanna

Copyright © 2022 Xianghe Zhang et al. This is an open access article distributed under the Creative Commons Attribution License, which permits unrestricted use, distribution, and reproduction in any medium, provided the original work is properly cited.

Background. The first-line treatment for patients with any type of pituitary adenoma is trans-sphenoidal surgery. Considering the prevalence of the condition globally, the treatment is quite common. The recurrence of pituitary adenoma is a recognized occurrence in the medical field; however, there is limited comprehensive research and analysis of the predictive factors of recurrence rates and the clinical factors impacting relapse rates. Identifying the recurrence rates of pituitary adenomas and the clinical factors associated with them could help increase the remission rate by increasing focus on the specific aspects for early diagnosis and improved treatment. **Objective.** The objective of the current systematic review and meta-analysis is to assess the recurrent rates based on previous studies and to explore the clinical factors after pituitary surgery. **Methods.** A search was performed on PubMed, APA PsycINFO, Scopus, CENTRAL, and Google Scholar databases for English articles published from 1st January 2010 to 1st August 2022. Systematic reviews, meta-analysis, evidence syntheses, editorials, commentaries, preclinical studies, abstracts, theses, and preprints were excluded. Meta XL statistical software was used to conduct a prevalence meta-analysis. **Results.** PubMed, PsycINFO, and Medline databases were searched. All of the articles were written between 2012 and 2022. In the beginning, 612 items were recognized. After removing duplicates and analyzing the remaining articles in terms of inclusion and exclusion criteria, 31 articles remained. **Conclusion.** There is a relationship between recurrence rates and the follow-up period. There were conflicting results about the clinical factors after pituitary adenoma surgery, specifically age and tumor size. Some included studies that there was an association between macroadenomas and high recurrence rates. No study reported that gender was a clinical factor affecting pituitary adenoma surgery outcomes or the recurrence rate. Studies also reported that there was a correlation between the remnant tumor factor and the recurrence rates; adenoma remnants after surgery increased the risk of recurrence rates for patients.

1. Introduction

Trans-sphenoidal surgery is one of the available treatments for patients with pituitary adenoma [1]. There are many types of pituitary adenomas including prolactinoma, acromegaly, and Cushing's disease [2]. Pituitary surgery is common for patients with acromegaly and prolactinoma; the treatment is known for quick relief of adenoma signs and symptoms. Unfortunately, despite the fact that the surgery is among the best treatment options, it does not guarantee high remission [3]. Recurrence of the tumor can occur in some cases. Some predictive factors are known in association with

recurrence of pituitary adenomas, but very few clinical factors are explored after the surgery [4].

A common type of pituitary adenoma is silent corticotroph adenoma which is characterized by positive immunostaining for adrenocorticotrophic hormone; it stems from a rise in adenohypophyseal cells of Tpit lineage [5]. It accounts for approximately 3%–19% of nonfunctioning adenoma, which shows that it is quite prevalent. There are two categories of pituitary adenomas including macroadenoma (greater than 1 centimeter) and microadenoma (smaller than 1 centimeter). Cushing's disease, a pituitary adenoma [6], is mostly attributed to microadenoma and

stems from prior exposure to dangerously high cortisol levels for a prolonged period. The benign tumor of the pituitary gland in those with Cushing’s disease produces a very high amount of adrenocorticotrophic hormone that stimulates the adrenal glands to release more cortisol [7]. Endogenous Cushing’s syndrome is rare. “Endogenous” means something inside your body is causing disorder rather than something outside your body, such as medicine. However, estimates vary, ranging from 40 to 70 people out of every million. There is a strong association with the development of pituitary adenomas [8].

Patients with pituitary adenomas who do not show hypersecretory symptoms, such as hyperprolactinemia, acromegaly, or Cushing’s syndrome, have nonfunctioning adenomas. Cushing’s disease is a rare kind of pituitary adenoma characterized by excessive adrenocorticotrophic hormone release, which causes hypertension, weight gain, morbidity, extreme tiredness, diabetes, and osteoporosis. The recurrence rate of pituitary surgery varies greatly based on a variety of variables. The present systematic review and meta-analysis aims to quantify recurrence rates based on prior research and to investigate clinical variables after pituitary surgery [9, 10].

1.1. Objectives and Research Questions. Despite the fact that trans-sphenoidal surgery is the first-line treatment for patients with pituitary adenoma, there is limited research on the recurrence rates of treatments, the clinical factors affecting them, and significant aspects after surgery. Therefore, the objective of the current systematic review is as follows:

- (i) Assess the recurrent rates of pituitary surgery
- (ii) Explore the clinical factors after pituitary surgery

Some characteristics of patients included in the study are shown in Tables 1 and 2.

1.2. Research Question. The research question for the current analysis was structured according to the PICO model.

Population: people with pituitary adenoma

Intervention: treatment using pituitary adenoma surgery

Comparison: no comparison

Outcome: recurrence rate

Question: what are the recurrent rates and the clinical factors after pituitary surgery?

2. Search Methods

2.1. Search Criteria and Information Sources. The current systematic review was reported by following the Preferred Reporting Items for Systematic Review and Meta-Analysis (PRISMA) guidelines. Numerous online databases were searched based on computer artificial intelligence system, including PubMed, MEDLINE, and APA PsycINFO. A search string was developed and applied in the databases; the results from each database are shown.

2.2. Inclusion Criteria. All articles had to have been published within the past twenty years and authored in English.

TABLE 1: Patient characteristics.

Characteristics	Patients overall registered
Female, n (%)	1378
Age (y), mean \pm SD	51.3 \pm 16.1
Age group (y), n (%)	
18–24	251
25–34	202
35–44	308
45–54	498
Diagnosed with,* n (%)	
Neck and back pain	995
Diabetes	736
Asthma/chronic obstructive	418
Pulmonary disease	
Mental health problems	383
Hearing or vision loss	370
Cancer	153
Lung disease	86
Stroke	80
Epilepsy	53

TABLE 2: Generalised features of patients.

Characteristics	
	<i>Gender</i>
Male/female	44/5
Median age at treatment (years)	59 (43–75)
	<i>Performance status (PS)</i>
Small-cell carcinoma/others	51/0
	<i>Stage</i>
Number of first-line chemotherapy courses	
1/2/3/4/5/6	1/4/3/38/2/1
Median (range)	5(0–3)
	<i>Number of regimens after progression</i>
After first-line chemotherapy	
0/1/2/3/4/5	5/18/13/8/3/2
Median (range)	3 (2–6)
Median sum of target lesion diameters (mm) (range)	99(61–305)

The study designs included randomized controlled trials, case series, prospective analysis, retrospective analysis, controlled trials, comparative studies, and experimental studies. No grey literature was included in the analysis. Only peer-reviewed articles were included. All articles had to have been published through proper channels. The participants in the included studies had to be 18 years or older. The articles had to be relevant to the research topic focusing on the recurrence rate and clinical factors affecting exploration of clinical factors after pituitary adenoma surgery. Different categories of pituitary adenoma were included for the analysis such as silent corticotroph adenoma, Cushing’s disease/syndrome, acromegaly, hypercortisolism, prolactinoma, and nonfunctioning pituitary adenoma. All the studies included had to focus exclusively on pituitary adenoma surgery; any other treatments such as radiotherapy were not allowed. The follow-up period had to be more than 12 months. The included studies also had to focus on primary pituitary adenoma surgery.

2.3. Exclusion Criteria. All articles published before 2010 (the past twelve years) were excluded from the systematic review and meta-analysis. As mentioned, no grey literature or articles published through unknown/unconventional channels were included in the current systematic review. All articles that were not peer-reviewed were also excluded. Any studies that were irrelevant to the research topic were not included. Studies focusing on secondary pituitary adenoma surgery or a combination of both primary and secondary surgeries were excluded since the objective of the systematic review and meta-analysis was to assess recurrence rates and clinical factors after the treatment. Systematic reviews, meta-analysis, evidence syntheses, editorials, commentaries, and preclinical studies that were authored before 2010 were also excluded. Studies that included radiotherapy intricately were excluded considering the fact that although the treatment may help in tumor control, it does not impact recurrence rates [11, 12]. The articles included also had to be available online; the source was excluded when only the abstract was available. Studies with participants less than 18 years such as cases of pediatric Cushing’s disease were not included.

2.4. Data Extraction. The data and findings from the included studies that passed the eligibility criteria are shown in Table 2. The extracted data included author, year of publication, study design, pituitary adenoma, follow-up period, and recurrence rates and clinical factors. The follow-up period was the mean/average since some studies failed to

report on the exact follow-up period related to the remission rate.

3. Results

3.1. Search Results. The Preferred Reporting Items for Systematic Reviews and Meta-Analysis (PRISMA) checklist 2020 guidelines were applied. The initial search in the online databases using the earlier mentioned keywords identified 612 studies. After the removal of duplicates, only 436 studies were left. The abstracts and titles of 274 studies were scanned to determine their significance for the systematic review. After elimination, 132 articles remained; they were scrutinized based on the eligibility criteria. Finally, 31 articles were identified that effectively passed the predefined eligibility criteria. Figure 1 shows the process of study selection presented in a flowchart (Figure 1 and Tables 1–3).

3.2. Follow-Up Periods and Recurrence Rates. Figure 2 shows findings from two studies by Jung et al. [2012] and Reddy et al. [13] that showed follow-up periods and their recurrence rates. As shown in Table 4, nonfunctioning pituitary adenomas have the highest recurrent rates.

3.3. Statistical Analysis. Figure 3 shows a meta-analysis of the studies that focused exclusively on silent corticotroph adenoma. IR (95% CI) figures are highlighted in the analysis.

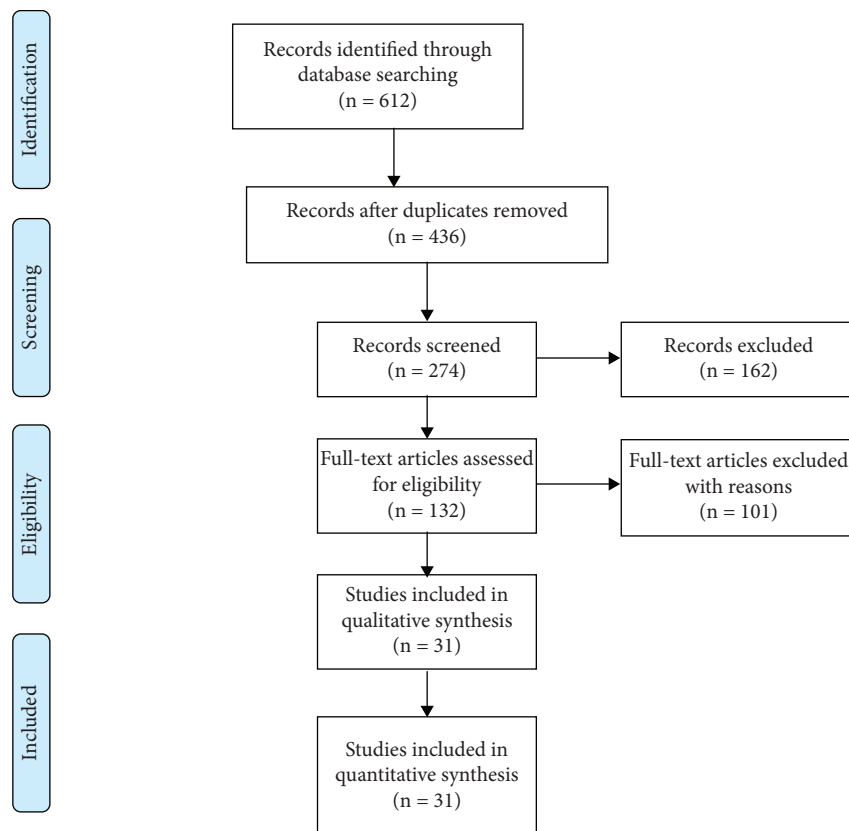


FIGURE 1: PRISMA flowchart diagram.

TABLE 3: Data extraction results.

Author and year	Study design	Recurrence rate (95% CI)	Adenoma type	Population	Follow-up	Clinical factors
Langlois et al. (2018)	Retrospective single-center study	36% for silent corticotroph adenomas, 10% for silent gonadotroph adenomas, $P = 0.001$	Silent corticotroph adenomas versus silent gonadotroph adenomas	814 pituitary surgeries	>5 years	
Watts et al. (2017)	Retrospective analysis	12.5% (6/48; $P = 0.003$)	Nonfunctioning pituitary macroadenomas	143 patients	12 months	
Jahangiri et al. (2013)	Retrospective analysis	34% for strongly ACTH-positive type I SCAs, 10% for weakly ACTH-positive type II SCAs	Silent corticotroph adenomas	75 patients	>3 years	
Alahmadi et al. (2012)	Retrospective analysis	14% for silent corticotroph adenomas, 10% for nonfunctioning pituitary macroadenomas	Silent corticotroph adenomas nonfunctioning pituitary macroadenomas	20 patients	41 months	
Ioachimescu et al. (2012)	Retrospective cohort study	6.0%	Silent corticotroph adenomas	33	42.5 months	
Reddy et al. (2011)	Comparative study	23.1% (5 years), 46.7% (10 years) 67.9% (15 years)	Nonfunctioning pituitary adenomas (NFAs)	155 patients	6.5 years	Pituitary tumor remnant after the first postoperative scan ($P \leq 0.001$) younger age at initial surgery ($P = 0.034$)
Cho et al. (2010)	Comparative study	25.0% for silent corticotroph adenomas and 26.9% for nonsilent corticotroph adenomas ($P = 0.839$)	Silent corticotroph adenomas	28 patients	5.2 years	Young patients had a higher frequency of multiple and late recurrences with more aggressive tumor behavior
Cooper et al. (2010)	Cohort analysis	54% for SCAs 17% for nonfunctioning adenomas ($P < 0.025$)	Silent corticotroph adenomas and nonfunctioning adenomas	25 SCA 84 nonfunctioning adenomas	1-15 years	
Brochier et al. (2010)	Retrospective study	24% for those who initially had complete macroscopic resection, 47% for initial surgical remnant	Nonfunctioning adenomas	142 patients	6.9 years	Initial complete macroscopic resection, initial surgical treatment
Raverot et al. (2010)	Cohort study	20%	Pituitary tumor	94 patients	138 ± 46 months	
Lindsay et al. (2011)	Retrospective analysis	12%	Cushing's disease	331 patients	10.5 ± 0.3 years	
Chang et al. (2010)	Retrospective analysis	8%	Inactive pituitary macroadenomas (EIA)	81 patients	5 years	
Brady et al. (2021)	Retrospective analysis	3%	Cushing's disease	39 patients	24 months	

TABLE 3: Continued.

Author and year	Study design	Recurrence rate (95% CI)	Adenoma type	Population	Follow-up	Clinical factors
Jang et al. (2016)	Retrospective analysis	19%	Pituitary adenoma	331 patients	68.5 months	
Ćirić et al. (2012)	Retrospective study	9.67%	Cushing's disease	136 patients	>12 months	Recurrence rates increased with the passage of time, mean immediate postoperative plasma cortisol (IPPC) of >2.0 µg/dL
Jung et al. (2012)	Retrospective study	32.4% (5 years) 54.6% (10 years)	Cushing's disease	54 patients	50.7 months	Recurrence rate increases with time and possibly increases the preoperative serum cortisol level and pathologic confirmation of adenoma
Barbot et al. (2013)	Retrospective analysis	42.11% (40 months)	Cushing's disease	57 patients	40 months	
Alwani et al. (2010)	Retrospective analysis	20%	Cushing's disease	79 patients	84 months	
Ammuni et al. (2011)	Prospective study	18.5%	Cushing's disease	97 patients	2.9 ± 2.1 years	
Ambrogio et al. (2017)	Prospective study	23%	Cushing's disease	56 patients		Most patients who had successful adenectomy did not respond to desmopressin after surgery
Espinosa-de-Los-Monteros et al. (2017)	Retrospective cohort study	26%	Cushing's disease	84 patients	6.3 years	
Mayberg et al. (2018)	Single-center retrospective cohort analysis	9.5%	Cushing's disease	69 patients	43.5 months	Immediate reoperation is associated with low recurrence rates
Shirvani et al. (2016)	Retrospective analysis	21.9%	Cushing's disease	96 patients	44 months	Age, preoperative basal cortisol levels, and follow-up duration influenced recurrence (there was a significant negative correlation between the patient's age and the follow-up period)
Johnston et al. (2017)	Prospective analysis	7%	Cushing's disease	101 patients	4.33 years	Presence of macroadenoma and tumor extension beyond the pituitary and sella were predictive of risk of late recurrence
Almeida et al. (2020)	Retrospective study	34% for GTR 39.5% for subtotal resection	Pituitary adenoma	98 patients	Median 144 months	
Dimopoulou et al. (2014)	Retrospective analysis	34% (54 months)	Cushing's disease	85 patients	79 months	Higher recurrence rates of CD after first TSS
Bou et al. (2011)	Retrospective analysis	20.8%	Cushing's disease	101 patients	44.7 months	A positive response to vasopressin analogs and/or CRH tests occurs early in recurrence

TABLE 3: Continued.

Author and year	Study design	Recurrence rate (95% CI)	Adenoma type	Population	Follow-up	Clinical factors
Feng et al. (2018)	Single-center retrospective analysis	2.42%	Cushing's disease	197 patients	12 to 36 months	
Maletkovic et al. (2019)	Retrospective analysis	9.4%	Nonfunctioning pituitary Tumors	85 patients		
Bansal et al. (2017)	Retrospective analysis	32%	Cushing's disease	151 patients	74 ± 61.1 months	
Chandler et al. (2016)	Retrospective analysis	17% (4 years)	Cushing's disease	219 patients	4 years	

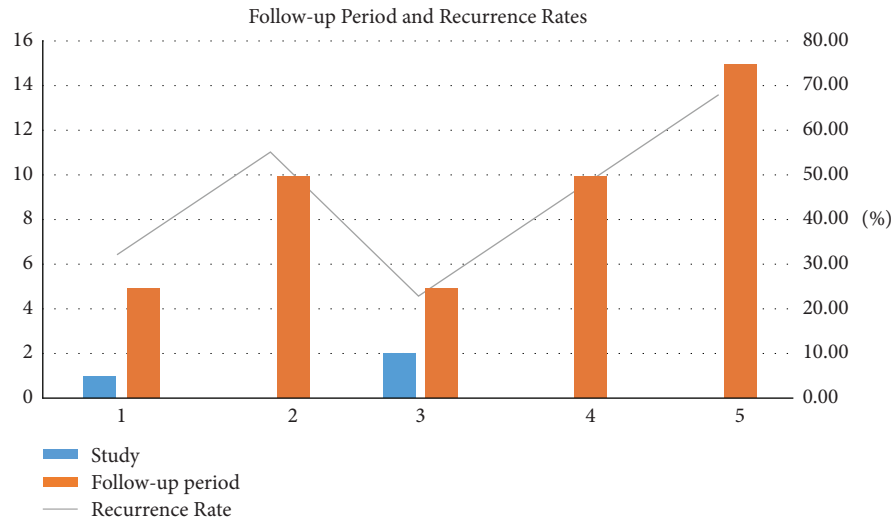


FIGURE 2: Correlation between follow-up periods and recurrence rates.

TABLE 4: Highest recurrence rates.

Author	Recurrence rate >30%	Pituitary adenoma
Langlois et al. (2018)	36%	Silent corticotroph adenoma
Jahangiri et al. (2013)	34%	Silent corticotroph adenoma
Reddy et al. (2011)	67.9% (highest after 15 years)	Nonfunctioning pituitary adenoma
Cooper et al. (2010)	54%	Silent corticotroph adenoma
Jung et al. (2012)	54.6%	Cushing's disease
Barbot et al. (2013)	42.11%	Cushing's disease
Bansal et al. (2017)	32%	Cushing's disease
Dimopoulou et al. (2014)	34%	Cushing's disease

3.4. *Cushing's Disease.* The mean recurrence rate for Cushing's disease was 18.888% for the included studies. The total number of participants was 2021. The average recurrence rate (95% CI) was found to be 18.88 (11.11–28.38), as shown in Figure 4.

3.5. *Recurrence Rate.* As shown in the figure, the recurrence rate for Cushing's disease has fluctuated through the years but continues to decrease through the past few years; there is no distinct way to forecast future recurrence, as shown in Figure 5.

4. Discussion

The objective of the current systematic review was to analyze the recurrence rate and explore clinical factors after pituitary adenoma surgery. The highest recurrence rates were recorded in patients with nonfunctioning adenoma as shown in Table 3 in comparison to Cushing's disease and silent corticotroph adenomas. As proposed by Shirvani et al. [2016] and Jung et al. [2012], there is a direct correlation between the follow-up period and recurrence rates; a comparison shown in Figure 2 highlights the relationship.

Some studies reported that age, gender, and tumor size impacted the recurrence rate, while some studies suggested the opposite. According to Shirvani et al. [2016], age influenced the recurrence rate; additionally, there was a

significant negative correlation between the follow-up period and patient's age in the same study. Additionally, in the study conducted by Cho et al. [14], younger patients had a higher frequency of numerous and late recurrences with more aggressive tumor behavior [15]. In a similar study conducted by Reddy et al., there was an increase in the recurrence rates for younger patients at initial surgery ($P = 0.034$) [16, 17]. Conversely, some previous studies found that the age factor did not affect the recurrence rate such as the study by Losa et al. [18]. The same findings reported by Watts et al. [19] showed that younger age was the predictor of recurrence/relapse in patients with non-functional pituitary adenomas; the recurrence rate was diminished every year by approximately 3% each increase in the age of the patient after surgery. However, in reference to previous studies, the question of age as a prognostic factor remains quite controversial and conflicted. None of the included studies in the systematic review and meta-analysis showed that gender influenced the recurrence rates [20, 21].

Johnston et al. [2017] found that macroadenoma (a benign tumor with glandular tissue more than 10 mm) presence and tumor extension beyond the pituitary and sella were predictive of risk of late recurrence [22, 23]; this shows that size of the tumor may be a clinical factor that impacts the recurrence rate. The same findings had been echoed by Amar et al. [4] who found that the probability of long-term

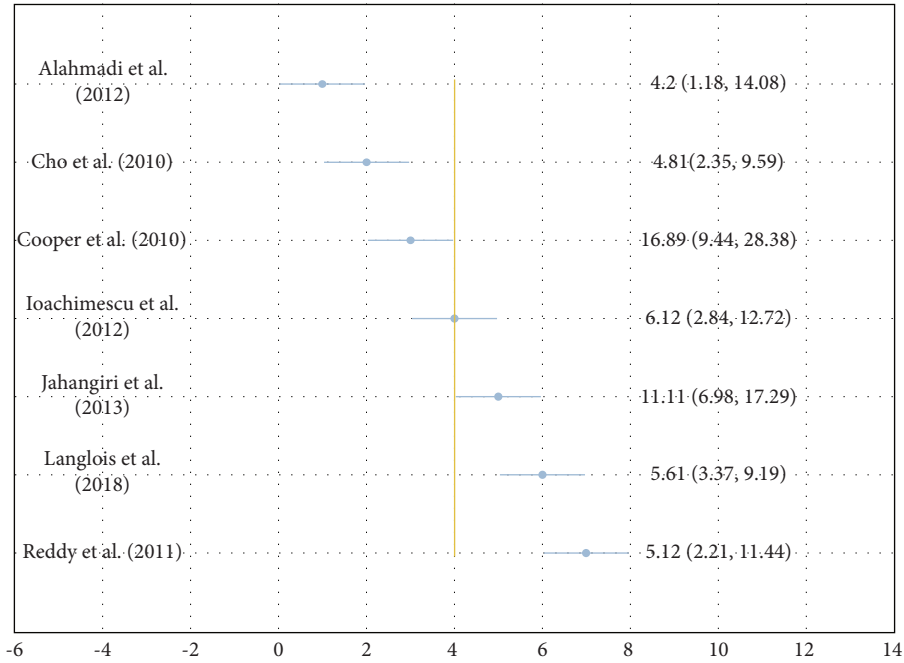


FIGURE 3: IR for silent corticotroph adenoma.

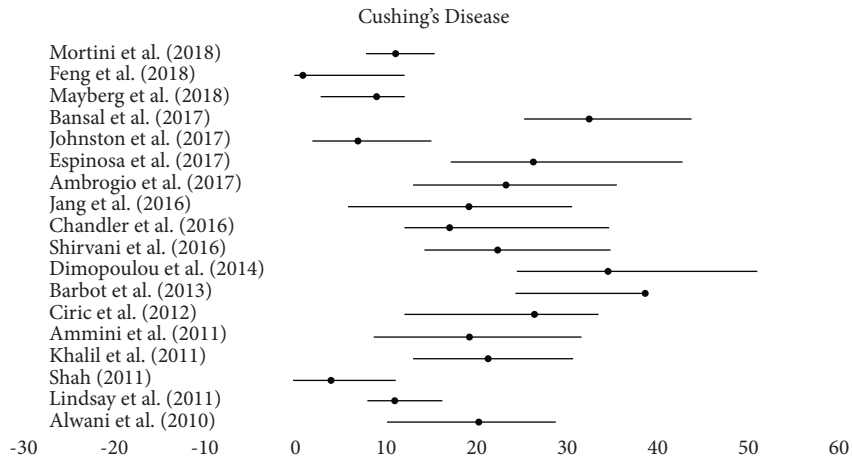


FIGURE 4: The mean recurrence rate for Cushing's disease.

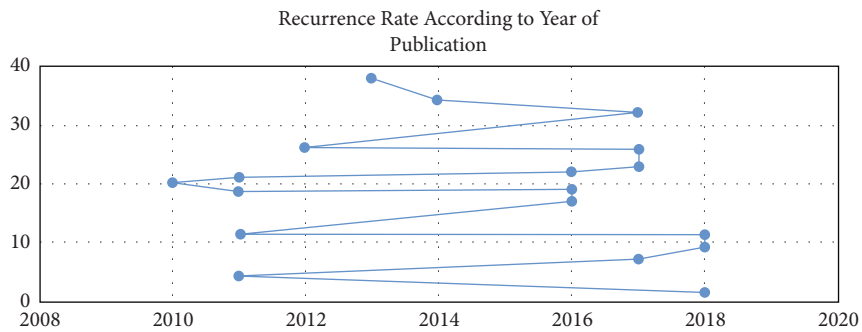


FIGURE 5: Recurrence rates through the years for Cushing's disease.

chemical cure was much higher (91) for patients with microadenomas than those with macroadenomas (33%).

Pituitary tumor remnant after the primary pituitary adenoma surgery is an additional clinical factor that could impact the recurrence and remission rates [18, 24]. According to the study by Reddy et al. [13], pituitary tumor remnant after the first postoperative scan ($P \leq 0.001$) increases the risk of relapse or recurrence of pituitary adenoma. Brochier et al. [10] recorded a very high recurrence rate of 47% after initial surgical remnant. No studies reported any relationships between remnant tumors and recurrence or remission rates.

The number of trans-sphenoidal surgeries/pituitary adenoma surgeries may be a clinical factor that may impact the treatment outcome. According to a study conducted by Dimopoulou et al. [16], higher recurrence rates of Cushing's disease were recorded after first trans-sphenoidal surgery; this means that revision pituitary surgeries could report higher remission rates and lower recurrence rates [10, 16]. Additionally, immediate reoperation of patients with pituitary adenoma was associated with low recurrence rates (Mayberg et al., 2018). There were some predicting factors of recurrence of pituitary adenomas highlighted by different studies. Bou et al. [9] found that a predictive factor of early recurrence was a positive response to CRH tests and/or vasopressin analogs.

According to Ambrogio et al. [5], a significant percentage of patients that had successful adenectomy failed to respond to desmopressin after pituitary adenoma surgery. Therefore, the test could be used as a predictive factor of the recurrence of the condition if the treatment was unsuccessful. Ciric et al. [2012] also found that the mean immediate plasma cortisol (IPPC) after pituitary adenoma surgery should not exceed $2.0 \mu\text{g/dL}$; a higher level shows that the operation was not fully successful and adenoma may recur after an unknown period. Such predictive factors are very significant in defining the follow-up period and possibly the behavior of adenoma after recurrence. At the same time, the control of surgical infection is also crucial. Therefore, the effects of commonly used anti-infective drugs, such as amoxicillin and ornidazole, should also be concerned [25–27].

5. Conclusion

All the studies included in the current systematic review and meta-analysis reported different recurrence rates depending on pituitary adenoma [13, 19]. As shown in the analysis, there is a relationship between the recurrence rates and the follow-up period. Therefore, the highest value recorded by the analysis (67.9%) for nonfunctioning adenoma may be due to a follow-up period of 15 years. Other than the relationship between the two aspects, there was no distinct factor in relation to the distinct factor. There were conflicting results about the clinical factors after pituitary adenoma surgery. Some studies suggested that age and tumor size impacted the recurrence rate, while others found no evidence of existence of such a relationship; some studies reported the correlation of macroadenomas with high

recurrence rates. No study reported that gender was a clinical factor affecting pituitary adenoma surgery outcomes or the recurrence rate. The most significant factor reported by studies with no conflicting results was the remnant tumor factor. According to the findings, initial surgical remnant adenomas increased the probability of low remission rates and high recurrence rates for patients. Additionally, some studies reported that the recurrence rates were lower for patients undergoing revision pituitary adenoma surgery than patients going through it for the first time.

5.1. Limitations. A significant limitation of the studies that passed the eligibility criteria for pituitary surgery was their noncomparative nature, restricting the analysis of within-study confounders. Additionally, there was a very high heterogeneity degree among the reported recurrence rates. Previous reports have attributed this heterogeneity to variations in the length of follow-up and criteria used to define remission and recurrence. Unfortunately, there were very few studies that highlighted numerous recurrence rates of different pituitary adenomas during the same follow-up period; this means that it was difficult to carry out a statistical analysis to analytically define the relationship between the follow-up period and the recurrence rates. The eligibility criteria were a significant limitation considering that few studies met the inclusion criteria. Some studies that failed to meet the inclusion criteria contained important data that could have helped to solve the existing conflicting results in relation to some clinical aspects such as the impact of age and tumor size. For instance, there have been few studies relevant to the research topic that have been published within the last twelve years (2010–2022). The findings from the current systematic review will form a foundation for future research into the treatment of pituitary adenomas. Future research should focus on highlighting clinical factors after pituitary adenoma surgery, especially conflicting aspects such as gender, age, and tumor size; additionally, they should consider highlighting more predictive factors of recurrence.

Data Availability

The data used in this study are available from the corresponding author upon request.

Conflicts of Interest

The authors declare no conflicts of interest.

Authors' Contributions

The authors, working with other experts, contributed significantly to the design and analysis of the systematic review. Additionally, they participated meaningfully in the process of study selection, screening, and scrutiny, extraction of data and information, quality assessment of randomized controlled trials, and data synthesis. The authors took part in the entire process of reviewing and approving the final manuscript.

References

- [1] H. Alahmadi, D. Lee, J. R. Wilson et al., "Clinical features of silent corticotroph adenomas," *Acta Neurochirurgica*, vol. 154, no. 8, pp. 1493–1498, 2012.
- [2] C. Alameda, T. Lucas, E. Pineda et al., "Experience in management of 51 non-functioning pituitary adenomas: indications for post-operative radiotherapy," *Journal of Endocrinological Investigation*, vol. 28, no. 3, pp. 18–22, 2005.
- [3] J. P. Almeida, R. Tabasinejad, A. Kalyvas et al., "The importance of long term follow up after endoscopic pituitary surgery: durability of results and tumor recurrence," *Neurology India*, vol. 68, pp. 92–S100, 2020.
- [4] A. P. Amar, W. T. Couldwell, J. C. T. Chen, and M. H. Weiss, "Predictive value of serum prolactin levels measured immediately after transsphenoidal surgery," *Journal of Neurosurgery*, vol. 97, no. 2, pp. 307–314, 2002.
- [5] A. G. Ambrogio, M. Andrioli, M. De Martin, F. Cavagnini, and F. Pecori Giraldi, "Usefulness of desmopressin testing to predict relapse during long-term follow-up in patients in remission from Cushing's disease," *Endocrine Connections*, vol. 6, no. 8, pp. 791–799, 2017.
- [6] A. C. Ammini, S. Bhattacharya, J. Praksh Sahoo et al., "Cushing's disease: results of treatment and factors affecting outcome," *Hormones*, vol. 10, no. 3, pp. 222–229, 2011.
- [7] L. M. Auer and G. Clarici, "The first 100 transsphenoidally operated pituitary adenomas in a non-specialised centre: surgical results and tumour-recurrence," *Neurological Research*, vol. 7, no. 3, pp. 153–160, 1985.
- [8] M. Barbot, N. Albiger, S. Koutroumpi et al., "Predicting late recurrence in surgically treated patients with Cushing's disease," *Clinical endocrinology*, vol. 79, no. 3, pp. 394–401, 2013.
- [9] R. Bou Khalil, C. Baudry, L. Guignat et al., "Sequential hormonal changes in 21 patients with recurrent Cushing's disease after successful pituitary surgery," *European Journal of Endocrinology*, vol. 165, no. 5, pp. 729–737, 2011.
- [10] S. Brochier, F. Galland, M. Kujas et al., "Factors predicting relapse of nonfunctioning pituitary macroadenomas after neurosurgery: a study of 142 patients," *European Journal of Endocrinology*, vol. 163, no. 2, pp. 193–200, 2010.
- [11] E. F. Chang, G. Zada, S. Kim et al., "Long-term recurrence and mortality after surgery and adjuvant radiotherapy for non-functional pituitary adenomas," *Journal of Neurosurgery*, vol. 108, no. 4, pp. 736–745, 2008.
- [12] L. Chen, W. L. White, R. F. Spetzler, and B. Xu, "A prospective study of nonfunctioning pituitary adenomas: presentation, management, and clinical outcome," *Journal of Neuro-Oncology*, vol. 102, no. 1, pp. 129–138, 2011.
- [13] R. Reddy, S. Cudlip, J. V. Byrne, N. Karavitaki, and J. A. H. Wass, "Can we ever stop imaging in surgically treated and radiotherapy-naive patients with non-functioning pituitary adenoma?" *European Journal of Endocrinology*, vol. 165, no. 5, pp. 739–744, 2011.
- [14] H. Y. Cho, S. W. Cho, S. W. Kim, C. S. Shin, K. S. Park, and S. Y. Kim, "Silent corticotroph adenomas have unique recurrence characteristics compared with other nonfunctioning pituitary adenomas," *Clinical Endocrinology*, vol. 72, no. 5, pp. 648–653, 2010.
- [15] O. Cooper, A. Ben-Shlomo, V. Bonert, S. Bannykh, J. Mirocha, and S. Melmed, "Silent corticotroph adenomas: clinical and cellular characteristics and long-term outcomes," *Hormones and Cancer*, vol. 1, no. 2, pp. 80–92, 2010.
- [16] C. Dimopoulou, J. Schopohl, W. Rachinger et al., "Long-term remission and recurrence rates after first and second transsphenoidal surgery for Cushing's disease: care reality in the Munich Metropolitan Region," *European Journal of Endocrinology*, vol. 170, no. 2, pp. 283–292, 2014.
- [17] A. L. Espinosa-de-Los-Monteros, E. Sosa-Eroza, E. Espinosa, V. Mendoza, R. Arreola, and M. Mercado, "Long-term outcome of the different treatment Alternatives for recurrent and Persistent Cushing disease," *Endocrine Practice*, vol. 23, no. 7, pp. 759–767, 2017.
- [18] M. Losa, P. Mortini, R. Barzaghi, L. Gioia, and M. Giovannelli, "Surgical treatment of prolactin-secreting pituitary adenomas: early results and long-term outcome," *The Journal of Clinical Endocrinology & Metabolism*, vol. 87, no. 7, pp. 3180–3186, 2002.
- [19] A. K. Watts, A. Easwaran, P. McNeill, Y. Y. Wang, W. J. Inder, and C. Caputo, "Younger age is a risk factor for regrowth and recurrence of nonfunctioning pituitary macroadenomas: results from a single Australian centre," *Clinical Endocrinology*, vol. 87, no. 3, pp. 264–271, 2017.
- [20] I. H. Hewedi, W. M. Osman, and M. M. El Mahdy, "Differential expression of cyclin D1 in human pituitary tumors: relation to MIB-1 and p27/Kip1 labeling indices," *Journal of the Egyptian National Cancer Institute*, vol. 23, no. 4, pp. 171–179, 2011.
- [21] C. Huan, Y. Qu, and Z. Ren, "Gender differences in presentation and outcome of patients with Cushing's disease in Han Chinese," *Bio-Medical Materials and Engineering*, vol. 24, no. 6, pp. 3439–3446, 2014.
- [22] J. H. Jang, K. H. Kim, Y. M. Lee, J. S. Kim, and Y. Z. Kim, "Surgical results of pure endoscopic Endonasal transsphenoidal surgery for 331 pituitary adenomas: a 15-year experience from a single Institution," *World neurosurgery*, vol. 96, pp. 545–555, 2016.
- [23] F. Langlois, D. S. T. Lim, C. G. Yedinak et al., "Predictors of silent corticotroph adenoma recurrence; a large retrospective single center study and systematic literature review," *Pituitary*, vol. 21, no. 1, pp. 32–40, 2018.
- [24] J. Maletkovic, A. Dabbagh, D. Zhang et al., "Residual tumor confers a 10-fold increased risk of regrowth in clinically nonfunctioning pituitary tumors," *Journal of the Endocrine Society*, vol. 3, no. 10, pp. 1931–1941, 2019.
- [25] X. Cheng, Q. Chen, and P. Sun, "Natural phytochemicals that affect autophagy in the treatment of oral diseases and infections: a review," *Frontiers in Pharmacology*, vol. 13, Article ID 970596, 2022.
- [26] X. Cheng, F. He, M. Si, P. Sun, and Q. Chen, "Effects of antibiotic Use on Saliva Antibody content and oral Microbiota in Sprague Dawley rats," *Frontiers in Cellular and Infection Microbiology*, vol. 12, Article ID 721691, 2022.
- [27] X. Cheng, F. Huang, K. Zhang, X. Yuan, and C. Song, "Effects of none-steroidal anti-inflammatory and antibiotic drugs on the oral immune system and oral microbial composition in rats," *Biochemical and biophysical research communications*, vol. 507, no. 1-4, pp. 420–425, 2018.

Research Article

A Method for Extracting Building Information from Remote Sensing Images Based on Deep Learning

Lianying Li ¹, Xi Chen ², and Lianchao Li ³

¹School of Art and Design, Harbin University, Harbin, Heilongjiang 150086, China

²School of Landscape Architecture, Zhejiang Agriculture and Forestry University, Hangzhou, Zhejiang 310000, China

³Harbin Xinguang Optoelectronic Technology Co.LTD, Harbin, Heilongjiang 150028, China

Correspondence should be addressed to Lianying Li; lilianying@hrbu.edu.cn

Received 28 July 2022; Revised 1 September 2022; Accepted 24 September 2022; Published 12 October 2022

Academic Editor: Ashish Khanna

Copyright © 2022 Lianying Li et al. This is an open access article distributed under the Creative Commons Attribution License, which permits unrestricted use, distribution, and reproduction in any medium, provided the original work is properly cited.

Semantic segmentation of remote sensing images is an important issue in remote sensing tasks. Existing algorithms can extract information more accurately, but it is difficult to capture the contours of objects and further reveal the interaction information between different objects in the image. Therefore, a deep learning-based method for extracting building information from remote sensing images is proposed. First, the deep learning semantic segmentation model DeepLabv3+ and Mixconv2d are combined, and convolution kernels of different sizes are used for feature recognition. Then, the regularization method based on Rdrop Loss improves the accuracy and efficiency of contour capture for objects of different resolutions, and at the same time improves the consistency of dataset fitting. Finally, the proposed remote sensing image information extraction method is verified based on the self-built dataset. The experimental results show that the proposed algorithm can effectively improve the algorithm efficiency and result accuracy, and has good segmentation performance.

1. Introduction

Remote sensing images can quickly obtain a wide range of building information data and can be widely used in the monitoring of building surface conditions, as well as in urban and rural layout planning and other fields. However, due to the inevitable influence of spatial resolution, spectral resolution, radiometric resolution, and other factors in the process of remote sensing image acquisition, the data volume of remote sensing images is huge and the types are diverse, and it is necessary to extract the image features quickly and accurately [1–3]. Therefore, designing a high-precision and high-efficiency information extraction method for remote sensing images of buildings has become one of the core tasks of computer vision.

The current state-of-the-art DeepLabv3+ algorithm combines the encoder-decoder framework and hole space pyramid pooling, which reduces the amount of computation

and improves the accuracy of segmentation [4–6]. Reference [7] uses the DeepLabv3+ algorithm to conduct research in the field of fire detection and explores the performance balance method of Dice and Tversky loss functions in the DeepLabv3+ algorithm by training the entire data set containing RGB and infrared images. However, there are few data points in the fire RGB image, and this method cannot meet the requirements of remote sensing image fitting speed. Reference [8] used convolutional neural networks and semantic segmentation to provide the location and scale of fires for forest fire warning. The study shows that the complexity of the DeepLabv3+ algorithm in terms of shape, texture, color, and intensity is difficult to segment correctly. Reference [9] uses deep convolutional neural networks to automatically generate training datasets in heterogeneous and cluttered backgrounds. However, the algorithm has a slow fitting speed, inaccurate segmentation of edge objects, inconsistency within large-scale object segmentation and

defects such as holes. Based on the above-given problems, aiming at the DeepLabv3+ algorithm widely used in the field of remote sensing images, this paper proposes a deep learning algorithm that can improve the fitting rate and segmentation efficiency. Aiming at the low fitting speed of the original model, the Rdrop Loss regularization method is used to forward the samples twice. The symmetric Kullback-Leibler(KL) divergence loss of these two distributions is added to the original cross-entropy loss to achieve joint backpropagation and parameter update [10, 11]. By minimizing the divergence loss, the expressive ability and generalization ability of remote sensing image segmentation are enhanced [12]. Aiming at the problem of low segmentation accuracy in the original model, this paper takes advantage of multiscale convolution kernels and mixes multiple convolution kernels in one convolution operation. A large-sized convolution kernel is used to obtain high-resolution remote sensing image pattern information, and a small-sized convolution kernel is used to capture low-resolution pattern information to compensate for the boundary segmentation accuracy problem of DeepLabv3+ in remote sensing image tasks [13, 14].

Aiming at the problem of low segmentation accuracy and efficiency in segmentation tasks caused by the dense arrangement of targets in remote sensing images and the large size variation of similar targets, this paper proposes the Super-DeepLabv3+ algorithm from the convolution method and the regularization method. Compared with the traditional algorithm, the innovation of the proposed method lies as follows:

- (1) By minimizing the loss function composed of KL divergence, the proposed algorithm achieves higher scores for the target class than for nontarget classes under different dropouts. Therefore, it has better robustness in remote sensing image scenes with a large amount of data.
- (2) By combining different sizes of convolution kernels, the proposed Mixconv2d method acts as a simple replacement for ordinary depthwise convolutions. Different size kernels can be used to learn information of different scales, which further improves the accuracy and efficiency of the algorithm.

Based on the remote sensing image segmentation task, this paper proposes a new deep learning algorithm Super-DeepLabv3+. The recent research progress in the field of remote sensing image classification and segmentation is investigated, and the achievements and defects of mainstream algorithms are summarized. We further propose a novel semantic segmentation algorithm that adopts DeepLabv3+ as encoder and decoder modules. Convolution kernels of different sizes are used to arbitrarily control the resolution of the extracted encoder features, and the Rdrop Loss method is used to improve the robustness of the model. The validity of the Super-DeepLabv3+ algorithm is verified through experiments. The experimental results show that this algorithm has better performance than the DeepLabv3+ algorithm and has great potential in segmentation tasks.

Section 2 of this paper describes related work on building information extraction. Section 3 introduces the method and innovation of this paper. Section 4 compares the proposed method with other methods and analyzes the results. Section 5 is the conclusion of the paper.

2. Related Work

Buildings in a broad sense refer to all artificially constructed structures, including structures and houses. There are many classification standards for buildings, which can usually be classified according to the nature of use. In addition, buildings are classified based on building height, building structure, etc. Generally, the basic image features of buildings in remote sensing images are mainly manifested in the following four aspects. (1) Spectral features. (2) Shape features. (3) Texture Features. (4) Contextual Features.

Based on the above-given features, building information can be extracted from remote sensing images. In order to meet the needs of military detection, urban planning, statistical census, disaster emergency assessment, and other fields in the basic geographic information system database.

2.1. Traditional Remote Sensing Image Information Extraction Method. In order to accurately extract building objects, traditional methods can be divided into three categories according to the specific technology used: (1) Methods based on traditional edge/line detection techniques. (2) Methods based on the curve propagation class techniques. (3) Methods based on segmentation class techniques.

The methods based on traditional edge detection technology generally form a closed contour by gradually combining edges or straight line segments by extracting edge or straight line segment information in the image. And, then use the prior information such as building shape to realize the extraction of the target contour of the complete closed building. For example, Reference [15] uses the canny edge detection method to extract and segment the selected area of the mouza map image system to realize the precise planning of the area. However, this method cannot robustly handle regions of interest (ROI) with different contrast or shadow conditions such as weak texture, noise, or occlusion. Therefore performance is limited by Gaussian similarity and continuity related measures. Reference [16] combined the Shi_Tomasi corner detection algorithm and scale-invariant feature transformation to realize the registration of remote sensing images before and after earthquakes. However, this method relies on the edge of the building, and it is difficult to realize the joint application of global and local multi-scale information, which affects the extraction accuracy of remote sensing images.

For traditional boundary detection/extraction methods, there are always many discontinuous edge segments. Some of these should actually be connected to each other to form a continuous boundary of meaningful objects. For this reason, based on the traditional edge detection results, additional

edge linking operations are often required to improve the accuracy and reliability of building detection, that is, methods based on curve propagation techniques. For example, Reference [17] uses an active contour model to verify the depiction of building contours in aerial images. But this method is limited by the extraction of building prior information. Reference [18] proposes a low-rank minimization problem and estimates fused features in a lower-dimensional subspace using a novel iterative algorithm based on a multiplier-based alternative direction approach. While these methods are able to give closed contours, they are sensitive to initially detected edges, and there is no guarantee that a globally optimal boundary can be found. Obviously, since this method cannot fully utilize the global information, its application in building object extraction has certain limitations.

Considering that the first two methods cannot fully utilize global and local building prior information, segmentation techniques have been widely used in building object extraction through object-oriented processing. Reference [19] used training data to obtain the optimal scale parameters for multiresolution segmentation and then segmented remote sensing images. Then perform multi-feature extraction on each object obtained by segmentation. Finally, the building object extraction is realized by classification. Such methods rely heavily on initial segmentation and are difficult to extract objects from complex buildings and dense building areas.

2.2. Remote Sensing Image Information Extraction Method Based on Deep Learning. Due to the complex process, low degree of automation, and limited promotion ability of traditional remote sensing image information extraction methods. Existing studies have used deep learning techniques to extract building objects. Deep learning has two characteristics of feature learning and deep structure, which is conducive to the improvement of remote sensing image classification accuracy. Feature learning can automatically learn the required high-level feature representation from massive data according to different applications, and can better express the inherent information of the data. Deep structures usually have multiple layers of hidden layer nodes and contain more nonlinear transformations, which greatly enhances the ability to fit complex models. Deep learning classification algorithms in remote sensing images can be divided into supervised learning and unsupervised learning. Typical application methods include Deep Belief Nets (DBN), Convolutional Neural Network (CNN), Sparse Auto-Encoder (SAE), and so on.

DBN is an improved network of restricted Boltzmann machine (RBM), which belongs to unsupervised learning. Reference [20] introduced local receptive field and weight sharing into Deep Boltzmann Machine (DBM), and established a local-global DBM. However, this method requires more computing resources and increases the

corresponding management cost. Reference [21] improves spectral-spatial classification of HSI by extracting meaningful features to learn and distinguish representations of hyperspectral samples in hidden layers. However, the inherent shortcomings of unsupervised learning make it possible that the results pursue local optimality and are sensitive to noise.

The essence of CNN is the mapping relationship between input and output. Before learning, there is no explicit mathematical model between input and output. CNN builds a model by training a convolutional network by learning a large number of mappings between input and output. Reference [22] proposed a multiscale CNN (MCNN) framework to solve the multiscale problem of optical remote sensing images. Trained simultaneously by a dual-branch structure of a fixed-scale network (F-net) and a variable-scale network (V-net). However, the gradient descent algorithm used can easily make the training result converge to the local minimum rather than the global minimum while ignoring the correlation between the local and the whole. Reference [23] proposed a feature learning method named Deep Lab Dilated Convolutional Neural Network (DL-DCNN) based on automatic semantic segmentation to improve the accuracy of detecting images. However, the accuracy of the results of this method is limited by the precision and parameter selection of preprocessing and requires higher computational performance.

SAE is an improved auto-encoder (AE). SAE is formed by the layer-by-layer superposition of AE. It obtains concise and effective features by encoding and decoding the feature expression of the observation data, and deeply captures the rules hidden in the data. In order to make full use of implicit information such as data categories and patterns, it is also necessary to supervised fine-tuning of its model parameters. For example, Reference [24] proposes a spectral-spatial method for hyperspectral image classification by modifying the traditional auto-encoder based on the Majorization Minimization (MM) technique. However, because this method extracts multiscale features, the parameters will have a greater impact on the accuracy of target detection results. Reference [25] proposed a deep neural network based on SAE and semisupervised to estimate the soft labels of a large amount of existing unlabeled data and then used the soft labels to improve the model training. However, this method is restricted by the environment configuration, which reduces its generalization and generalization ability.

To sum up, there are still many problems in the application of typical target extraction methods in remote sensing images. For example, the mining of spatial relationships and the computational complexity are high. In practical applications, it is necessary to extract from massive high-resolution images, and the use of spectral information is insufficient. Compared with natural image target extraction in other fields, the extraction of building target prior information runs through all key links of building target extraction, and the available information is diverse. How to

effectively select relevant information for building target extraction is still a scientific issue that needs to be deeply explored.

3. Methods

This chapter proposes a CNN model that can improve the accuracy and efficiency of remote sensing image segmentation tasks. The method is based on the DeepLabv3+ algorithm and uses the Rdrop Loss method to enhance the consistency of training and inference models, making it suitable for remote sensing image segmentation tasks. The improved model further employs Mixconv2d convolutions to enable the extraction of features computed by deep convolutional neural networks at arbitrary resolutions. On this basis, Super-DeepLabv3+ also detects convolution features on multiple scales by applying convolution kernel functions with different sizes and further realizes batch extraction of remote sensing image features.

3.1. Mixconv2d. The main idea of Mixconv2d is to fuse multiple convolution kernels with different sizes in one depthwise convolution operation, which greatly reduces the difficulty of capturing different types of features from the input image.

The Mixconv2d feature map is shown in equation (1). Here, s is the kernel size, c is the input channel size, and n is the channel multiplier.

$$T_{x,y,z} = \sum_{-s/2 \leq a \leq s/2, -s/2 \leq b \leq s/2} E_{x+a,y+b,z/n} \cdot R_{a,b,z}, \forall z = 1, \dots, n \cdot c. \quad (1)$$

Unlike general depthwise convolution, Mixconv2d divides the channels into groups and defines kernels of different sizes for each group. For example, l sets of virtual tensors $\langle E^{\wedge(g,k,c_1)}, \dots, E^{\wedge(g,k,c_l)} \rangle$, the height g of the tensors is consistent with the width k , and their total channel size is equal to the original input tensors. Then, the virtual output corresponding to the p th virtual input vector and the kernel can be obtained as shown in the following formula.

$$\hat{T}_{x,y,z} = \sum_{-s_p/2 \leq a \leq s_p/2, -s_p/2 \leq b \leq s_p/2} \hat{E}_{x+a,y+b,z/n}^P \cdot \hat{R}_{a,b,z}^P, \forall z = 1, \dots, n \cdot c_p. \quad (2)$$

The final output tensor is the concatenation of all formulas (2), $\langle \hat{T}_{x,y,z_1}^1, \dots, \hat{T}_{x,y,z_p}^P \rangle$ is shown in the following formula:

$$T_{x,y,z_0} = \text{Concat} \left(\hat{T}_{x,y,z_1}^1, \dots, \hat{T}_{x,y,z_p}^P \right). \quad (3)$$

Mixconv2d can be implemented as a single operation and optimized using group convolutions. The TensorFlow code of Mixconv2d is shown in Algorithm 1. As shown in the figure, Mixconv2d can be seen as a simple replacement for ordinary depthwise convolution.

MixConv has a variety of design options. The optimal design can be made from a single input tensor using different types of kernel sizes, kernel sizes per group, number of channels per group size, and dilated convolutions.

3.2. RDrop Loss. Dropout performs implicit ensemble by simply dropping a certain percentage of hidden units from the neural network during training. However, this method has certain risks. Research has shown that the Dropout model has obvious inconsistencies in the training and inference stages. R-Drop introduces a simple consistency training strategy based on Dropout to regularize Dropout so that the outputs of its sub-models are consistent. That is, for each training sample, R-Drop minimizes the bidirectional KL divergence between the output distributions of the two sub-models that drop samples. R-Drop regularizes the output of two sub-models that are randomly sampled from the dropout for each data sample in training. In this way, the inconsistency between the training phase and the inference phase can be mitigated. Compared with the Dropout strategy in traditional neural network training, R-Drop only adds a KL-divergence loss without any structural changes.

R-Drop regularization requires a given training dataset $E = \{(x_j, y_j)\}_{j=1}^m$. The training objective is to learn the model $Q^z(y|x)$. Where m is the number of training samples, (x_j, y_j) is the data pair, x_j is the input data, and y_j is the label. The input data is further regarded as the probability distribution of the mapping function, and the KL divergence between the two distributions Q_1 and Q_2 is denoted as $S_{KL}(Q_1 || Q_2)$.

The loss function that minimizes the negative log-likelihood given training data is expressed as follows:

$$L_{\text{null}} = \frac{1}{n} \sum_{i=1}^n -\log Q^z(y_i | x_i). \quad (4)$$

With a given input, the input signal is fed back to the forward channel of the network twice, and two distributions are predicted by the model, $Q_1^z(y_i | x_i)$ and $Q_2^z(y_i | x_i)$, are obtained. The R-Drop method attempts to regularize model predictions by minimizing the bidirectional KL divergence between these two output distributions for the same sample, namely,

$$L_{KL}^i = \frac{1}{2} \left(E_{KL} \left(Q_1^z(y_i | x_i) || Q_2^z(y_i | x_i) \right) \right) + E_{KL} \left(Q_1^z(y_i | x_i) || Q_2^z(y_i | x_i) \right). \quad (5)$$

The basic negative log-likelihood learning objective using two prequels is

$$L_{NLL}^i = -\log Q_1^z(y_i | x_i) - \log Q_2^z(y_i | x_i). \quad (6)$$

```

def Mixconv2d(x, filters, args):
    #parameter define:
    #x: the features of input tensor;
    #filters: the list of specific filters' shape;
    #args: reference variable
    L = len(filters)
    #groups of number.
    y = [ ]
    for xi, fi in zip (tf.split(x, G, axis = -1), filters):
        y.append(tf.nn.depthwise_conv2d(xi, fi, args))
    return tf.concat(y, axis = -1)

```

ALGORITHM 1: A demo of TensorFlow Mixconv2d.

The final training objective is to minimize the L^i of the data $(y_i | x_i)$:

$$\begin{aligned}
 L^i &= L_{\text{NLL}}^i + \beta \cdot L_{\text{NLL}}^i = -\log Q_1^z(y_i | x_i) - \log Q_2^z(y_i | x_i) \\
 &+ \frac{\beta}{2} E_{KL} \left(Q_1^z(y_i | x_i) \parallel Q_2^z(y_i | x_i) \right) \\
 &+ \frac{\beta}{2} E_{KL} \left(Q_2^z(y_i | x_i) \parallel Q_1^z(y_i | x_i) \right), \quad (7)
 \end{aligned}$$

where β is the parameter weight assignment.

The specific algorithm is shown in Algorithm 2.

3.3. Super DeepLabv3+. Super-DeepLabv3+ performs R-Dropout Loss regularization based on Mixconv2d convolution. This method can greatly improve the segmentation accuracy and efficiency of remote sensing images.

For remote sensing image segmentation tasks, there are many data points and a large amount of computation. The segmentation algorithm needs to improve the training efficiency as much as possible without losing image features. Using Super-DeepLabv3+ to perform the segmentation task requires building two image network datasets with the same number of sampling points and regularization during the data training process. By composing the minimization training objective based on the negative log-likelihood and the KL divergence as the basis functions, the complete newness of the model and the effect and efficiency of regularization are improved. On this basis, the Mixconv2d convolution is further used to replace the original 3×3 depth convolution network. Reduce the number of parameters while maintaining the same accuracy. The algorithm framework of Super-DeepLabv3+ is shown in Figure 1.

4. Experimental Results and Analysis

In order to verify the accuracy and related performance of the algorithm proposed in this paper, the experimental environment and hardware related configuration are shown in Table 1.

4.1. Network Parameter Settings. Adam optimizer is used during training. The primary parameter is the learning rate, which refers to back-propagating the output error to the network parameters to fit the output of the sample. In essence, the optimization process tends to the optimal solution step by step, but how much error each update parameter utilizes needs to be controlled by a parameter. This parameter is the learning rate Learning rate, and the initial learning rate is set to 0.001. At the same time, the optimal learning rate is not a fixed value, but a variable value that decays with the number of training sessions. That is, in the early stage of training, the learning rate is relatively large, and as the training progresses, the learning rate continues to decrease until the model converges. In the experiment, the median frequency balanced cross-entropy loss function is used to assist training, and the learning rate is attenuated by the Poly decay strategy, and the weight decay is 0.0005. That is, use formula (8) to adjust the learning rate.

$$pr_{\text{epoch}} = pr_{\text{epoch}-1} \left(1 - \frac{\text{epoch}}{\text{max_epoch}} \right)^{0.9}. \quad (8)$$

In the formula, pr_{epoch} represents the learning rate of the current epoch, $pr_{\text{epoch}-1}$ represents the learning rate of the previous epoch, and max_epoch represents the set maximum epoch. An epoch means that all data is sent to the network, and a process of forward calculation + backpropagation is completed. As the number of epochs increases, so does the number of updates to the weights in the neural network. The curve goes from the initial unfit state to the optimal fitting state, and finally to overfitting. According to the actual verification, the maximum epoch of this experiment is set to 200, and the validation set is used for evaluation after each epoch. If the evaluation index does not improve for 10 consecutive epochs, the training is terminated.

4.2. Evaluation Indicators. The experimental evaluation indicators include algorithm efficiency and algorithm accuracy. The performance of the remote sensing image building information extraction algorithm can be relatively comprehensively summarized and described.

Input: Training data $E = \{(x_j, y_j)\}_{j=1}^m$;
Output: model data z .

- (1) Initialize model with parameters z .
- (2) **while** not converged **do**
- (3) randomly sample data pair $(x_j, y_j) \sim L$
- (4) repeat input data twice and then obtain the output distribution
- (5) calculate L_{NLL}^i
- (6) calculate L_{KL}^i
- (7) update the model parameters by minimizing L^i
- (8) **end while**

ALGORITHM 2: Pseudo-code for R-Drop training algorithm routines.

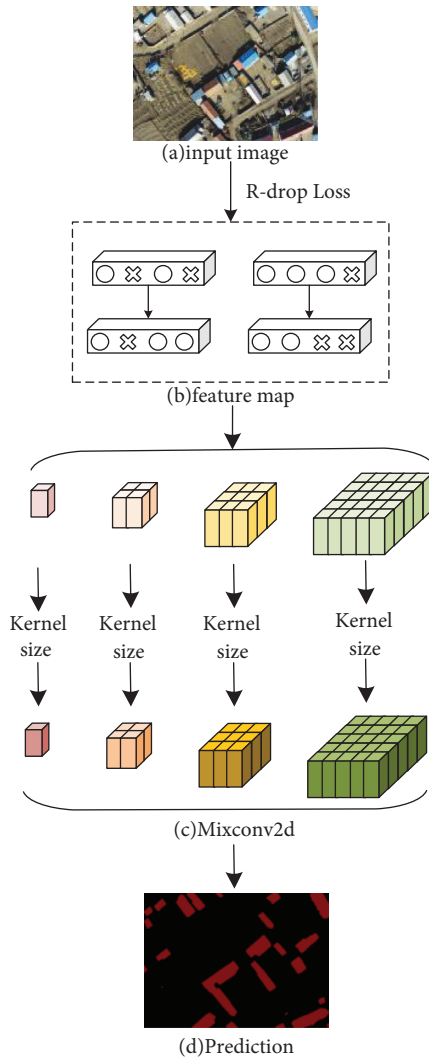


FIGURE 1: The overall framework of proposed super DeepLabv3+.

4.2.1. *Algorithm Efficiency Related Evaluation Index.* In terms of algorithm efficiency, the convergence time, inference occupied video memory and inference speed are selected as the evaluation criteria.

TABLE 1: Experimental environment.

Name	Related configuration
CPU	Intel(R) Xeon(R) CPU 6258R × 2
RAM	DDR4 2400 MHz 256 GB
Acceleration library	CUDA11.1, cudnn8.0.4
GPU	RTX3090 × 4
Operating system	Ubuntu 16.04
Processing software	Python 3.7, PIL, OpenCV
Framework	Pytorch 1.7.0
Python version	3.7

- (1) The convergence time of the algorithm refers to whether the algorithm can finally find the global optimal solution of the problem, and the time required to find the optimal solution. Therefore, the meaning of fast convergence is that relatively accurate values can be obtained with fewer iterations.
- (2) In inference tasks, there are three main parts that occupy GPU memory: model weights, input and output, and intermediate results. Deep learning models are often stacked with layers with similar structures, such as convolutional layers, pooling layers, fully connected layers, and activation function layers. Some layers have parameters. For example, the parameter of the convolutional layer is a high-dimensional convolution kernel, and the parameter of the fully connected layer is a two-dimensional matrix. There are also some layers without parameters, such as activation function layers, pooling layers, etc. Therefore, different model weights are formed. In the forward calculation, the output of the previous layer corresponds to the input of the next layer, and the intermediate results connecting the two adjacent layers also need GPU memory to save. Compared to the model weights and intermediate results, the GPU memory occupied by the input and output is relatively small. At the same time, due to the existence of backpropagation in the training phase, the usage of GPU memory will be more complicated.
- (3) In deep learning, inference refers to a forward propagation process of a neural network. That is, the

process of feeding input data into a neural network and then getting an output from it. The inference speed is the time from the image input model after preprocessing to the model output result. The inference speed of a model on a specific hardware is not only affected by the amount of computation, but also affected by many factors such as the inventory, hardware characteristics, software implementation, and system environment.

4.2.2. Algorithm Accuracy Related Evaluation Index. In terms of algorithm accuracy, with the ground truth map as a reference, the evaluation index can be used to quantitatively analyze the segmentation results. First, it is assumed that there are $n + 1$ classification categories ($0 - n$) in the ground object segmentation dataset, and category 0 represents the background. Using p_{ij} to indicate that the true classification label of a certain pixel is i , and the label predicted by the network model is j . When $i = j$, the prediction is called true positive (TP) if i is a foreground sample, and true negative (TN) if i is a background sample. When $i \neq j$, if i is a foreground sample, the prediction is called a false negative (FN), and if i is a background sample, the prediction is called a false positive (FP). Select the accuracy rate (Acc), class accuracy rate (Acc_class), mean intersection over union (mIoU), and frequency weight intersection over union (FWIoU) several evaluation indicators to evaluate the accuracy of the model.

Acc represents the proportion of correctly classified pixels in all pixels, and the calculation method is shown in the following equation:

$$Acc = \frac{TP + TN}{TP + TN + FN + FP}. \quad (9)$$

Acc_class indicates that for each class, the number of correct predictions for this class/the number of all predictions for this class. Calculate the proportion of correctly classified pixels to all predicted pixels of that class, and then accumulate and average, as shown in the following equation:

$$Acc_{class} = \frac{1}{N} \frac{TP}{TP + FP}. \quad (10)$$

IoU refers to the ratio of the intersection and union between the true set of each classification category and the correctly classified predicted set, as shown in the following equation:

$$IoU = \frac{TP}{TP + FP + FN} = \frac{\sum_{i=1}^N n_{ii}}{\sum_{i=1}^N (m_i + \sum_{j=1}^N n_{ji} - n_{ii})}. \quad (11)$$

Here, mIoU refers to the average of the ratio of the intersection and union between the label value and the correct predicted value of each classification category, as shown in the following formula:

$$mIoU = \frac{1}{N} \frac{TP}{TP + FP + FN} = \frac{1}{N} \frac{\sum_{i=1}^N n_{ii}}{\sum_{i=1}^N (m_i + \sum_{j=1}^N n_{ji} - n_{ii})}. \quad (12)$$

FWIoU is to set weights according to the frequency of occurrence of each class, and the weights are multiplied by the IoU of each class and summed. The formula is as follows:

$$\begin{aligned} FWIoU &= \frac{TP}{TP + FP + FN} \frac{TP + FN}{TP + FP + FN} \\ &= \frac{1}{\sum_{j=1}^N \sum_{i=1}^N n_{ii}} \sum_{i=1}^N \frac{\sum_{j=1}^N n_{ii} n_{ij}}{\sum_{i=1}^N (m_i + \sum_{j=1}^N n_{ji} - n_{ii})}. \end{aligned} \quad (13)$$

4.3. Remote Sensing Image Dataset. In order to verify the performance of the Super-DeepLabv3+ model for extracting building information from remote sensing images, a self-built dataset was selected to evaluate the model results. The dataset has a total of 127 images, covering a variety of scenes containing sparse and dense buildings. The number of images in each scene varies from 50 to 60. The horizontal and vertical resolution of each image is 96 dpi. To facilitate training, by randomly splitting between tiles. The dataset is divided into training set, validation set, and test set according to the ratio of 8 : 1 : 1. That is, 104 images are divided into training set, 11 images are divided into a validation set, and 12 images are divided into test set.

Usually, the size of remote sensing images is large, and it is difficult to directly input into the model. The remote sensing image needs to be cropped into multiple small-sized subimages, then input into the model for prediction, and then stitched to obtain the final segmentation result. If no measures are taken, stitching marks may occur. The main reason is that the original remote sensing image has been cropped, and the feature information at the edge of the small-size subimage is incomplete, resulting in the loss of some of the above-given information in the small-size subimage. In order to eliminate the stitching traces, the remote sensing images need to be cropped into small-sized subimages by overlapping sliding windows. The prediction results of the small-sized subimages are obtained by the model and then stitched in sequence. It should be noted that the edge regions of the prediction results of small-sized subimages are ignored during stitching. In the experiment, the dataset is cropped into subimages of 256 pixels \times 256 pixels according to the sliding window overlap step size of 40 pixels. At the same time, the images of the training set are expanded by scaling, flipping, color transforming, adding noise, and random erasing to improve the generalization ability of the model.

4.4. Experimental Results. In the experiment, five semantic segmentation networks were trained on remote sensing feature segmentation datasets, including Unet network model [26], Mix_DeepLabv3+ network model, DeepLabv3+ network model [7], Rdrop_DeepLabv3+ network model, and Super-DeepLabv3+ network model. And, a more comprehensive comparison and reason analysis are carried out on the algorithm execution efficiency and accuracy of the trained model. The segmentation

TABLE 2: Efficiency comparison of various network models.

Network name	Convergence time (h)	Inference occupies video memory (GB)	Inference speed (fps)
Unet	6	3.3	20.5
Mix_DeepLabv3+	8	4.2	16.7
DeepLabv3+	10	4.3	17.6
Rdrop_DeepLabv3+	7	3.7	15.1
Super_DeepLabv3+	7	3.6	14.8

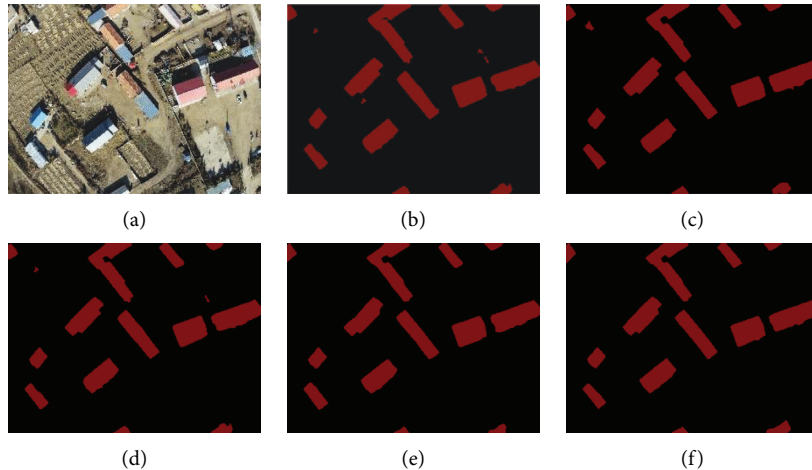


FIGURE 2: Schematic diagram of segmentation results. (a) Input image. (b) Unet. (c) Mix_DeepLabv3+. (d) DeepLabv3+. (e) Rdrop_DeepLabv3+. (f) Super_DeepLabv3+.

performance of the network model is further intuitively evaluated by data analysis, and its shortcomings are analyzed.

4.4.1. Comparison of the Execution Efficiency of Different Remote Sensing Image Information Extraction Methods.

In Table 2 shows the comparison of video memory occupied, convergence time and inference speed for each network model training.

For the model convergence time, from the training results, the Unet network model has the fastest convergence speed, which takes 6 hours. The slowest is the DeepLabv3+ network model, which takes 10 hours to train from start to convergence. Although the five network models have long or short convergence times in a fixed training period, the overall difference is not large. This is because the batch normalization layer is used in the implementation of the network model, which can prevent the gradient from exploding. The mean and standard deviation calculated on the mini-batch are used to dynamically adjust the segmentation of the output of the intermediate layer of the deep convolutional neural network, so that the entire network is more stable in the intermediate output of each layer, thereby accelerating the convergence speed. The learning rate decay strategy used in training enables the network model to avoid the explosion of loss values during the training process, and then achieve convergence.

For inference that occupies video memory, when the training batch size and input image size are fixed, a network model with a large number of parameters will occupy

more video memory. It can be seen from Table 2 that the Unet network model inference occupies 3.3 GB of video memory, and the inference occupies the least video memory. Because the Unet network model uses skip connections between each corresponding layer of the encoder network and the decoder network to perform feature fusion. Therefore, the intermediate feature maps of each stage in the encoder network need to be stored during training. Although this will lead to a larger video memory occupied by inference, the total occupancy is minimal because the number of intermediate feature map channels in Unet is designed to be less. DeepLabv3+ network model inference occupies the largest video memory, which is 4.3 GB. This is because the DeepLabv3+ network model also performs feature fusion with the shallow feature map of the encoder network in the process of restoring the resolution of the feature map, which requires additional storage of the intermediate feature map of the encoder during training.

For inference speed, the Super-DeepLabv3+ network model has the fastest inference speed of 14.8 fps. This is because the Super-DeepLabv3+ network model is regularized during data training. On this basis, the Mixconv2d convolution is further used to replace the original deep convolution network, which reduces the number of parameters while ensuring the same accuracy. Compared with other methods, the proposed Super-DeepLabv3+ method significantly improves the efficiency and performance of the algorithm on the basis of ensuring convergence and ensures the effective execution of remote sensing image information extraction.

TABLE 3: Accuracy comparison of each network model.

Network name	Acc	Acc_class	mIoU	FWIoU
Unet	0.8630	0.9065	0.8539	0.9006
Mix_DeepLabv3+	0.9832	0.9406	0.8958	0.9681
DeepLabv3+	0.9830	0.9371	0.8939	0.9676
Rdrop_DeepLabv3+	0.9836	0.9429	0.8985	0.9689
Super_DeepLabv3+	0.9834	0.9538	0.8993	0.9688

4.4.2. *Comparison of Accuracy of Different Remote Sensing Image Information Extraction Methods.* In terms of the accuracy comparison of different remote sensing image information extraction methods, a typical remote sensing building image is taken as an example to compare the performance between the models. Figures 2(a)–2(f) are the original images of remote sensing buildings, and the extraction results of building information using each model.

As can be seen from Figure 2, for the denser buildings in the wilderness environment, the difficulty in extracting building information mainly lies in how to eliminate environmental influences and avoid misidentification of small-area objects. Compared with the existing algorithms, the proposed Super-DeepLabv3+ method can eliminate the interference of two small-area objects in the upper left corner and upper right part of the screen and identify the outline of the building more clearly and accurately. The following will quantitatively compare the accuracy of each network model from the perspective of data analysis, as shown in Table 3.

The proposed Super-DeepLabv3+ method is only 0.02% lower than the Rdrop_DeepLabv3+ method in terms of Acc. Compared with Unet, Mix_DeepLabv3+, DeepLabv3 and Rdrop_DeepLabv3+ methods, Acc_class is improved by 4.73%, 1.32%, 1.67%, and 1.09% respectively. Overall, the Super-DeepLabv3+ method achieves the best segmentation accuracy.

In terms of mIoU and FWIoU, the proposed Super-DeepLabv3+ method is also at a higher level than other methods. This is due to the fact that the proposed Super-DeepLabv3+ method takes KL divergence minimization as the objective constraint training dataset based on regularization to optimize the segmentation results. So that the resolution of the predicted segmentation map can be restored, and it can be fused with the shallow feature map rich in localization information. While improving the performance of building information extraction, the division of building edges is also smoother, and a higher segmentation accuracy is achieved.

Combining the four accuracy evaluation indicators, the Super-DeepLabv3+ method has the best remote sensing image segmentation performance, which significantly improves the accuracy and quality of building information extraction.

5. Conclusion

Aiming at the characteristics of a large amount of remote sensing image data and various types, a remote sensing image feature recognition method combining DeepLabv3+ and Mixconv2d is proposed. (1) The deep learning semantic segmentation model DeepLabv3+ and Mixconv2d are combined, and convolution kernels of different sizes are used for feature recognition. (2) The regularization method based on Rdrop Loss improves the accuracy and efficiency of contour capture for objects of different resolutions, and at the same time improves the consistency of dataset fitting. (3) Experiments based on self-built datasets show that Super-DeepLabv3+ has good accuracy and execution efficiency, which fully proves the effectiveness of the method. In the next step, we will deeply study how to further extend the applicability of the algorithm on the basis of ensuring the efficiency and calculation accuracy of the algorithm.

Data Availability

The data used to support the findings of this study are included within the article.

Conflicts of Interest

The author declares that there are no conflicts of interest regarding the publication of this paper.

References

- [1] H. Caesar, J. Uijlings, and V. Ferrari, "Coco-stuff: thing and stuff classes in context," in *Proceedings of the IEEE Conference on Computer Vision and Pattern Recognition*, pp. 1209–1218, Salt Lake City, UT, USA, June 2018.
- [2] Y. Bazi, L. Bashmal, M. M. A. Rahhal, R. A. Dayil, and N. A. Ajlan, "Vision transformers for remote sensing image classification," *Remote Sensing*, vol. 13, no. 3, pp. 516–523, 2021.
- [3] Z. Zhou, S. Li, W. Wu et al., "NaSC-TG2: natural scene classification with Tiangong-2 remotely sensed imagery," *Ieee Journal of Selected Topics in Applied Earth Observations and Remote Sensing*, vol. 14, no. 3, pp. 3228–3242, 2021.
- [4] N. Mboga, S. Georganos, T. Grippa, M. Lennert, S. Vanhuyse, and E. Wolff, "Fully convolutional networks and geographic object-based image analysis for the classification of VHR imagery," *Remote Sensing*, vol. 11, no. 5, pp. 597–612, 2019.
- [5] Y. H. Robinson, S. Vimal, M. Khari, F. C. L. Hernandez, and R. G. Crespo, "Tree-based convolutional neural networks for object classification in segmented satellite images," *International Journal of High Performance Computing Applications*, vol. 8, no. 2, 2020.
- [6] E. Li, A. Samat, W. Liu, C. Lin, and X. Bai, "High-resolution imagery classification based on different levels of information," *Remote Sensing*, vol. 11, no. 24, pp. 2916–2921, 2019.

- [7] H. Houda, J. M. P. Nascimento, and A. Bernardino, "Fire detection using residual deeplabv3+ model," in *Proceedings of the 2021 Telecoms Conference (ConfTELE)*. IEEE, pp. 1–6, Leiria, Portugal, February 2021.
- [8] S. Frizzi, M. Bouchouicha, and E. Moreau, "Comparison of two semantic segmentation databases for smoke detection," in *Proceedings of the 2021 22nd IEEE International Conference on Industrial Technology (ICIT)*, IEEE, vol. 1, pp. 856–863, Valencia, Spain, March 2021.
- [9] V. Varatharasan, H. S. Shin, A. Tsourdos, and N. Colosimo, "Improving Learning Effectiveness for Object Detection and Classification in Cluttered Backgrounds," in *Proceedings of the e2019 Workshop On Research, Education And Development Of Unmanned Aerial Systems (RED UAS)*, pp. 78–85, IEEE, Cranfield, UK, November 2019.
- [10] V. Raj and S. Kalyani, "Design of communication systems using deep learning: a variational inference perspective," *IEEE Transactions on Cognitive Communications and Networking*, vol. 6, no. 4, pp. 1320–1334, 2020.
- [11] L. Zhu, G. Wang, F. Huang, Y. Li, W. Chen, and H. Hong, "Landslide susceptibility prediction using sparse feature extraction and machine learning models based on GIS and remote sensing," *IEEE Geoscience and Remote Sensing Letters*, vol. 19, no. 4, pp. 1–5, 2022.
- [12] S. Susan, S. Tandon, S. Seth, M. Mohdi-Tariq, C. Ritika, and B. Nikhil, "Kullback-leibler divergence based marker detection in augmented reality," in *Proceedings of the 2018 4th International Conference on Computing Communication and Automation (ICCCA)*, pp. 1–5, IEEE, Greater Noida, India, December 2018.
- [13] X. Wang, S. Yin, H. Li, J. Wang, and L. Teng, "A network intrusion detection method based on deep multi-scale convolutional neural network," *International Journal of Wireless Information Networks*, vol. 27, no. 4, pp. 503–517, 2020.
- [14] H. T. Mustafa, J. Yang, and M. Zareapoor, "Multi-scale convolutional neural network for multi-focus image fusion," *Image and Vision Computing*, vol. 85, no. 11, pp. 26–35, 2019.
- [15] Y. A. Akter, M. A. Rahman, and M. Osiur Rahman, "Quantitative analysis of Mouza map image to estimate land area using zooming and Canny edge detection," *TELKOMNIKA (Telecommunication Computing Electronics and Control)*, vol. 18, no. 6, pp. 3293–3302, 2020.
- [16] X. Zhao, H. Li, P. Wang, and L. Jing, "An image registration method for multisource high-resolution remote sensing images for earthquake disaster assessment," *Sensors*, vol. 20, no. 8, pp. 2286–2297, 2020.
- [17] A. Hatamizadeh, D. Sengupta, and D. Terzopoulos, "End-to-end trainable deep active contour models for automated image segmentation: delineating buildings in aerial imagery," in *Proceedings of the European Conference on Computer Vision*, pp. 730–746, Glasgow, UK, October 2020.
- [18] B. Rasti and P. Ghamisi, "Remote sensing image classification using subspace sensor fusion," *Information Fusion*, vol. 64, no. 1, pp. 121–130, 2020.
- [19] R. Attarzadeh and M. Momeni, "Object-based rule sets and its transferability for building extraction from high resolution satellite imagery," *Journal of the Indian Society of Remote Sensing*, vol. 46, no. 2, pp. 169–178, 2018.
- [20] J. Yang, Y. Guo, and X. Wang, "Feature extraction of hyperspectral images based on deep Boltzmann machine," *IEEE Geoscience and Remote Sensing Letters*, vol. 17, no. 6, pp. 1077–1081, 2020.
- [21] A. Sellami and I. R. Farah, "Spectra-spatial Graph-Based Deep Restricted Boltzmann Networks for Hyperspectral Image Classification," in *Proceedings of the 2019 Photonics & Electromagnetics Research Symposium-Spring (PIERS-Spring)*, pp. 1055–1062, IEEE, Rome, Italy, June 2019.
- [22] Y. Liu, Y. Zhong, and Q. Qin, "Scene classification based on multiscale convolutional neural network," *IEEE Transactions on Geoscience and Remote Sensing*, vol. 56, no. 12, pp. 7109–7121, 2018.
- [23] N. Venugopal, "Automatic semantic segmentation with DeepLab dilated learning network for change detection in remote sensing images," *Neural Processing Letters*, vol. 51, no. 3, pp. 2355–2377, 2020.
- [24] E. Kordi Ghasrodashti and N. Sharma, "Hyperspectral image classification using an extended Auto-Encoder method," *Signal Processing: Image Communication*, vol. 92, p. 116111, 2021.
- [25] E. Protopapadakis, A. Doulamis, N. Doulamis, and E. Maltezos, "Stacked autoencoders driven by semi-supervised learning for building extraction from near infrared remote sensing imagery," *Remote Sensing*, vol. 13, no. 3, p. 371, 2021.
- [26] N. He, L. Fang, and A. Plaza, "Hybrid first and second order attention Unet for building segmentation in remote sensing images," *Science China Information Sciences*, vol. 63, no. 4, pp. 140305–140312, 2020.

Retraction

Retracted: Factors Analysis of the Compliance Rate of Hypertension Detection Control and Self-Assessment Control in Community Outpatient Clinics

Computational Intelligence and Neuroscience

Received 17 October 2023; Accepted 17 October 2023; Published 18 October 2023

Copyright © 2023 Computational Intelligence and Neuroscience. This is an open access article distributed under the Creative Commons Attribution License, which permits unrestricted use, distribution, and reproduction in any medium, provided the original work is properly cited.

This article has been retracted by Hindawi following an investigation undertaken by the publisher [1]. This investigation has uncovered evidence of one or more of the following indicators of systematic manipulation of the publication process:

- (1) Discrepancies in scope
- (2) Discrepancies in the description of the research reported
- (3) Discrepancies between the availability of data and the research described
- (4) Inappropriate citations
- (5) Incoherent, meaningless and/or irrelevant content included in the article
- (6) Peer-review manipulation

The presence of these indicators undermines our confidence in the integrity of the article's content and we cannot, therefore, vouch for its reliability. Please note that this notice is intended solely to alert readers that the content of this article is unreliable. We have not investigated whether authors were aware of or involved in the systematic manipulation of the publication process.

Wiley and Hindawi regrets that the usual quality checks did not identify these issues before publication and have since put additional measures in place to safeguard research integrity.

We wish to credit our own Research Integrity and Research Publishing teams and anonymous and named external researchers and research integrity experts for contributing to this investigation.

The corresponding author, as the representative of all authors, has been given the opportunity to register their agreement or disagreement to this retraction. We have kept a record of any response received.

References

- [1] Z. Chen and R. Xiong, "Factors Analysis of the Compliance Rate of Hypertension Detection Control and Self-Assessment Control in Community Outpatient Clinics," *Computational Intelligence and Neuroscience*, vol. 2022, Article ID 9432202, 9 pages, 2022.

Research Article

Factors Analysis of the Compliance Rate of Hypertension Detection Control and Self-Assessment Control in Community Outpatient Clinics

Zhigao Chen¹ and Rui Xiong² 

¹Hospital of Wuhan University of Science and Technology, Wuhan 430061, China

²Wuchang District Shouyilu Street Community Health Service Center, Wuhan 430061, China

Correspondence should be addressed to Rui Xiong; 19404171@masu.edu.cn

Received 11 August 2022; Revised 15 September 2022; Accepted 22 September 2022; Published 12 October 2022

Academic Editor: Ashish Khanna

Copyright © 2022 Zhigao Chen and Rui Xiong. This is an open access article distributed under the Creative Commons Attribution License, which permits unrestricted use, distribution, and reproduction in any medium, provided the original work is properly cited.

Objective. To understand the related influencing factors of outpatient hypertension detection and control and self-test control compliance rate. **Methods.** A total of 637 hypertensive patients who visited the outpatient clinic of our hospital from January 2021 to December 2021 were selected for investigation and research, and the relevant information such as blood pressure, treatment detection, and other related information of the patients were counted, and the detection and control of outpatient hypertension were explored through regression analysis and the related factors of the self-test control compliance rate. **Results.** There was no statistically significant difference in the number of patients who met the standard or not under the gender difference ($P > 0.05$), and it can be found that there was no statistically significant difference in the age of patients who met the standard and those who did not ($P > 0.05$). The proportion of patients with self-test hypertension control at home was 64.68%, and the compliance rate of self-test blood pressure was 42.54%. The compliance rate of blood pressure control in outpatient testing was 61.85%. Heart rate, exercise, smoking, medication compliance, and other factors are important factors affecting the control of hypertension. Knowing hypertension-related knowledge, regular follow-up, office blood pressure compliance, smoking, excessive salt intake, and hypertension complications are important factors affecting the self-test control of hypertension in the family. **Conclusion.** By urging patients to do daily physical exercise, admonishing patients to quit smoking, and improving patients' medication compliance, the control rate of hypertension in outpatient clinics can be effectively improved. Understanding the knowledge of hypertension, controlling the salt content in the diet, and receiving regular follow-up surveys from doctors can effectively improve the effect of self-measurement and control of blood pressure at home and further improve the control rate of hypertension.

1. Introduction

At present, scholars have proved that bad habits such as smoking and drinking lead to poor blood pressure control in patients with hypertension. Family history of cardiovascular disease, long-term excessive drinking, smoking, diabetes, hyperlipidemia, and compliance with medical compliance are risk factors affecting blood pressure control in patients with hypertension. These factors should be paid attention to in clinical practice. But these studies are not in depth and need to be further explored.

Hypertension is a common chronic disease, often accompanied by heart, kidney, and other target organ dysfunction or organic discoloration and is also a major risk factor for cardiovascular and cerebrovascular diseases such as stroke and coronary heart disease [1, 2]. In recent years, with the rapid improvement of the economic level, people's living patterns have changed, and the social population is aging. The fatality rate is also high, and it is one of the important causes of death [3–5]. Effective hypertension prevention and control is of great significance to reduce the prevalence and incidence of hypertension and can help

hypertensive patients control their own blood pressure levels and improve their quality of life. In addition, the prevention and control of hypertension is also conducive to reducing the risk of related cardiovascular and cerebrovascular diseases and reducing people's disease burden.

Hypertension, as a common disease, seriously affected the physical condition of patients with hypertension. If the blood pressure of patients with hypertension is not well controlled, the increase in the range of blood pressure fluctuations can increase the cerebral perfusion pressure and lead to dizziness. Without timely treatment, it will even progress to small focal bleeding, causing amaurosis, or even fainting. Therefore, the common clinical symptoms of hypertension patients are dizziness, headache, blurred vision, blackening, and even fainting. Excessive drug dose in patients with hypertension may lead to low blood pressure. Similarly, insufficient cerebral perfusion can also cause transient ischemic attack, leading to dizziness, headache, and darkness. In severe cases, patients will also have symptoms of fainting. Low blood pressure caused by acute cerebral infarction will not only cause severe headaches but also cause coma [6].

Hypertension is a long-term chronic disease that requires patients to maintain long-term medication treatment to maintain a stable blood pressure state. Even if the patient's blood pressure level generally reaches the safe standard, there is still a certain residual risk of cardiovascular events [7, 8]. At present, the commonly used hypertension control method is a combined treatment mode including blood pressure monitoring, drug treatment, and life intervention, and strict blood pressure monitoring ensures stable blood pressure control of patients [9, 10]. Outpatient blood pressure testing can provide reference for doctors to diagnose and treat and provide accurate blood pressure data for patients. The economic cost and time cost of self-measurement of blood pressure at home are lower, and self-monitoring of blood pressure by patients outside medical institutions can effectively help hypertensive patients to quickly understand their blood pressure status in the home environment and prompt patients to take corresponding measures in a timely manner [11–13]. Therefore, the study analyzed the relevant factors of hypertension self-testing and the compliance rate of blood pressure detection and control in community outpatient clinics, in order to provide a reference for improving the blood pressure control compliance rate of hypertensive patients.

Through the analysis of community outpatient hypertension detection control and self-test control compliance rate-related factors, we can more accurately grasp the blood pressure control of patients with hypertension to help patients with hypertension stable condition; normal life is of great significance.

2. Materials and Methods

2.1. General Information. The study cases were 637 hypertensive patients who visited the outpatient department of our hospital from January 2021 to December 2021. The inclusion criteria of the surveyed patients were as follows: (1) meet the diagnostic criteria of hypertension in the “Chinese Guidelines

for the Prevention and Treatment of Hypertension 2010” and meet the systolic blood pressure ≥ 140 mmHg or diastolic blood pressure ≥ 90 mmHg. (2) Age > 18 years old. (3) Have self-behavior, clear consciousness, and no communication barriers. The exclusion criteria are as follows: (1) patients with secondary hypertension. (2) Patients with severe cardiovascular and cerebrovascular complications in the past. (2) Suffering from mental illness and cognitive dysfunction. (3) Women who are pregnant or breastfeeding. All patients participated in the investigation and research voluntarily, and the patients and their families had signed the informed consent, and the research was approved by the ethics committee of our hospital. The general data of the study cases are shown in Table 1.

2.2. Research Methods. This study focuses on the analysis of the factors related to the compliance rate of hypertension detection control and self-test control in community clinics. On the premise of considering the age and gender factors of patients, the relevant evaluation criteria are measured by grouping patients in different groups. The effect of age on blood pressure control and the effect of gender on blood pressure control were also analyzed.

The clinicians who have received unified training and passed the examination will conduct a questionnaire survey and physical examination on the subjects. They will learn about the age, disease, medication, physical exercise, family history, diabetes history, smoking and alcohol history, medication compliance, and other information of the subjects in the form of a questionnaire. After completing the questionnaire, they will review the questionnaire items in time and supplement the missing information. Physical examination included height, weight, and blood pressure measurements of the subjects. The height and weight of the subjects were measured according to standard methods. The subjects were required to take off their shoes and hats and wear single clothes. When measuring height, the subjects were required to stand barefoot close to the scale, keep their heels close together, and keep their shoulder blades, hips, and heels close to the scale. The height data reading was accurate to 0.1 cm. A platform scale was used to measure the weight of the subjects, and the weight data were accurate to 0.1 kg. The blood pressure of the subjects was measured according to the international common blood pressure measurement methods and quality control methods, and the standard mercury sphygmomanometer was used for measurement. Before the measurement, the subjects were required to sit and rest for at least 5 min and measure three times, ensuring that the interval between the two measurements was 1–2 min and taking the average value of the three measurements.

2.3. Judgment Criteria. In the examination of blood pressure in the consulting room, if the systolic blood pressure of the subjects under 60 years old is ≥ 140 mmHg or the diastolic blood pressure is ≥ 90 mmHg, the examination is unqualified. If the systolic blood pressure is ≥ 150 mmHg or diastolic blood pressure is ≥ 90 mmHg of subjects over 60

TABLE 1: General information ($n = 637$).

Variable	Number of cases	Composition ratio (%)
Gender	Male	41.92
	Female	58.08
Age	60 \leq , <70	48.35
	\geq 70	51.65
Educational level	Elementary school and below	59.81
	Secondary school and above	40.19
BMI	Normal	27.32
	Overweight	72.68
Family history	Parents with high blood pressure	31.55
	Parents without hypertension	68.45
Smoking history	Yes	57.61
	No	42.39
Hypertension comorbidities	Stroke	41.44
	Heart failure	32.34
	Dyslipidemia	26.53
Target organ damage	Cardiac enlargement and hypertrophy	33.44
	Carotid artery thickening and plaque	30.93
	Proteinuria and elevated serum creatinine	35.64

years old, the test is not up to the standard. In the family self-test, if the systolic blood pressure of the subject is ≥ 135 mmHg or the diastolic blood pressure is ≥ 85 mmHg, the test is unqualified. Salt intake ≥ 6 G per day is considered as excessive salt intake. The study subjects who smoke or have quit smoking are smoking history, which refers to smoking and smoking more than 1 cigarette a day for more than 1 year or smoking more than 1 cigarette a day in the past but have quit smoking now. Drinking history refers to drinking more than 50 ml of baijiu, 150 ml of red wine, or 500 ml of beer every day. In the evaluation of physical exercise indicators, if the average number of exercises per week is ≥ 3 and the duration of each exercise is ≥ 30 min, it is judged that there is physical exercise. If the number of days of taking medicine according to the doctor's instructions exceeds 90% of the total number of days, it is judged that the medication compliance is good. Subjects with BMI ≥ 50 were obese, and BMI was the square of body weight divided by height.

If the study object meets one of the conditions of plasma cholesterol rise ≥ 5.7 mmol/l, low-density lipoprotein cholesterol > 3.6 mmol/l, or triglyceride rise ≥ 1.7 mmol/l, it is judged that the study object is dyslipidemia. The subjects with a history of typical angina pectoris and coronary artery stenosis $\geq 50\%$ shown by coronary CTA or coronary angiography, or a history of myocardial infarction, were recorded as coronary heart disease. Cerebral hemorrhage and cerebral infarction were recorded as stroke complications, and heart failure included acute heart failure and chronic heart failure. If the daily urine protein quantity of the study object is more than 150 mg, or the urine protein qualitative test result is positive, or the urine protein/creatinine is more than 200 mg/g, the study object is judged to be proteinuria. Serum creatinine was higher than 133 $\mu\text{mol/L}$ in males and 124 $\mu\text{mol/L}$ in females. Left ventricular hypertrophy was diagnosed by the left ventricular mass index. If female ≥ 110 g/m^2 and male ≥ 125 g/m^2 , left ventricular hypertrophy was judged. If there is atrial

enlargement or left ventricular thickening in each atrium and ventricle of the study object, the study object is marked as cardiac enlargement and hypertrophy. If the carotid intima-media thickness of the subject is ≥ 1 cm, or there are single or multiple atherosclerotic plaques, the subject is marked as carotid artery thickening and plaque.

The above are diseases that interact with hypertension, but they are not comprehensive. If other diseases occur during the survey, they can be listed separately for analysis.

2.4. Statistical Analysis. Statistical software SPSS22.0 was used for data analysis, and measurement data were expressed as the mean \pm standard deviation ($\bar{x} \pm s$). Due to the large amount of data in the sample and all of them being numerical data, the average value of the sample variance can be calculated. Therefore, the *t*-test is used for intergroup comparison, the count data are compared between the groups by the test, and the related factors are analyzed by binary logistic stepwise regression. $P > 0.05$ indicates that the difference is statistically significant.

3. Results

3.1. Analysis of Related Factors of Hypertension Detection and Control. Table 2 shows the results of univariate analysis of blood pressure control in community outpatient clinics. Among 637 hypertensive patients, 394 had blood pressure control, and the compliance rate was 61.85%. The patients were grouped according to whether blood pressure detection and control reached the standard. It can be seen that the difference in the number of people who reached the standard or not under the gender difference was not statistically significant ($P > 0.05$). There were statistically significant differences between those who reached the standard and those who did not reach the standard under such indicators as BMI, heart rate, exercise, smoking, drinking, medication compliance, and excessive salt intake ($P < 0.05$).

TABLE 2: Univariate analysis results of outpatient hypertension detection and control.

Variable		Up to standard ($\bar{x} \pm s, n$)	Not to standard ($\bar{x} \pm s, n$)	t/χ^2	P
Gender	Male	196 (49.75%)	119 (48.97%)	0.139	0.772
	Female	198 (50.25%)	124 (51.03%)		
Age		66.37 ± 10.62	66.83 ± 10.24	0.543	0.587
BMI (kg/m^2)		24.65 ± 3.31	24.53 ± 3.33	2.395	0.017
Heart rate (times/min)		75.31 ± 5.54	76.36 ± 5.71	2.280	0.023
Exercise	YES	189 (47.97%)	97 (39.92%)	8.269	0.004
	NO	205 (52.03%)	146 (60.08%)		
Smoking	YES	216 (54.82%)	155 (63.79%)	21.064	0.001
	NO	178 (45.18%)	88 (36.21%)		
Drinking	YES	117 (29.70%)	132 (54.32%)	10.617	0.001
	NO	277 (70.30%)	111 (45.68%)		
Medication compliance	GOOD	381 (96.70%)	192 (79.01%)	28.643	0.001
	LACK	13(3.30%)	51(20.99%)		
Excessive salt intake	YES	372 (94.42%)	232 (95.47%)	5.024	0.025
	NO	22 (5.58%)	11 (4.53%)		

TABLE 3: Multivariate logistic analysis results of outpatient hypertension detection and control.

Elements	β	SE	Wald χ^2	P	OR (95%CI)
Heart rate	0.059	0.031	10.352	0.002	0.997 (0.824–1.039)
Exercise	0.972	0.442	15.776	0.001	0.325 (0.303–0.464)
Smoking	0.936	0.439	32.364	0.001	2.579 (1.929–3.816)
Medication compliance	1.157	0.507	44.853	0.001	0.153 (0.127–0.221)

The multivariate analysis results of the influencing factors of hypertension detection and control are shown in Table 3. Logistic regression analysis was used to evaluate the degree of influence of the indicators. Whether the patient's control was up to the standard was used as the dependent variable, and BMI, heart rate, exercise, smoking, drinking, and medication were used as the dependent variable. The factors affecting compliance and excessive salt intake, namely independent variables, were analyzed by logistic regression. The results showed that the multivariate analysis P value of the heart rate, exercise, smoking, and medication compliance was less than 0.05, indicating that factors such as the heart rate, exercise, smoking, and medication compliance were important influencing factors for hypertensive patients to be controlled. It is a risk factor for hypertension control, and regular exercise and high medication compliance are protective factors for hypertension control.

The ROC curve is used to reflect the diagnostic performance of the heart rate, exercise, smoking, and medication compliance indicators in hypertension clinics. The OR value of the heart rate was 0.997, between 0.824 and 1.039, so heart rate block was a risk factor for high snow pressure control. Smoking is also a risk factor for blood pressure control. Conversely, exercise and medication adherence are protective factors for blood pressure control. The ROC curve of the heart rate, exercise, smoking, and medication compliance in the prediction of blood pressure control compliance in patients with hypertension is shown in Figure 1, and the areas under the ROC curve of the heart rate, exercise, smoking, and medication compliance were 0.779, 0.752, 0.821, and 0.704, respectively.

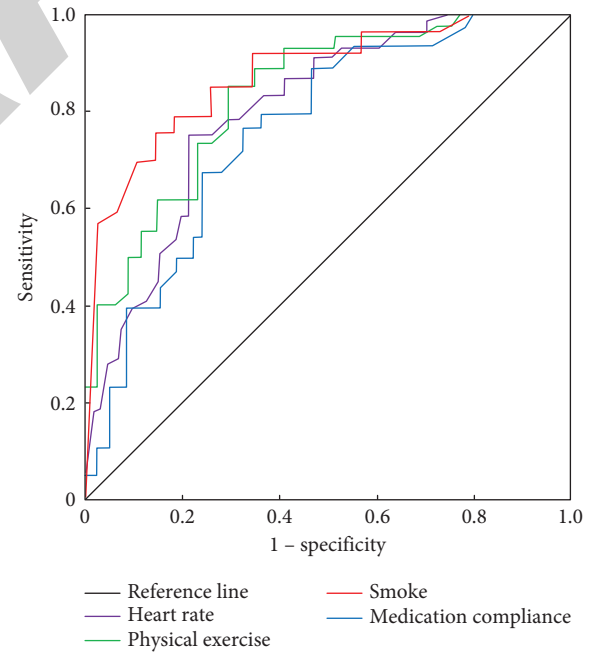


FIGURE 1: ROC curve of risk factors for hypertension detection.

3.2. Analysis of Influencing Factors of Self-Assessment and Control of Hypertension. The results of blood pressure self-testing in community outpatient clinics are shown in Table 4. Among 637 hypertensive patients, 412 had self-measured blood pressure, and 225 had not performed home blood pressure self-measurement. Grouped by educational background, 51.71% of hypertensive patients with primary school

TABLE 4: Data of patients with hypertension controlled by self-testing at home.

project	Education		Hypertension complications			Parental history of hypertension	
	Elementary school and below	Secondary school and above	Stroke	Myocardial failure	Dyslipidemia	Yes	No
Self-test	197 (51.71%)	184 (71.88%)	101 (38.26%)	82 (39.81%)	55 (32.93%)	184 (91.54%)	217 (49.77%)
Not self-tested	184 (48.29%)	72 (28.12%)	163 (61.74%)	124 (60.19%)	112 (67.07%)	17 (5.46%)	219 (50.23%)
χ^2	10.127		8.523			14.339	
P	<0.05		<0.05			<0.05	

TABLE 5: Univariate analysis results of hypertension self-assessment and control compliance

Variable	Up to standard ($\bar{x} \pm s, n$)	Not to standard ($\bar{x} \pm s, n$)	t/χ^2	P	
Gender	Male	138 (49.08%)	72 (51.06%)	0.139	0.772
	Female	133 (50.902%)	69 (48.94%)		
Age		66.26 ± 10.72	66.65 ± 10.57	0.543	0.587
Profession	Brain power	127 (46.86%)	63 (44.68%)	1.264	0.642
	Physical strength	144 (53.14%)	78 (55.32%)		
Exercise	Yes	103 (38.01%)	52 (36.88%)	8.269	0.004
	No	168 (61.99%)	89 (63.12%)		
Smoking	Yes	113 (41.70%)	61(43.26%)	21.064	0.001
	No	158 (58.30%)	80 (56.74%)		
Drinking	Yes	117 (43.17%)	63 (44.68%)	10.617	0.001
	No	154 (56.83%)	78 (55.32%)		
High blood pressure-related knowledge	Know	126 (46.49%)	43 (30.50%)	28.643	0.001
	Do not know	145 (53.51%)	98 (69.50%)		
Excessive salt intake	Yes	142 (52.40%)	88 (62.41%)	5.024	0.025
	No	129 (47.60%)	53 (37.59%)		
Follow-up	Regular	163 (60.15%)	79 (56.03%)	10.332	0.037
	Irregular	108 (39.85%)	62 (43.97%)		
Sleep quality	Good	123 (45.39%)	59 (15.60%)	6.727	0.029
	Poor	148 (54.61%)	82 (58.16%)		
Hypertension complications	Yes	192 (70.85%)	141 (84.40%)	12.369	0.007
	No	79 (29.15%)	22 (15.60%)		
Target organ damage	Heart enlargement and hypertrophy	81 (29.15%)	51 (29.89%)	9.379	0.014
	Carotid thickening and plaque	93 (34.32%)	42 (15.80%)		
	Proteinuria, increased serum creatinine	97(35.79%)	48(17.71%)		
Office blood pressure up to the standard	Yes	194 (71.59%)	78 (55.32%)	5.337	0.009
	No	77 (28.41%)	63 (44.68%)		

and below took blood pressure self-testing at home, and 71.88% of hypertensive patients with high school education or above took home self-testing; the proportions of hypertensive patients with failure and dyslipidemia were 38.26%, 39.81%, and 32.93%, respectively; the proportion of hypertensive patients with a history of hypertension at home was 91.54%. 49.77% of hypertensive patients with no history of hypertension had self-measured blood pressure at home.

Table 5 shows the results of univariate analysis of blood pressure self-assessment and control compliance, in which the number of blood pressure self-assessment compliance was 271, and the compliance rate was 42.54%. Gender, age, and occupation had no significant effect on the number of hypertensive patients who met the control standard at home ($P > 0.05$); hypertension, smoking, drinking, salt intake,

follow-up, sleep quality, exercise, and hypertension complications were investigated; there was a statistically significant difference between the number of people who reached the standard and those who did not meet the standard of target organ damage and outpatient blood pressure ($P < 0.05$). Thus, education has a significant impact on home control of hypertension ($P < 0.05$), complications of hypertension also have a significant impact on home control of hypertension ($P < 0.05$), and the same history of hypertension in parents also has a significant impact on home control of hypertension. ($P < 0.05$).

Logistic regression analysis was used to determine the main influencing factors that affect the self-assessment and control of hypertension. The multivariate analysis results of the self-assessment and control of hypertension are shown in Table 6. Knowledge of hypertension, regular follow-up, and

TABLE 6: Multivariate analysis results of self-assessment and control in hypertensive patients.

elements	β	SE	Wald χ^2	P	OR (95%CI)
Smoking	0.574	0.298	8.185	0.002	0.543 (0.264–0.710)
Office blood pressure up to the standard	1.072	0.556	12.349	0.001	1.201 (0.915–1.318)
Know about high blood pressure	0.825	0.407	5.446	0.005	0.526 (0.415–0.618)
Excessive salt intake	0.092	0.047	15.299	0.007	0.235 (0.129–0.307)
Regular follow-up	1.123	0.784	7.553	0.001	0.997 (0.829–1.054)
Have high blood pressure	1.256	0.539	11.265	0.005	1.127 (1.063–1.198)

meeting the blood pressure in the office are the most important factors for family high blood pressure. The protective factors of blood pressure self-assessment and control, smoking, high salt intake, and hypertension complications are the risk factors for family blood pressure self-assessment and control.

The ROC curve is used to reflect the knowledge about hypertension, regular follow-up, meeting the blood pressure in the office, exercise, smoking, high salt intake, and suffering from hypertension complications. The ROC curve of the main factors controlling the compliance is shown in Figure 2. The areas under the ROC curve of knowledge of hypertension, regular follow-up, standard office blood pressure, smoking, excessive salt intake, and hypertension complications were 0.719, 0.704, 0.807, 0.725, 0.694, and 0.757.

4. Discussion

Hypertension is a common disease among middle-aged and elderly people. The occurrence of hypertension can lead to cardiovascular diseases such as myocardial failure and cerebral apoplexy in the middle-aged and elderly, which seriously endangers the normal life of middle-aged and elderly people [14, 15]. For hypertensive diseases, drug therapy is a common basic treatment method for hypertensive patients, but the role of drug therapy alone in blood pressure control is limited. For this reason, in order to improve the effect of hypertension control, it is important to understand the relevant factors affecting hypertension control [16, 17]. In medical research, it is found that the detection and control of hypertension includes two ways: outpatient hypertension detection and control and patient self-test control at home. In general, outpatient hypertension detection and control is to use drugs to help patients suppress blood pressure, and self-test control of blood pressure at home is to promote patients to change bad habits in daily life by improving patients' cognition of hypertension. Drug therapy and living habits play a supporting role in taking medicine while developing a good life schedule, such as getting up early and going to bed and exercising actively, can help patients with hypertension in better recovery. In general, outpatient hypertension detection and control is to use drugs to help patients suppress elevated blood pressure. Home blood pressure self-test control is to promote patients to change bad habits in daily life by improving their awareness of hypertension [18, 19]. Medication and lifestyle habits play an auxiliary role in taking medication, while making a good life plan, such as getting up early and going to bed, and taking

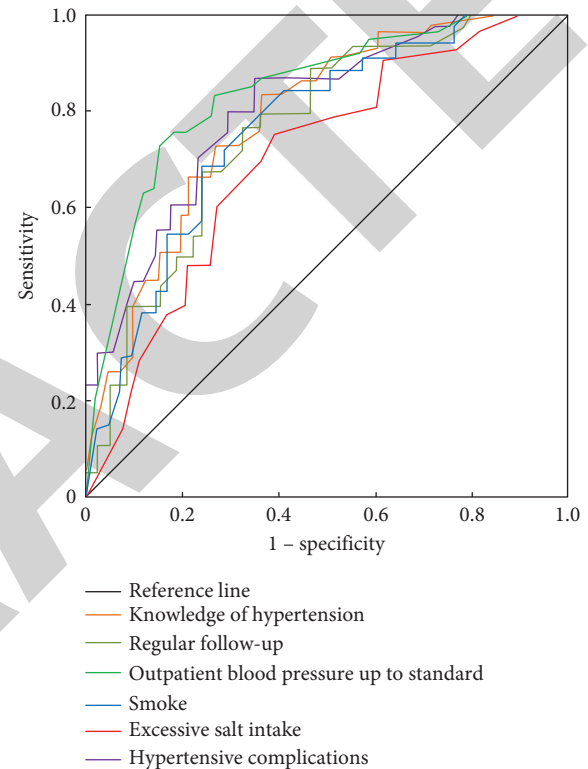


FIGURE 2: Multifactor ROC curve of hypertension self-assessment and control compliance.

active exercise, can help people with hypertension recover better. In general, outpatient hypertension detection and control is to use drugs to help patients suppress blood pressure rise, and home blood pressure is automatically controlled. Measurement and control is to promote patients to change their bad habits in daily life by improving their awareness of hypertension [18, 19]. Therefore, in order to effectively control blood pressure in hypertensive patients, the study starts from two aspects of outpatient detection and control and home self-measurement control, and it analyzes the relevant factors that affect outpatient detection and control and self-measurement control treatment and control rates [20].

The study conducted an analysis of the compliance rate of hypertension outpatient testing and control in community outpatient clinics. The results showed that the blood pressure control compliance rate in outpatient testing was 61.85%. Through univariate analysis, it was concluded that BMI, heart rate, exercise, smoking, drinking, medication

compliance, and excessive salt intake can affect the compliance rate of outpatient hypertension detection and control. Multivariate logistic regression analysis showed that the rapid heart rate and smoking were risk factors for hypertension control, while regular exercise and high medication compliance were protective factors for hypertension control. The increased heart rate can lead to an excited state of the sympathetic nerves, which promotes the production of thyroxine, which in turn causes the arterioles to constrict and raise blood pressure [21–23]. Smoking stimulates the central and sympathetic nerves, which in turn promotes the contraction of small arteries and increases blood pressure. Exercise is an important way to improve personal physical fitness. Exercise can relax the patient's mood, reduce abnormal vasoconstriction caused by emotional stress, and reduce the probability of blood pressure increase [24, 25]. Medication compliance can help patients use antihypertensive drugs regularly, reduce the occurrence of drug side effects, and achieve the effect of blood pressure control, which is consistent with previous research results [26–28]. At the same time, there is also an interaction effect between them. Active exercise and taking drugs will have a positive feedback effect. There is a negative feedback effect between taking drugs and smoking and the increased heart rate. In other words, smoking and the increased heart rate will reduce the effect of drugs, while active exercise will make the effect of drugs better. Therefore, in the detection and control of hypertension in outpatient clinics, instructing patients to quit smoking, exercising more, and taking medicine regularly can improve the effect of blood pressure control and improve the quality of life of patients [29].

The study showed that 64.68% of the experimental subjects took home self-measured hypertension control, and the self-measured blood pressure compliance rate was 42.54%. Through univariate analysis, the influencing factors of hypertension patients' self-measured blood pressure at home included hypertension-related knowledge, smoking, drinking, salt intake, follow-up, sleep quality, exercise, hypertension complications, and outpatient blood pressure compliance. Multivariate analysis was performed to determine the risk factors affecting the self-measured blood pressure control of patients. Using multivariate logistic regression analysis, the results showed that smoking, excessive salt intake, and suffering from hypertension complications were the risk factors for home hypertension self-assessment control. Knowledge of hypertension, regular follow-up, and meeting the standard of blood pressure in the office are the protective factors for the self-measured control of hypertension at home. It is known from numerous studies that increased salt intake can lead to increased water and sodium retention in the body, which in turn can lead to increased blood pressure. Hypertensive complications are malignant consequences of hypertension, and hypertensive complications can also feedback the status of hypertension, further aggravating the condition of hypertension [30–32]. For patients with hypertension at home, their awareness of hypertension is the basis for prompting

patients to reasonably control their hypertension. Regular follow-up by doctors can help patients conduct regular monitoring and control. In addition, meeting the standard of blood pressure detection in the office can help patients with hypertension to scientifically control their hypertension. Knowing the status of their own blood pressure control will also induce patients to measure their blood pressure control at home [33, 34]. The above results show that for hypertensive patients who control their blood pressure at home, they need to reduce the frequency of smoking, control their diet, and pay attention to their own hypertension complications. They also need to participate in surveys of regular follow-up visits by physicians.

To sum up, in the detection and control of hypertension, urging patients to participate in daily physical exercise, admonishing patients to quit smoking, and improving medication compliance can improve the control rate of hypertension in outpatient clinics. Blood pressure and regular follow-up surveys by doctors can effectively improve the control effect of blood pressure self-measurement at home in hypertensive patients and further improve the control rate of hypertension. There are still some limitations in the study. The selection of hypertensive patients is affected by regional and cultural factors, which makes the selection of relevant factors difficult to be universal. Therefore, in the follow-up research, the research scope needs to be gradually expanded, and the detection and control of hypertension should be discussed in depth.

This study starts with a large amount of data and studies the factors related to the compliance rate of hypertension detection control and self-test control in community clinics under the premise of eliminating gender factors, age factors, complication factors, family history factors, and others. It has great research significance and has a significant effect on improving the self-behavior management and quality of life of patients with hypertension. There are still some limitations in the study. There are regional cultural factors in the selection of hypertension patients, which makes the selection of relevant factors difficult to have universality. Therefore, in the follow-up study, the scope of the study needs to be gradually expanded, and the risk factors and protective factors of hypertension detection and control are discussed in depth.

Data Availability

The datasets used and/or analyzed during the current study are available from the corresponding author on reasonable request.

Conflicts of Interest

The authors declare no conflicts of interest.

Authors' Contributions

Zhigao Chen and Rui Xiong contributed equally to this work. They are co-first authors.

References

- [1] J. W. Wang, Q. L. Fan, and Y. Z. Xu, "Analysis on the prevalence of hypertension, prehypertension and hypertension control and influencing factors in Kazakh elderly herdsmen," *Modern Preventive Medicine*, vol. 46, no. 16, pp. 2965–2969+3000, 2019.
- [2] B. B. Li, Q. Mao, and Z. Y. Huang, "Analysis of the control of hypertension and its influencing factors in rugao city, jiangsu province," *Clinical Journal of Practical Hospitals*, vol. 18, no. 6, pp. 43–46, 2021.
- [3] J. J. Chu, W. Zhang, and R. Fang, "Study on the control and influencing factors of hypertension in communities in Bengbu City," *Journal of Bengbu Medical College*, vol. 45, no. 2, pp. 263–266, 2020.
- [4] S. J. Wang, Q. H. Gong, and S. X. Li, "Analysis of new-onset hypertension control and influencing factors among community residents in Ningbo City," *China Chronic Disease Prevention and Control*, vol. 29, no. 3, pp. 195–197, 2021.
- [5] J. Yan, Y. Yao, S. Yan, R. Gao, W. Lu, and W. He, "Chiral protein supraparticles for tumor suppression and synergistic immunotherapy: an enabling strategy for bioactive supramolecular chirality construction," *Nano Letters*, vol. 20, no. 8, pp. 5844–5852, 2020.
- [6] K. Jin, Y. Yan, M. Chen et al., "Multimodal deep learning with feature level fusion for identification of choroidal neovascularization activity in age related macular degeneration," *Acta Ophthalmologica*, vol. 100, no. 2, pp. 512–520, 2022.
- [7] H. K. Chopra and C. V. S. Ram, "Recent guidelines for hypertension: a clarion call for blood pressure control in India," *Circulation Research*, vol. 124, no. 7, pp. 984–986, 2019.
- [8] A. Paczkowska, K. Hoffmann, W. Bryl et al., "Obesity related hypertension- pharmacotherapy regimen and blood pressure control among young adult patients in Poland and Germany," *Acta Poloniae Pharmaceutica - Drug Research*, vol. 77, no. 5, pp. 815–822, 2020.
- [9] K. Kario, A. Sakima, and Y. Ohya, "STEP to estimate cardiovascular events by home blood pressure in the era of digital hypertension," *Hypertension Research*, vol. 45, no. 1, pp. 11–14, 2022.
- [10] Y. Gu, X. B. Zhang, and J. S. Zhou, "Influence of home blood pressure monitoring on medication compliance and blood pressure control in patients with essential hypertension," *Chinese Journal of Hypertension*, vol. 29, no. 8, pp. 772–775, 2021.
- [11] D. Zhao, L. Liu, and K. L. Margolis, "Cardiovascular events and costs after home blood pressure monitoring and pharmacist management in patients with uncontrolled hypertension," *Zhonghua Hypertension Journal*, vol. 28, no. 11, p. 1018, 2020.
- [12] Q. H. Li, L. Xia, and D. Liu, "A clinical study on optimizing the medication regimen to improve the control rate of hypertension," *Chongqing Medical Journal*, vol. 50, no. 20, pp. 3514–3517, 2021.
- [13] Z. Li, M. Teng, Y. Jiang et al., "YTHDF1 negatively regulates treponema pallidum-induced inflammation in THP-1 macrophages by promoting SOCS3 translation in an m6A-Dependent manner," *Frontiers in Immunology*, vol. 13, no. 13, Article ID 857727, 2022.
- [14] Y. F. Hu, Y. P. Ding, and H. Y. Lv, "The relationship between hypertension control and obesity in the elderly in Jiang'an District, Wuhan City," *Public Health and Preventive Medicine*, vol. 31, no. 5, pp. 135–138, 2020.
- [15] S. Raghavan, Y. L. Ho, V. Kini et al., "Association between early hypertension control and cardiovascular disease incidence in veterans with diabetes," *Diabetes Care*, vol. 42, no. 10, pp. 1995–2003, 2019.
- [16] M. F. Shapiro, S. B. Shu, N. J. Goldstein et al., "Impact of a patient-centered behavioral economics intervention on hypertension control in a highly disadvantaged population: a randomized trial," *Journal of General Internal Medicine*, vol. 35, no. 1, pp. 70–78, 2020.
- [17] R. Poggio, S. E. Melendi, A. Beratarrechea et al., "Cluster randomized trial for hypertension control: effect on lifestyles and body weight," *American Journal of Preventive Medicine*, vol. 57, no. 4, pp. 438–446, 2019.
- [18] A. Kollias, G. Katsimagklis, A. Mastrokostopoulos, and G. S. Stergiou, "Therapeutic approach for hypertension management and control in patients receiving olmesartan-based treatment: the "family" non-interventional study in primary care in Greece," *Journal of Hypertension*, vol. 39, no. Supplement 1, pp. e345–e346, 2021.
- [19] M. T. Mefford, P. Goyal, G. Howard et al., "The association of hypertension, hypertension duration, and control with incident heart failure in black and white adults," *Journal of Clinical Hypertension*, vol. 22, no. 5, pp. 857–866, 2020.
- [20] S. Xu, H. Tao, W. Cao et al., "Ketogenic diets inhibit mitochondrial biogenesis and induce cardiac fibrosis," *Signal Transduction and Targeted Therapy*, vol. 6, no. 1, p. 54, 2021.
- [21] N. R. Poulter, "Additive association of knowledge and awareness on control of hypertension: a cross sectional survey in rural India," *Journal of Hypertension*, vol. 39, no. 1, pp. 44–45, 2021.
- [22] C. A. Dézsi, M. Glezer, Y. Karpov, R. Brzozowska-Villatte, and C. Farsang, "Effectiveness of perindopril/indapamide single-pill combination in uncontrolled patients with hypertension: a pooled analysis of the fortissimo, forsage, aces and picasso observational studies," *Advances in Therapy*, vol. 38, no. 1, pp. 479–494, 2021.
- [23] D. Wang, F. Wang, K. H. Shi et al., "Lower circulating folate induced by a fidgetin intronic variant is associated with reduced congenital heart disease susceptibility," *Circulation*, vol. 135, no. 18, pp. 1733–1748, 2017.
- [24] S. P. Zheng, J. B. Jin, and X. Chen, "Analysis of the application effect of the community intensive management model in patients with uncontrolled hypertension," *Chinese Journal of General Practitioners*, vol. 18, no. 4, pp. 328–332, 2019.
- [25] M. Xie, Y. Zeng, and S. Q. Yuan, "The effect of the interaction between overweight/obesity and hyperhomocysteinemia on the pathogenesis of hypertension," *Chinese Journal of Disease Control*, vol. 25, no. 11, pp. 1269–1275, 2021.
- [26] X. H. Zhi, S. M. Duan, and Z. Zhang, "A systematic review of the effect of remote blood pressure monitoring by nurses on blood pressure control in urban hypertensive patients," *Nursing Research*, vol. 36, no. 6, pp. 966–972, 2022.
- [27] Y. Wu, Y. Zhang, and W. W. Tang, "Blood pressure status, prevalence of hypertension and its influencing factors in middle-aged people with positive family history of hypertension," *West China Medicine*, vol. 34, no. 9, pp. 1022–1027, 2019.
- [28] J. R. Hou, B. Liu, and L. F. Xie, "Effects of two antihypertensive drugs on early morning hypertension on blood pressure variability," *Shanxi Medicine Journal*, vol. 48, no. 23, pp. 2909–2911, 2019.
- [29] X. Zhang, Y. Y. Qu, L. Liu et al., "Homocysteine inhibits pro-insulin receptor cleavage and causes insulin resistance via

Review Article

Observation on the Clinical Efficacy of Traditional Chinese Medicine Non-Drug Therapy in the Treatment of Insomnia: A Systematic Review and Meta-Analysis Based on Computer Artificial Intelligence System

Jingqing Zhuang ¹, Jian Wu,² Liang Fan,³ and Chongnan Liang ¹

¹Department of Nursing, Haikou Hospital of Traditional Chinese Medicine, Haikou, Hainan 570216, China

²Department of Massage, Haikou Hospital of Traditional Chinese Medicine, Haikou, Hainan 570216, China

³Department of Quality Control, Haikou Hospital of Traditional Chinese Medicine, Haikou, Hainan 570216, China

Correspondence should be addressed to Chongnan Liang; liangchongnan66599@163.com

Received 8 September 2022; Accepted 24 September 2022; Published 11 October 2022

Academic Editor: Ashish Khanna

Copyright © 2022 Jingqing Zhuang et al. This is an open access article distributed under the Creative Commons Attribution License, which permits unrestricted use, distribution, and reproduction in any medium, provided the original work is properly cited.

Objective. Insomnia is a common and frequently occurring disease affecting the health of the population, which can seriously affect the work and life of patients. Drug treatment of insomnia has a rapid onset of action but has a large adverse reaction incidence rate. Traditional external treatment of traditional Chinese medicine (TCM) belongs to a type of non-drug therapy, the treatment of insomnia has a long history, but the methods of non-drug treatment of TCM are diverse, and the efficacy is also different. This study investigated the efficacy of TCM non-drug therapy in the treatment of insomnia by means of literature search and meta-analysis. **Methods.** We searched Embase, Pubmed, OVID, WOS, CNKI, and CBM for randomized controlled trials (RCTs) on the use of TCM as a non-drug treatment for primary insomnia. After doing a literature search according to the inclusion and exclusion criteria, we used Cochrane rob v2.0 to assess the potential for bias in the studies that were included, and we did a combined analysis and assessment of the effectiveness of the therapy. **Results.** 16 articles were included in this study for quantitative analysis, and a total of 1285 patients participated in the study, including 643 patients in the intervention group and 642 patients in the control group. Meta-analysis showed that non-drug therapy of TCM could improve the treatment response rate of insomnia patients [$OR = 6.88$, 95%CI (4.40,10.74), $Z = 8.48$, $P < 0.0001$], reduce post-treatment PSQI total score [$MD = -3.42$, 95%CI (-4.62, -2.22), $Z = -5.60$, $P < 0.0001$], and improved patient anxiety [$SMD = -1.25$, 95%CI (-2.13, -0.37), $Z = -2.78$, $P = 0.01$] and degree of depression [$SMD = -1.53$, 95%CI (-2.84, -0.21), $Z = -2.28$, $P = 0.02$]. The heterogeneity survey showed that treatment time was one of the sources of heterogeneity. Meta-regression analysis revealed that publication year, patient age, sample size, and intervention characteristics were not specific factors affecting the combined results. **Discussion.** TCM non-drug therapy (acupuncture, moxibustion, massage, and auricular point pressing beans) can significantly improve the PSQI score of patients after treatment and improve the degree of anxiety and depression of patients, with significant effect, which is worthy of clinical promotion.

1. Introduction

Insomnia is characterized by difficulty falling asleep, easy awakening, and early awakening; it is a common and frequently occurring disease in clinical practice. According to epidemiological surveys, about 25%–30% of adults meet the diagnostic criteria of insomnia [1]. Insomnia is especially

likely to occur in the elderly, women, family history, life stress, anxiety, perfectionism, and psychological diseases, and its predisposing factors include physical, psychological, environmental, lifestyle, drugs, and other factors [2]. The treatment of insomnia emphasizes comprehensive treatment, and identifying the cause is the key to the treatment of insomnia, while sleep hygiene education, psychotherapy,

TABLE 1: Baseline conditions of participating study patients. Basic characteristics of the informed consent form.

Factors	Number of patients (%)
Gender (%)	
Male	31 (88.5)
Female	4 (11.5)
Median age, years (range)	50 (34–72)
Median follow-up months	14
Median time interval between initial and reirradiation	51 (12–240)

physical therapy, drug therapy, and traditional Chinese medicine (TCM) treatment are used to achieve the purpose of improving sleep quality, increasing effective sleep time, and restoring normal life and work [3]. Drug treatment for insomnia has a rapid onset of action but has a large adverse reaction incidence rate [4]. Related studies [5] have found that non-drug therapy for insomnia has the advantages of significant efficacy, high safety, and less adverse reactions, so the study of non-drug therapy for insomnia has become one of the hotter topics in recent years. Non-drug therapy mainly includes modern medical therapy and traditional external treatment of TCM. Modern medical therapy includes cognitive behavioral therapy, relaxation therapy, music therapy, and Morita therapy. Traditional external treatment of TCM includes acupuncture, auricular point pressing beans, massage, and other methods [6]. Insomnia belongs to the category of “sleeplessness” in TCM, and TCM has a long history of treating insomnia, but the methods of non-drug treatment in TCM are diverse and the efficacy varies [7]. There was not a significant change in PSQI score (Pittsburgh sleep quality index) between patients and controls after 4 weeks of acupuncture therapy, according to a paper written by Wang et al. [8]. The study was conducted on patients with insomnia. The PSQI score of insomnia patients following acupuncture therapy was substantially different from that of the control group, according to a controlled clinical investigation that was conducted by Yin et al. [9]. The study was conducted in a hospital setting. As a result of the aforementioned dispute, we decided to carry out this meta-analysis research in order to investigate whether or not quantitative meta-analysis is an effective way for resolving it.

2. Materials and Methods

2.1. Database and Search Strategy. We searched Embase, Pubmed, OVID, WOS, CNKI, and CBM databases until April 2022 for articles related to the treatment of primary insomnia with TCM using a keyword free search strategy containing: “TCM,” “Traditional Chinese medicine,” “Acupuncture,” “Massage,” “Chronic insomnia,” and “Primary insomnia.” Baseline conditions of participating study patients are shown in Table 1.

2.2. Inclusion Criteria. (1) Class of research: the works that we looked at were all randomized controlled trials (RCTs), and there were no language restrictions placed on them. (2) Study subjects: all study subjects were patients with continuous insomnia for more than one month and poor sleep

quality, were over the age of 18, and were clinically diagnosed with insomnia [10]. (3) The intervention group: using TCM, it can be an intervention measure in acupuncture, moxibustion, decoction, Chinese patent medicine, and massage. (4) The control group: sham treatment or no intervention or general traditional western medicine treatment measures were taken. (5) The results of the study showed that the intervention group treatment results are effective. (6) Outcome indicators: it is possible to offer at least one outcome indicator, such as the response rate, the score on the Pittsburgh sleep quality index (PSQI), the recurrence rate, anxiety, depression, the incidence of adverse reactions, and comprehensive post-intervention data.

2.3. Exclusion Criteria. Exclusion criteria include the following: (1) patients who suffer from non-primary insomnia such as those whose sleeplessness is brought on by conditions such as maintenance blood diseases, menopause in women, cancer-related issues, moderate to severe anxiety disorders, moderate to severe depression, convalescent strokes, Parkinson’s disease, schizophrenia, and other medical conditions. The following types of research will not be considered: (2) literatures on combined Chinese and Western medicine treatment in interventions; (3) investigations, case analyses, and reviews of non-randomized controlled studies will not be considered; (4) studies with missing outcome indicators, unavailable data, or untransformable data will not be considered (Figure 1).

2.4. Screening of Literature. After literature retrieval, the repeated literatures were excluded by software. Two researchers read the title and abstract, screened according to the inclusion and exclusion criteria, and obtained the full text of the remaining literatures. If the original text could not be obtained from the Internet, the author of the original text was contacted, read the full text of the literatures, and further screened.

2.5. Interview Participants. Interview participants will be invited from 5 practices from each of the three trial recruitment centres. The practices will be selected to reflect a range of practice types (e.g., based on practice size or membership of a consortium). One practice nurse, one trial participant, and one practice manager or GP will be interviewed from each selected practice. We have added further information to clarify.

Informed Consent Form

Please take a moment to read our informed consent before completing the form. We thank you for your support in helping us conduct this clinical research study.

Title of Study

Purpose of Study

Principal Investigator Email

Name

First	Last

Date

I have read all the information and am willing to participate in the clinical research study.

Signature

FIGURE 1: Informed consent form template.

2.6. Data Extraction. Two researchers independently extracted literature data: literature author, publication year and month, grouping method, number of cases in each group, patient age, gender ratio, initial *PSQI* score, duration of insomnia, intervention measures, treatment time, follow-up time, and outcome indicators. After data extraction was completed by both researchers, each other's results were cross-checked and discrepancies were discussed and finalized.

2.7. Statistical Methods. (1) Effect sizes were reported as Odd Ratio (*OR*) with 95%CI for discrete variables; (2) effect sizes were reported using Mean Difference (*MD*) or Standard Mean Difference (*SMD*) with 95%CI for continuous variables; (3) comparisons were performed using forest plot descriptive statistics; (4) literature heterogeneity was analyzed using I^2 analysis and *Q* test with $I^2 > 50\%$ or $P < 0.1$ indicating heterogeneity of the results; (5) if there was no heterogeneity between the literature, it was calculated by Mantel-haenszel method; if there was heterogeneity between the literatures, it was calculated by Dersimonian-Laird method; (6) heterogeneity survey: subgroup analysis was used to investigate heterogeneity; (7) meta-regression analysis: meta-regression analysis was used to investigate factors that were significant for effect size; (8) sensitivity analysis: detect literature with the greatest impact on effect size; and (9) detect publication bias using Egger's test and present using funnel plot.

3. Results

3.1. Literature Screening Results. The literature selection flow chart is shown in Figure 2, 1100 articles were initially

retrieved, and after de-duplication and screening, 16 articles were finally included in the quantitative analysis, as shown in Table 2.

3.2. Literature Quality and Bias Evaluation. In this study, the literature [22] grouped according to the order of admission and did not strictly use the random sequence process, which may have a large bias; all other literatures described the generation method of random sequence (using permuted block randomization method or computer random sequence generation method). Literatures [17–23, 25, 26] did not describe allocation concealment method and blinding method; others used sealed opaque envelopes to conceal numbers and implemented blinding method. All literatures recorded dropout cases in detail, without significant selective reporting bias and other biases. The overall quality was excellent, as shown in Figure 3.

3.3. Meta-Analysis Results

3.3.1. Effective Rate of TCM Non-Drug Therapy Acting on Primary Insomnia. In the literatures [13–15, 17, 18, 21–24], a total of 9 literatures reported the effective rate after intervention. There was no statistical heterogeneity between the literatures ($I^2 = 49\%$, $P = 0.05$), using fixed effect mode, and meta-analysis showed that TCM non-drug therapy could improve the effective rate of insomnia patients [$OR = 6.88$, 95%CI (4.40,10.74), $Z = 8.48$, $P < 0.0001$], as shown in Figure 4.

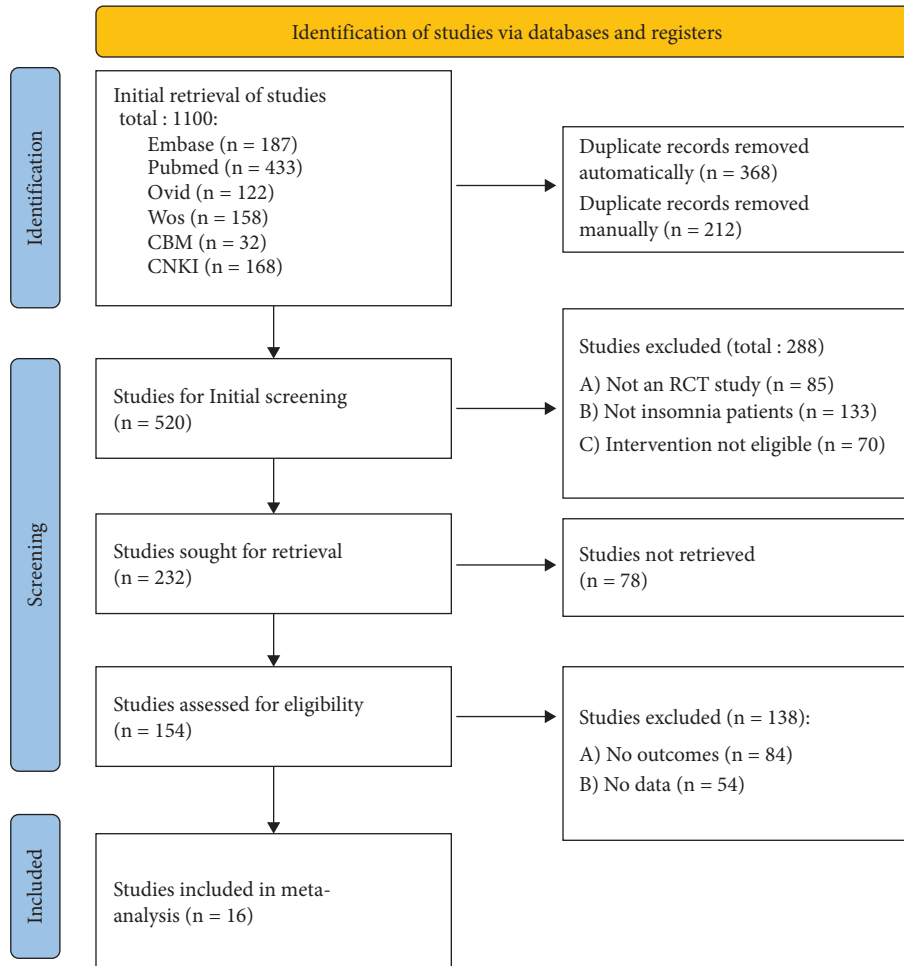


FIGURE 2: Literature selection flow chart.

3.3.2. *Effect of TCM Non-Drug Therapy on PSQI Index in Patients with Primary Insomnia.* PSQI indicators after intervention were reported in all 12 literatures [8, 9, 13–19, 21, 25, 26], and there was statistical heterogeneity between the literature ($I^2 = 98\%$, $P < 0.01$), using random effect model, and meta-analysis statistics showed that TCM non-drug therapy could reduce the total PSQI score after treatment [$MD = -3.42$, 95%CI (-4.62, -2.22), $Z = -5.60$, $P < 0.0001$], as shown in Figure 5.

3.3.3. *Effect of TCM Non-Drug Therapy on Other Indicators in Patients with Primary Insomnia.* 3 articles [13, 14, 16] reported the recurrence rate after treatment, 4 articles reported the degree of anxiety and depression of patients after treatment, and 3 articles reported the incidence of adverse reactions after treatment, as shown in Table 3.

3.3.4. *Investigation of Sources of Heterogeneity.* In the analysis of PSQI indicators, there was statistical heterogeneity between the literatures ($I^2 = 98\%$, $P < 0.01$). Subgroup analysis was performed for the literatures according to “intervention method,” “control group method,” and “intervention time.” The heterogeneity test between subgroups

after grouping only “intervention time” showed $P < 0.05$, indicating that “intervention time” was one of the sources of heterogeneity in this study, as shown in Table 4.

3.3.5. *Meta-Regression Analysis.* In the analysis of PSQI index, we regressed pooled ES using “publication year of literature,” “study sample size,” “mean age,” and “intervention method + control group method + treatment time” and found that the P values of the effects of these four factors on PSQI index ES were 0.32, 0.90, 0.15, and 0.23. That means none of these factors could linearly affect the results of the meta-analysis (Figure 6).

3.3.6. *Sensitivity Analyses.* Our impact analysis on the combined effect size of PSQI outcome indicators showed that the literature [18] was the most influential literature, and excluding these two articles, the combined effect size of PSQI outcome indicators remained statistically significant, showing good stability of the results (good sensitivity) as shown in Figure 7.

3.3.7. *Publication Bias Analysis.* For the pooled effect analysis of PSQI outcome indicators, publication bias was

TABLE 2: Basic characteristics, intervention measures, treatment time, and outcome indicators of included literatures.

Author and publication date	Number of cases	Number (E/C)	Age (years)	Intervention category	Intervention measures	Control intervention	Treatment time	Rehabilitation index
Wang et al. [8] 2021	75	37/38	57.9 ± 8.76	Acupuncture	Acupoints: HT 7 and KI 7	Sham treatment	3 weeks	②
Yin et al. [9] 2017	72	36/36	39.7 ± 12.9	Acupuncture	Acupoints: Baihui (GV20), Shenting (GV24), Yintang (GV29), Bilateral Anmian (EX-HN22), Bilateral Shenmen (HT7), Bilateral Sanyinjiao (SP6)	Sham treatment	4 weeks	②⑤⑥
Chen et al. [13] 2018	60	30/30	45.3 ± 11.2	Moxibustion	Pricking and penetrating moxibustion therapy	Conventional treatment	3 weeks	①②
Gao et al. [14] 2013	116	57/59	40 ± 13	Moxibustion	Moxibustion at Baihui (GV20) and Sishengcong (EX-HN1)	Conventional treatment	3 weeks	①②
Zhang et al. [15] 2020	96	48/48	37.9 ± 14.1	Acupuncture	Acupoints: Anmian (EX-HN22), nNeiguan (PC6), Shenmen (HT7), Hegu (L4), Zusanli (ST36), Zhaohai (KI6), Shenmai (BL62) and Taichong (LR3)	Sham treatment	4 weeks	①②③⑤⑥
Liu et al. [16] 2021	60	30/30	47.17 ± 14.08	Acupuncture	Acupoints: Baihui (GV20), Yintang (GV29), Shenmen (HT7, bilateral), and Sanyinjiao (SP6, bilateral)	Sham treatment	4 weeks	②⑤⑥
Huo et al. [17] 2013	60	30/30	46.00 ± 10.7	Acupuncture	Acupoints: Baihui (DU20), bilateral Zusanli (ST36), Neiguan (PC6), Shenmen (HT7), Sanyinjiao (SP6), Taichong (LR3), and Yongquan (KI1)	Conventional treatment	4 weeks	①②
Zhang et al. [18] 2017	80	40/40	37.45 ± 4.25	Acupuncture	Acupuncture and moxibustion points: Shenmen, Neiguan, Fengchi, Taichong, Xingjian, Zusanli, Taixi, and Sanyinjiao points	Sham treatment	8 weeks	①②
Yin et al. [19] 2020	60	30/30	47.3 ± 14.9	Electroacupuncture	Baihui (GV20), Shenting (GV24), Yintang (GV29), Bilateral Anmian (EX-HN22), Shenmen (HT7), Sanyinjiao (SP6), and Neiguan (PC6)	Sham treatment	8 weeks	②③⑤⑥
Xing et al. [20] 2020	63	31/32	54.45 ± 12.1	Electroacupuncture	Acupuncture points used were DU-20, EX-HN1, EX-HN22, SP-6, HT-7, PC-6, BL-62, and KI-6	Conventional treatment	4 weeks	⑤⑥
Fan et al. [21] 2019	99	50/49	68.52 ± 5.38	Acupuncture	Acupuncture: Acupuncture at Anmian point	Conventional treatment	4 weeks	①②③④

TABLE 2: Continued.

Author and publication date	Number of cases	Number (E/C)	Age (years)	Intervention category	Intervention measures	Control intervention	Treatment time	Rehabilitation index
Wang et al. [22] 2005	78	40/38	NR	Acupuncture	Acupuncture and moxibustion points: the main points are Zhaohai and Shenmai. Acupoints: according to syndrome differentiation, liver stagnant fire type to take Neiguan, Xingjian, Ganshu; phlegm-heat internal disturbance type to take Shenmen, Neiguan, Gongsun, Fenglong; Yin deficiency and fire excess type to take Taixi, Xinshu, Shenshu; heart and spleen deficiency type to take Xinshu, Pishu, Zusanli, sanyinjiao; heart and gallbladder qi deficiency type to take Daling, Danshu, Ganshu, Yin Xie	Sham treatment	2 weeks	①
He et al. [23] 2019	60	30/30	41.4 ± 11.0	Acupuncture + auricular point pressing	Acupuncture points: Shanggen, Yintang, Anmian, Xingjian (bilateral), Taichong (double side) Auricular point pressing beans: select Shenmen, sympathetic, subcortical, heart and liver as the main acupoints	Conventional treatment	4 weeks	①
Huang et al. [24] 2011	84	44/40	44.6 ± 12.5	Massage	Foot bath + plantar massage	Conventional treatment	2 weeks	①
Pang et al. [25] 2015	160	80/80	45.83 ± 9.02	Massage	Acupoints on head: Yangbai, Benshen, Head Lin Weeping, Zhengying, Chengling, Rugu, Tianchong, Bubai, Tip Yin, Fengchi	Conventional treatment	4 weeks	②
Zhong et al. [26] 2015	80	40/40	33.0 ± 4.1	Massage	Acupressure	Conventional treatment	3 weeks	②⑤

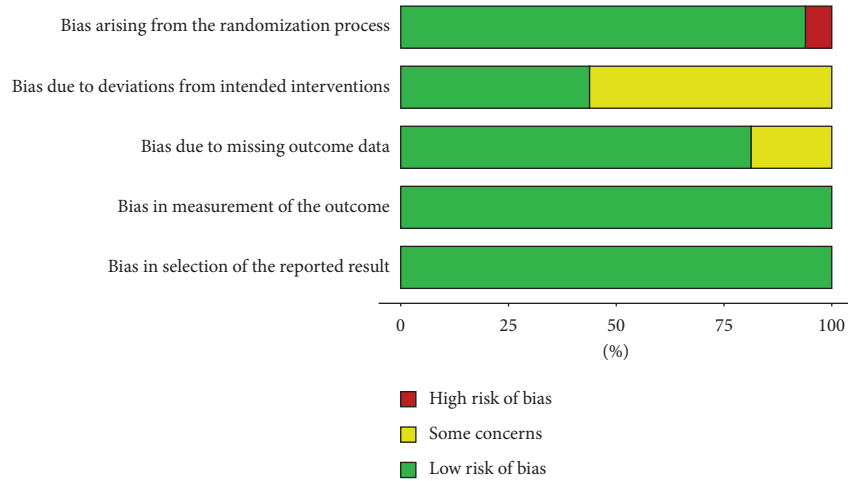


FIGURE 3: Bias analysis of randomized controlled intervention based on ROB 2.0.

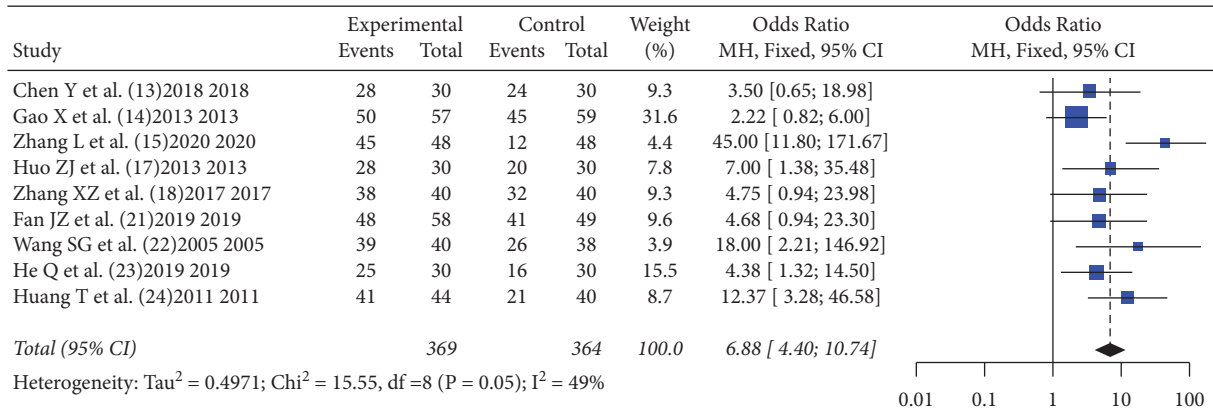


FIGURE 4: Effect of TCM non-drug therapy on the treatment efficiency of patients with primary insomnia.

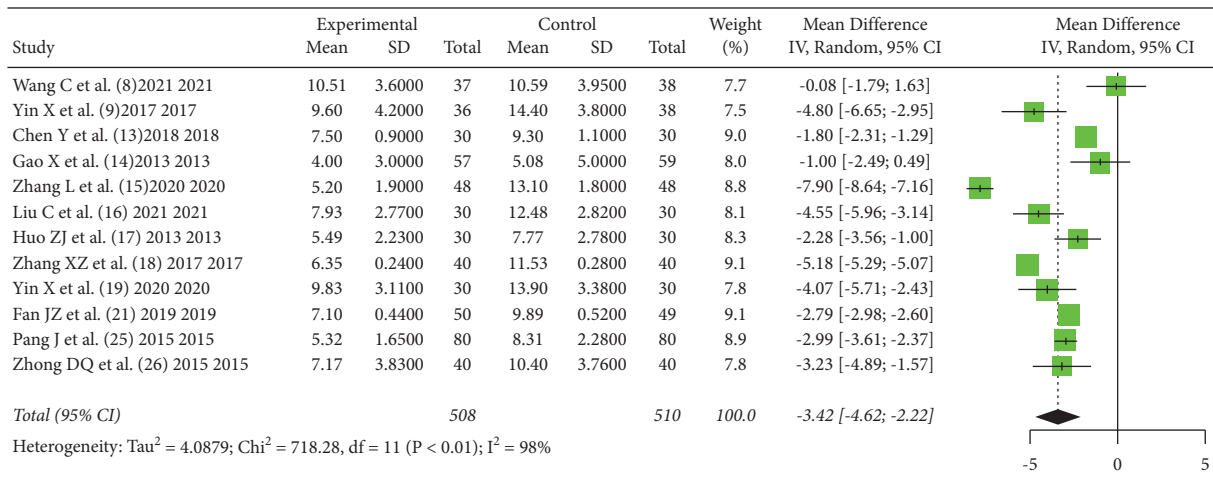


FIGURE 5: Effect of TCM non-drug therapy on PSQI score of patients with primary insomnia after treatment.

TABLE 3: Meta-analysis results of other outcome indicators.

Factors	Reported literature	Literature number	Analysis mode	I^2 C with P value	Effect size	Pooling value	Z, P value
Relapse rate	21, 23	2	Random effect mode	85.8% with 0.008	OR	0.04[0.00, 0.97]	-1.98, 0.05
Anxiety level	9, 15-16, 19-20, 26	6	Random effect mode	93.0% with 0.001	SMD	-1.25[-2.13, -0.37]	-2.78, 0.01
Degree of depression	9, 15-16, 19-20	5	Random effect mode	95.5% with 0.001	SMD	-1.53[-2.84, -0.21]	-2.28, 0.02
Incidence of adverse reactions	14-15, 21	3	Random effect mode	54.0% with 0.11	OR	0.47[0.11, 2.04]	-1.02, 0.31

TABLE 4: Subgroup analysis of PSQI indicators.

No.	Grouping method	Subgroup	Literature number	Heterogeneity		P value
				I^2	P	
1	Intervention methods	Acupuncture	7	94.5%	<0.001	0.08
		Moxibustion	3	88.6%	0.05	
		Massage	2	0	0.99	
2	Control group method	Sham intervention	6	94.3%	<0.001	0.05
		Traditional treatment	6	74.2%	0.04	
		3 weeks	4	61.0%	0.03	
3	Intervention time	4 weeks	6	97.2%	<0.001	0.0001
		8 weeks	2	42.6%	—	

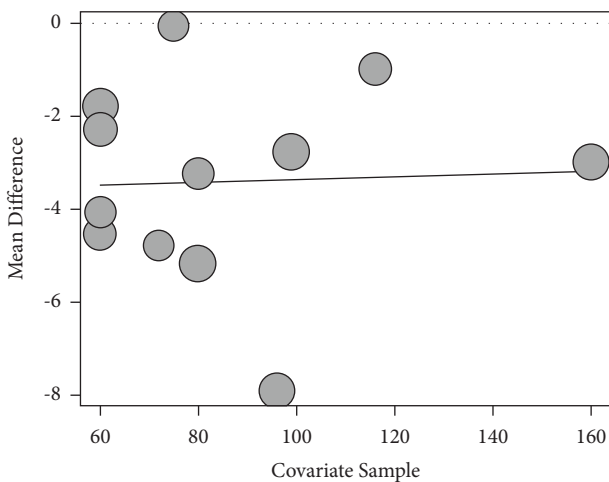


FIGURE 6: Meta-regression analysis of PSQI score outcome indicators: publication year factor.

detected by Egger’s test: $P = 0.30$, which did not indicate the existence of asymmetry in the funnel plot, which is shown in Figure 8.

4. Discussion

At present, the main means of insomnia treatment is drug therapy, sedative hypnotics represented by benzodiazepines are effective, but adverse reactions are obvious, long-term medication can lead to psychomotor impairment, memory impairment, drug addiction, aggravation of depression and rebound insomnia after withdrawal, and other negative effects. In addition, it is easy to produce adverse reactions such as fatigue, dizziness, and drowsiness [27, 28]. Physical

therapy emerging in recent years has been able to improve sleep quality in patients to varying degrees with less adverse reactions, but it has not been clinically promoted because its mechanism of action is not clear [29]. TCM characteristic therapy has been gradually paid attention and widely used in the treatment of insomnia, especially the traditional external treatment of TCM such as acupuncture and massage developed on the basis of the theory of meridians and viscera in TCM, which has the advantages of good clinical efficacy and less adverse reactions [30].

In this study, 16 high-quality RCT studies with a total of 1285 participants were included, and the results showed that non-drug therapy of TCM (acupuncture, moxibustion, massage, and auricular point pressing beans) could significantly improve the PSQI score of patients after treatment, the effective rate was significantly higher than that of the control group, and the improvement of anxiety and depression was better than that of the control group. Acupuncture therapy is the most widely used, long-standing treatment and is clinically mainly based on dialectical acupoint selection but also using specific acupoints for treatment. The main points mainly take Baihui, Sishencong, Shenmen, Sanyinjiao, hypnosis, and so on. At the same time, a group of matching points were selected based on syndrome differentiation: if the liver stagnated fire, Taichong, Fengchi, Yanglingquan, and Zhimen points were taken; if the phlegm-heat internal disturbance, Fenglong, Houxi, Shenmai, Daling, and Lidui points were taken; if the heart and spleen were deficient, Neiguan, Zusanli, Xinshu, and Pishu points were taken; if the *yin* deficiency and fire flourishing, Taixi, Taichong, Xinshu, Shenshu, Zhaohai, Daling, and Fuliu points were taken [8, 9, 15–18]. Acupuncture can regulate viscera in the treatment of insomnia and has the

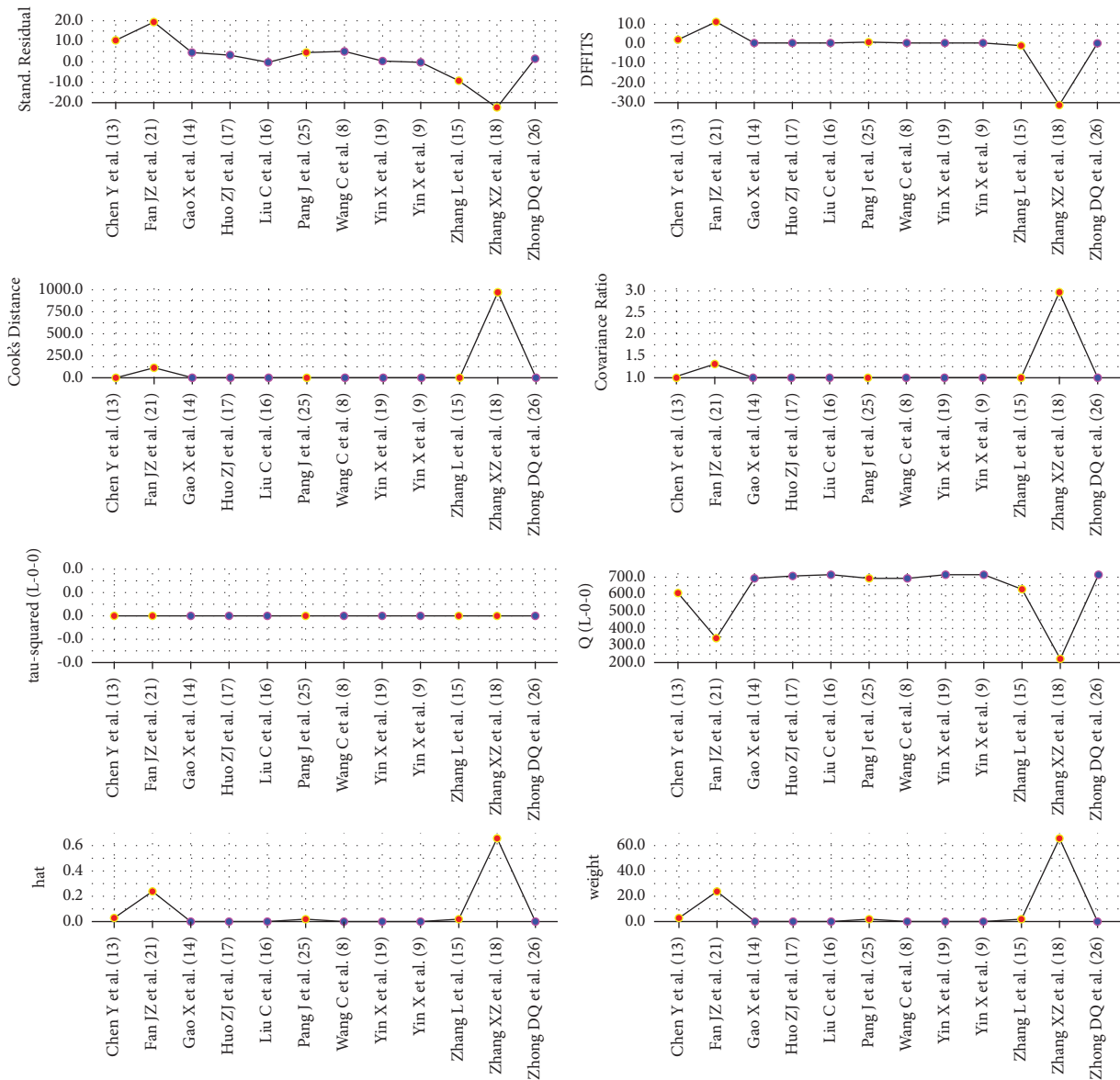


FIGURE 7: PSQI score effect size impact analysis.

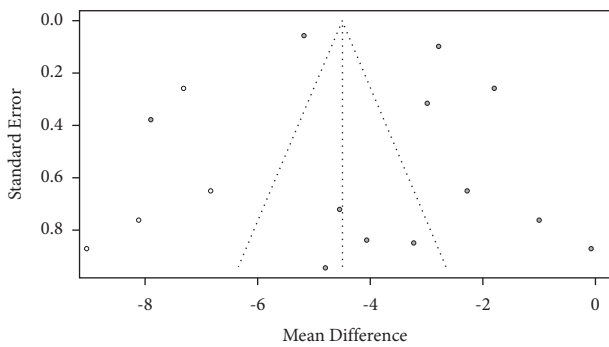


FIGURE 8: Funnel plot for PSQI outcome indicators.

advantages of safety and no side effects. Massage is also commonly used in the treatment of insomnia, manipulation mostly acts on the head of the human body, healers often massage with acupuncture, so that the effect is significantly

and lasting. Massage therapy for insomnia is to use certain techniques to stimulate the fixed parts of the human body and play a role in stimulating meridians and *qi* and balancing *yin* and *yang*. In addition, it can dredge *qi* and blood, improve tissue oxygen supply, and regulate the relative balance of excitation and inhibition of the nervous system. Repeated stimulation of the head and face with gentle maneuvers can excite peripheral nerves, increase blood circulation in the head and face, improve brain tissue nutrition, and play a role in inhibiting the central nervous system, ultimately achieving tranquilizing purposes [24–26]. Moxibustion uses the heat of fire to give the patient warm stimulation of the human body, through the action of meridians, to achieve the effect of improving insomnia [13, 14]. Other methods such as auricular acupressure, acupoint injection, cupping, and fumigation are effective, but there is a lack of clinical controlled studies, so this study was not included.

Although all studies with subjects with non-primary insomnia (women with menstrual insomnia, tumor-induced insomnia, post-stroke insomnia) were strictly screened out in this study, significant heterogeneity between the literature was still observed when combining the analyses. In this study, subgroup analysis was performed according to different interventions, and it was found that although the interventions taken in the literature were different and the interventions in the control group were also different, the intervention methods were not the cause of heterogeneity, but the treatment time contributed the most to heterogeneity and was one of the sources of heterogeneity. We failed to find all the heterogeneity contributors, and statistically significant heterogeneity remained within the subgroups after passing through the subgroup groups, the source of which may be related to the characteristics of the different participants.

We tried to find factors affecting the combined results by meta regression analysis but did not find statistically significant factors. According to the impact analysis, the literature [18] contributed the most to the difference in the results, but excluding the literature [18] did not change the combined results of the meta-analysis, which indicated that this analysis was stable.

In this study, it was also found that there was no significant difference in the recurrence rate and incidence rate of adverse reactions between the observation group and the control group, but there were still too few literatures included for these two indicators.

In this study, the funnel plot showed that both sides were symmetrically distributed, suggesting that the publication bias was small (which was also confirmed by Egger's test). However, there are still some literatures with high risk of bias included in this meta-analysis, and there are still few literatures included in each intervention method. Therefore, RCT studies with larger sample size are still required to be further explored for the study on this topic.

A total of 1285 patients were included in 16 literatures in this meta-analysis. The results showed that TCM non-drug therapy (acupuncture, moxibustion, massage, and auricular point pressing) could significantly improve the *PSQI* score of patients after treatment, with an effective rate significantly higher than that of the control group, and the improvement of anxiety and depression was better than that of the control group. However, due to the small number of articles included in this study, randomized controlled studies with larger sample sizes remain to be explored in depth on this topic. On the other hand, the influence of commonly used anti infective drugs or anti-tumor drugs on the mental state of patients also deserves attention [11, 12, 31–33].

Data Availability

The data used in this study are available from the author upon request.

Disclosure

Jingqing Zhuang and Jian Wu are co-first authors.

Conflicts of Interest

The authors declare that there are no conflicts of interest.

Authors' Contributions

Jingqing Zhuang and Jian Wu contributed equally to this work.

Acknowledgments

This work was supported by the Hainan Medical and Health Research Project (No: 20A200307).

References

- [1] L. Culpepper, "Insomnia: a primary care perspective," *Journal of Clinical Psychiatry*, vol. 66, no. 9, pp. 14–17, 2005.
- [2] J. N. O'Byrne, M. Berman Rosa, J. P. Gouin, and T. Dang-Vu, "Neuroimaging findings in primary insomnia," *Pathologie Biologie*, vol. 62, no. 5, pp. 262–269, 2014.
- [3] S. Salter and S. Brownie, "Treating primary insomnia - the efficacy of valerian and hops," *Australian Family Physician*, vol. 39, no. 6, pp. 433–437, 2010.
- [4] M. T. Samara, M. Huhn, V. Chiocchia et al., "Efficacy, acceptability, and tolerability of all available treatments for insomnia in the elderly: a systematic review and network meta-analysis," *Acta Psychiatrica Scandinavica*, vol. 142, no. 1, pp. 6–17, 2020.
- [5] J. A. Dopheide, "Insomnia overview: epidemiology, pathophysiology, diagnosis and monitoring, and non-pharmacologic therapy," *American Journal of Managed Care*, vol. 26, no. 4, pp. S76–S84, 2020.
- [6] W. F. Yeung, K. F. Chung, K. C. Tso, S. P. Zhang, Z. J. Zhang, and L. M. Ho, "Electroacupuncture for residual insomnia associated with major depressive disorder: a randomized controlled trial," *Sleep*, vol. 34, no. 6, pp. 807–815, 2011.
- [7] X. L. Yan, Y. D. Yu, and D. D. Yang, "Clinical efficacy of acupuncture combined with modified Xiangfu Decoction in treatment of menopausal insomnia cause by liver Qi stagnation," *Zhongguo Zhongyao Zazhi*, vol. 45, no. 6, pp. 1460–1464, 2020.
- [8] C. Wang, W. L. Xu, G. W. Li et al., "Impact of acupuncture on sleep and comorbid symptoms for chronic insomnia: a randomized clinical trial," *Nature and Science of Sleep*, vol. 13, pp. 1807–1822, 2021.
- [9] X. Yin, M. Gou, J. Xu et al., "Efficacy and safety of acupuncture treatment on primary insomnia: a randomized controlled trial," *Sleep Medicine*, vol. 37, pp. 193–200, 2017.
- [10] M. L. Perlis and S. D. Youngstedt, "The diagnosis of primary insomnia and treatment alternatives," *Comprehensive Therapy*, vol. 26, no. 4, pp. 298–306, 2000.
- [11] D. J. Buysse, C. F. Reynolds 3rd, T. H. Monk, S. R. Berman, and D. J. Kupfer, "The pittsburgh sleep quality index: a new instrument for psychiatric practice and research," *Psychiatry Research*, vol. 28, no. 2, pp. 193–213, 1989.
- [12] J. A. C. Sterne, J. Savović, M. J. Page et al., "RoB 2: a revised tool for assessing risk of bias in randomised trials," *BMJ*, vol. 366, p. 14898, 2019.
- [13] C. Yan, G. Xiyan, and S. Cuiying, "Pricking and penetrating moxibustion therapy in patients with refractory insomnia: a randomized and controlled clinical trial," *Journal of Traditional Chinese Medicine*, vol. 38, no. 5, pp. 754–762, 2018.

- [14] X. Gao, C. Xu, P. Wang et al., “Curative effect of acupuncture and moxibustion on insomnia: a randomized clinical trial,” *Journal of Traditional Chinese Medicine*, vol. 33, no. 4, pp. 428–432, 2013.
- [15] L. Zhang, Y. Tang, R. Hui et al., “The effects of active acupuncture and placebo acupuncture on insomnia patients: a randomized controlled trial,” *Psychology Health & Medicine*, vol. 25, no. 10, pp. 1201–1215, 2020.
- [16] C. Liu, Y. Zhao, S. Qin, X. Wang, Y. Jiang, and W. Wu, “Randomized controlled trial of acupuncture for anxiety and depression in patients with chronic insomnia,” *Annals of Translational Medicine*, vol. 9, no. 18, p. 1426, 2021.
- [17] Z. J. Huo, J. Guo, and D. Li, “Effects of acupuncture with meridian acupoints and three Anmian acupoints on insomnia and related depression and anxiety state,” *Chinese Journal of Integrative Medicine*, vol. 19, no. 3, pp. 187–191, 2013.
- [18] X. Z. Zhang, “Clinical control study on acupuncture combined with traditional Chinese medicine in the treatment of insomnia of liver depression and fire transformation type,” *Liaoning Journal of traditional Chinese medicine*, vol. 44, no. 1, pp. 143–145, 2017.
- [19] X. Yin, W. Li, H. Wu et al., “Efficacy of electroacupuncture on treating depression-related insomnia: a randomized controlled trial,” *Nature and Science of Sleep*, vol. 12, pp. 497–508, 2020.
- [20] J. Xing, X. Wu, H. Liu et al., “Effects of electroacupuncture therapy and cognitive behavioral therapy in chronic insomnia: a randomized controlled study,” *Evidence-based Complementary and Alternative Medicine*, vol. 2020, Article ID 5630130, 12 pages, 2020.
- [21] J. Z. Fan, J. Y. Xiong, and X. He, “Clinical study on the treatment of senile insomnia with Yangxin Hewei Yimian decoction combined with acupuncture at Anmian point,” *Chinese Journal of traditional Chinese medicine*, vol. 37, no. 2, p. 4, 2019.
- [22] S. G. Wang, “Clinical observation on insomnia treated mainly by acupuncture according to Haishen pulse,” *China acupuncture*, vol. 25, no. 11, p. 2, 2005.
- [23] Q. He, Y. F. Yang, and C. L. Wu, “A clinical trial of treatment of primary insomnia of patients with qi-stagnation constitution by shallow acupuncture combined with ear-acupoint pellet-pressing,” *Zhen Ci Yan Jiu*, vol. 44, no. 4, pp. 293–296, 2019.
- [24] T. Huang, Q. Y. Zhou, and X. L. Li, “Effect of Chinese medicine foot bath combined with plantar massage on sleep quality of insomniacs,” *Chinese Journal of practical nursing*, vol. 27, no. 3, p. 2, 2011.
- [25] J. Pang, Z. Chen, and H. L. Tang, “A multicenter randomized controlled clinical study of massage of Shaoyang meridian in the treatment of insomnia,” *Chinese Journal of traditional Chinese medicine*, vol. 30, no. 10, pp. 3788–3790, 2015.
- [26] D. Q. Zhong, X. J. Jiang, and D. F. Zeng, “Application of progressive relaxation training combined with acupoint massage in patients with chronic insomnia and emotional disorders,” *Chongqing Medical Journal*, vol. 44, no. 27, pp. 3829–3832, 2015.
- [27] X. Yin, W. Li, T. Liang et al., “Effect of electroacupuncture on insomnia in patients with depression: a randomized clinical trial,” *JAMA Network Open*, vol. 5, no. 7, Article ID e2220563, 2022.
- [28] N. Jing, W. Bin, W. Fuzhuang et al., “Effectiveness and safety of auricular acupoint bloodletting in treatment of insomnia: an assessor-blinded pilot randomized controlled trial,” *Journal of Traditional Chinese Medicine*, vol. 38, no. 5, pp. 763–768, 2018.
- [29] X. Wen, Q. Wu, J. Liu et al., “Randomized single-blind multicenter trial comparing the effects of standard and augmented acupuncture protocols on sleep quality and depressive symptoms in patients with depression,” *Psychology Health & Medicine*, vol. 23, no. 4, pp. 375–390, 2018.
- [30] L. C. Li, H. J. Xing, Y. Liang et al., “Comparison of therapeutic effects between thermosensitive moxibustion and medication in the treatment of insomnia of liver- qi stagnation pattern,” *Zhen Ci Yan Jiu*, vol. 43, no. 9, pp. 573–575, 2018.
- [31] X. Cheng, F. Huang, K. Zhang, X. Yuan, and C. Song, “Effects of none-steroidal anti-inflammatory and antibiotic drugs on the oral immune system and oral microbial composition in rats,” *Biochemical and Biophysical Research Communications*, vol. 507, no. 1–4, pp. 420–425, 2018.
- [32] X. Cheng, F. He, M. Si, P. Sun, and Q. Chen, “Effects of antibiotic use on saliva antibody content and oral microbiota in sprague dawley rats,” *Frontiers in Cellular and Infection Microbiology*, vol. 12, Article ID 721691, 2022.
- [33] X. Cheng, Q. Chen, and P. Sun, “Natural phytochemicals that affect autophagy in the treatment of oral diseases and infections: a review,” *Frontiers in Pharmacology*, vol. 13, Article ID 970596, 2022.

Research Article

Artificial Intelligence Algorithm-Based Feature Extraction of Computed Tomography Images and Analysis of Benign and Malignant Pulmonary Nodules

Yuantong Gao , **Yuyang Chen**, **Yuegui Jiang**, **Yongchou Li**, **Xia Zhang**, **Min Luo**, **Xiaoyang Wang**, and **Yang Li**

Department of Radiology, The Third Affiliated Hospital of Wenzhou Medical University, Rui'an, Wenzhou 325200, Zhejiang, China

Correspondence should be addressed to Yuantong Gao; b1230125@stu.cpu.edu.cn

Received 3 July 2022; Revised 15 August 2022; Accepted 25 August 2022; Published 14 September 2022

Academic Editor: Ashish Khanna

Copyright © 2022 Yuantong Gao et al. This is an open access article distributed under the Creative Commons Attribution License, which permits unrestricted use, distribution, and reproduction in any medium, provided the original work is properly cited.

This study was aimed to explore the effect of CT image feature extraction of pulmonary nodules based on an artificial intelligence algorithm and the image performance of benign and malignant pulmonary nodules. In this study, the CT images of pulmonary nodules were collected as the research object, and the lung nodule feature extraction model based on expectation maximization (EM) was used to extract the image features. The Dice similarity coefficient, accuracy, benign and malignant nodule edges, internal signs, and adjacent structures were compared and analyzed to obtain the extraction effect of this feature extraction model and the image performance of benign and malignant pulmonary nodules. The results showed that the detection sensitivity of pulmonary nodules in this model was 0.955, and the pulmonary nodules and blood vessels were well preserved in the image. The probability of burr sign detection in the malignant group was 73.09% and that in the benign group was 8.41%. The difference was statistically significant ($P < 0.05$). The probability of malignant component leaf sign (69.96%) was higher than that of a benign component leaf sign (0), and the difference was statistically significant ($P < 0.05$). The probability of cavitation signs in the malignant group (59.19%) was higher than that in the benign group (3.74%), and the probability of blood vessel collection signs in the malignant group (74.89%) was higher than that in the benign group (11.21%), with statistical significance ($P < 0.05$). The probability of the pleural traction sign in the malignant group was 17.49% higher than that in the benign group (4.67%), and the difference was statistically significant ($P < 0.05$). In summary, the feature extraction effect of CT images based on the EM algorithm was ideal. Imaging findings, such as the burr sign, lobulation sign, vacuole sign, vascular bundle sign, and pleural traction sign, can be used as indicators to distinguish benign and malignant nodules.

1. Introduction

In recent years, with changes in living environments and habits, cancer has become an important disease endangering human health. Approximately 5,161 people died of cancer last year, according to the Ministry of Health. In terms of the number of deaths caused by cancer, lung cancer ranks first in China [1]. At present, research on the causes and pathogenesis of lung cancer is probably related to smoking cigarettes, living environment, eating habits, patients' own basic chronic diseases, and genetic factors [2, 3]. Lung cancer is a common malignant tumor mainly caused by bronchial

mucosal lesions. Therefore, after the onset of lung cancer, patients mainly present with throat and lung discomfort, such as cough, chest pain, dysphonia, and other symptoms, which may also be accompanied by various complications, such as lung inflammation and malignant pleural effusion. The symptoms and precursors of lung cancer are related to its metastasis and progression [4]. The progression of lung cancer includes primary lung cancer, intrathoracic expansion of primary lung cancer, and metastasis to other sites of lung cancer [5]. The symptoms and precursors are mainly the following kinds. The first is primary lung cancer. Patients with primary lung cancer often have symptoms of cough and

expectoration, which is characterized by irritant dry cough. The effect of cough suppressants is not obvious, and yellow purulent expectoration is associated with infection [6]. The second chapter is primary lung cancer with intrathoracic expansion. Patients may have hoarseness because the cancer compresses the recurrent laryngeal nerve. It may also be due to the metastasis of lung cancer cells to the mediastinum, the formation of mediastinal tumors, or mediastinal lymph node enlargement, resulting in compression of the esophagus and swallowing difficulties. The third chapter is lung cancer metastasis. Metastasis of lung cancer cells to corresponding tissues or organs will produce corresponding functional disorders, such as metastasis to the thoracic vertebra and the formation of bone tumors, which will cause pain in the thoracic vertebra [7, 8]. The progression of lung cancer in each period has the following precursor. First is a chronic cough. Patients often present with recurrent dry cough and a high metallic sound. The second is fever, with lung cancer fever at approximately 38°C. The third is hemoptysis, mostly with blood in sputum or intermittent blood sputum, occasionally with massive hemoptysis [9]. The fourth is dyspnea. Patients manifested chest tightness and asthma, and some patients exhibited chest pain. Fifth, lymphadenopathy may occur for unknown reasons. Unexplained emaciation may also occur [10].

Pulmonary nodules are a common clinical sign, mostly round or irregular lesions with a diameter ≤ 3 cm in the lung, which can be single or multiple with clear or unclear boundaries [11]. The early stage of lung cancer is often characterized by pulmonary nodules, so the detection of pulmonary nodules plays a vital role in the diagnosis and treatment of lung cancer. At present, the examination methods of pulmonary nodules mainly rely on imaging methods, and different examination methods have their own advantages and disadvantages. In clinical practice, chest X-ray and computed tomography (CT) scans are usually the main examination methods, and CT examination is the main means for the detection and follow-up observation of pulmonary nodules [12]. Chest CT, as a noninvasive examination, is currently recognized as the most reliable and sensitive imaging examination method for pulmonary diseases. Compared with the X-ray film, the density resolution is significantly improved. In addition, CT images show the anatomical structure of the human cross section, which can provide more valuable information for the accurate localization of pulmonary nodules. Therefore, chest CT scans have an irreplaceable advantage over X-ray in the examination of lung diseases [13, 14]. Clinical evaluation and follow-up of pulmonary nodules mainly rely on CT scanning, especially high-resolution CT (HRCT), which can clearly show the location and morphological characteristics of nodules, so it is the preferred method for the detection and evaluation of pulmonary nodules at present [15]. Conventional CT scans can judge benign and malignant pulmonary nodules according to their morphology and density as well as the relationship between pulmonary nodules and adjacent tissues, with low specificity. Enhanced CT scans can reflect the blood supply of lesions to a certain extent, and the blood supply of malignant lung tumors is more abundant than that

of most benign nodules [16]. In addition, with the rapid development of radiographic imaging technology in recent years, an increasing number of imaging techniques, such as enhanced scanning, energy spectrum technology, perfusion imaging, and magnetic resonance examination, have been applied in the detection, benign and malignant determination, and disease staging of pulmonary nodules. This provides more information for further detection and accurate diagnosis of pulmonary nodules [17].

In this study, an artificial intelligence algorithm was applied to extract CT image features of pulmonary nodules, and the accuracy of the algorithm model extraction and classification was compared and verified. On this basis, the imaging performance of benign and malignant pulmonary nodules was observed to provide a reference for the clinical diagnosis of pulmonary nodules.

2. Materials and Methods

2.1. The Research Object. This was a retrospective experiment, and the CT image data of pulmonary nodules in the hospital from December 2019 to December 2021 were collected as the research object. There were a total of 298 patients with a total of 330 nodules, including 167 males and 131 females, ranging from 25 to 73 years old with an average age of 61.12 ± 10.46 years. There were 223 malignant nodules (malignant group) and 107 benign nodules (benign group). The experiment was approved by the ethics committee of the hospital.

Inclusion criteria were as follows: (i) all patients were confirmed by thoracic surgery or clinical follow-up and had an accurate pathological diagnosis and definite clinical diagnosis results. (ii) The patient's CT image was clear, and the focus was clear, which was conducive to labeling. (iii) The relevant clinical data of patients were complete.

Exclusion criteria were as follows: (i) patients with pulmonary nodules who had not been pathologically confirmed or clinically diagnosed; (ii) incomplete patient data; (iii) the patient's CT image parameters did not meet the requirements, and the definition was not enough.

2.2. The Research Methods. The CT imaging data of patients with pulmonary nodules were collected as the research objects. Based on the original lung nodule image, the EM algorithm [18] was used to extract the image features of lung nodules. The detection sensitivity and nodule feature extraction of the model were observed and recorded and compared with the existing pulmonary nodule classification model to judge its classification efficiency. On this basis, the imaging characteristics of patients with lung nodules were observed, the structural characteristics of benign and malignant lung nodules were compared and analyzed, and the imaging characteristics of benign and malignant lung nodules were summarized. The specific experimental process is shown in Figure 1.

2.3. Pulmonary Nodule Detection. The images containing pulmonary nodules were input into the flow and processed by the first five groups of convolutional neural networks of

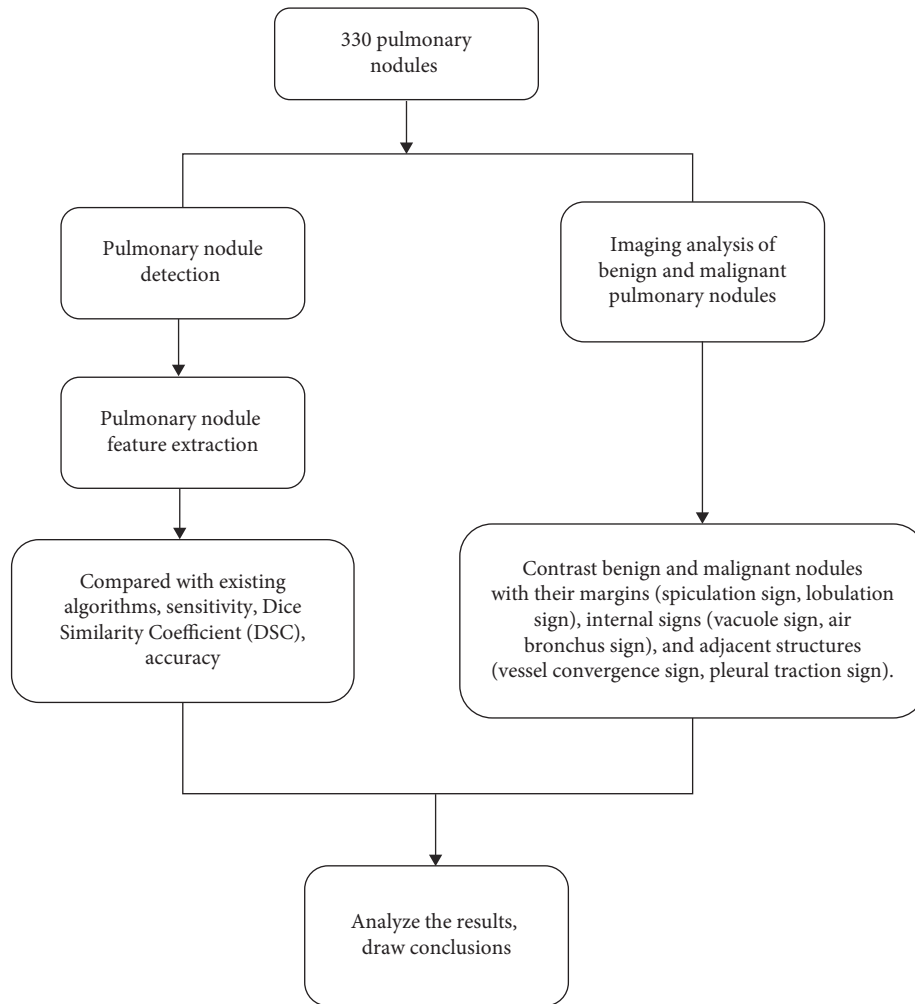


FIGURE 1: Technology roadmap.

the ResNet50 network model, and the characteristic images of pulmonary nodules were obtained after processing. After the feature image, twelve anchor boxes generated by the RPN neural network sliding window were used for further processing to lock the area where the pulmonary nodules were located. The RPN neural network further eliminated the repeated regions in the selected regions, and the remaining regions after elimination were regions of interest (ROIs). The ROI containing location information was classified and regressed to obtain the probability value and location coordinates of pulmonary nodules [19].

2.4. Pulmonary Nodule Extraction. First, the lung parenchyma image was acquired, and the segmentation process was as follows. Binarization, domain filling, image fusion, and other operations were used for the basic lung CT images, and the lung binarization image of Figure 2(a), chest binarization image of Figure 2(b), and chest image of Figure 2(c) were successively obtained. Figure 2(c) was subtracted from Figure 2(b) to obtain the binarization image of the lung parenchyma. Mask and fusion were performed to obtain the final image of the lung parenchyma. Next, the

initial contour mask image of the lung nodule was generated according to the position coordinates of the lung nodule, and then, the initial contour image of the lung nodule was generated by fusion with the lung parenchyma image (Figure 2).

Next, the initial contour mask image of pulmonary nodules was generated according to the position coordinates of pulmonary nodules and then fused with the pulmonary parenchyma image to generate the initial contour map of pulmonary nodules. An expectation-maximization algorithm (EM) was used to segment the initial contour of pulmonary nodules. The steps were (1) initializing the distribution parameters; (2) according to the known distribution parameters, the expected value P of the optimal hidden variable was inferred through the training data set; (3) making maximum likelihood estimation on the basis of P and obtaining the distribution parameter M ; and (4) circulating steps (2) and (3) until the expected value was reached to obtain the accurate contour map of pulmonary nodules [20]. The relevant equations of specific steps (2) and (3) are as follows.

The measured data are a , the unmeasured data are b , and the sum of a and b is complete data, represented by y . M is a

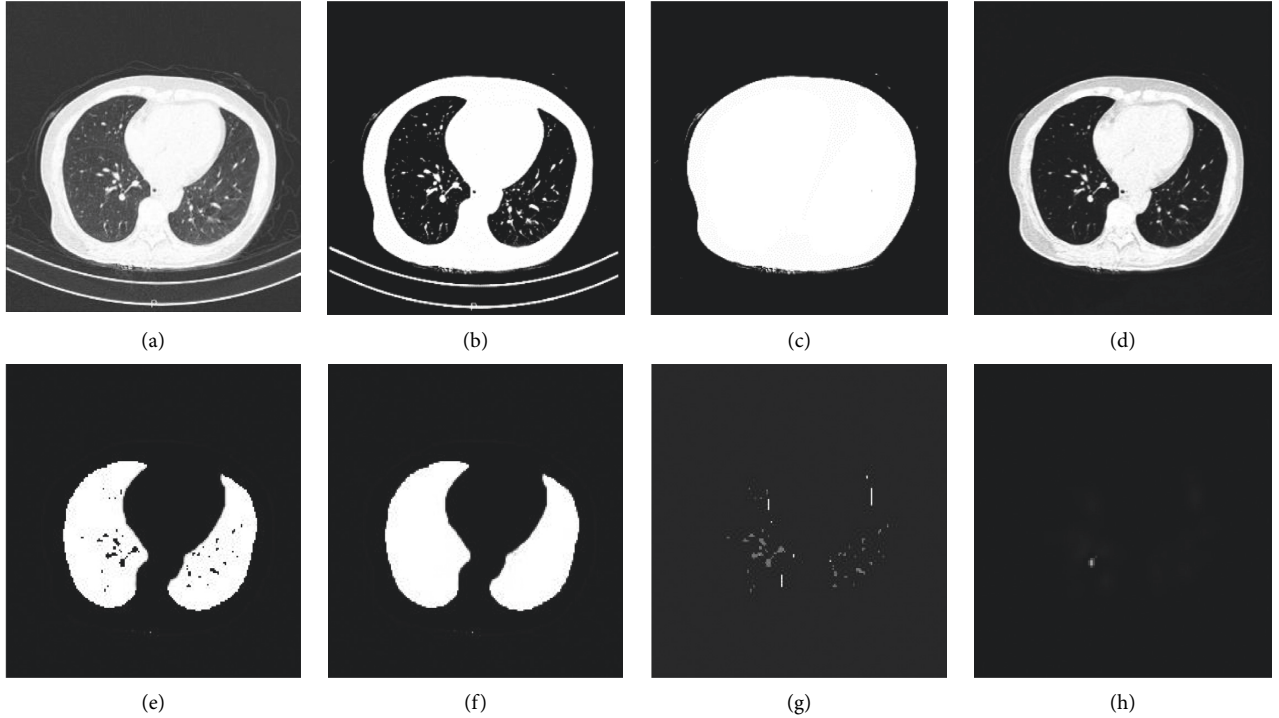


FIGURE 2: Effect drawings of lung parenchyma image segmentation at each stage. (a) CT image of lung; (b) binarized lung CT image; (c) thoracic image; (d) chest cavity image; (e) binarized lung parenchyma image; (f) pulmonary parenchyma mask; (g) lung parenchyma image; (h) initial contour of lung nodules.

distribution parameter, the joint probability of complete data y is $x(a, b|M)$, and the logarithmic likelihood function $Z(a, M)$ of a can be expressed as

$$Z(a, M) = \log y(a | M) = \int Z(a, b | M) d_b. \quad (1)$$

Then, the maximum likelihood estimation of M is shown in the following equation:

$$Z_{\max}(a, M) = \log y(a, b/M). \quad (2)$$

When iterated $n + 1$ times, the expectation $T(M|M(n))$ of the logarithmic likelihood function $Z(a, M)$ of y is shown in the following equation:

$$T(M|M(n)) = E\{Z_{\max}(M; y)|a; M(n)\}. \quad (3)$$

When iterated $n + 1$ times, $M(n + 1)$ is expressed as

$$M(n + 1) = \arg_M \max T(M|M(n)). \quad (4)$$

2.5. Image Representation Analysis. The images of pulmonary nodules processed by the algorithm were observed. The marginal (spiculation sign and lobulation sign), internal (vacuole sign and bronchial inflation sign), and adjacent structures (vessel convergence sign and pleural traction sign) of benign and malignant nodules were compared.

2.6. Observation Indicators. The Dice similarity coefficient (DSC) and accuracy were calculated. Benign and malignant nodule margins (spiculation sign and lobulation sign),

internal signs (vacuole sign and bronchial inflation sign), and adjacent structures (vessel convergence sign and pleural traction sign) were calculated. The DSC calculation is shown in (5), where m_1 represents the image of lung nodules segmented by the gold standard, and m_2 represents the image segmented by the algorithm.

$$DSC = \frac{2(m_1 \cap m_2)}{|m_1| + |m_2|} \times 100\%. \quad (5)$$

2.7. Statistical Methods. SPSS 20.0 was used for data analysis. The χ^2 test was used for disordered variables, and Spearman rank correlation was used for ordered variables. $P < 0.05$ suggested that the difference was statistically significant.

3. Results

3.1. Analysis of Pulmonary Nodule Detection Results. The total number of nodules was 330. In this study, the pulmonary nodule detection model based on the ES algorithm model detected 315 nodules, with a sensitivity of 0.955, which was higher than the existing three types of pulmonary nodule detection models (Table 1). The free-response ROC (FROC) curve can measure the performance of the pulmonary nodule detection system, and the coordinates indicate the sensitivity of the system. The FROC curves and scores of the number of false positives in each case were compared. The FROC values of the pulmonary nodule detection model, ETROCAD model, M5LCAD model, and ZNET model in this study were 0.841, 0.665, 0.597, and

TABLE 1: Sensitivity of three existing pulmonary nodule detection models.

Model	Sensitivity	Proposed year
ETROCAD	0.929	2011
M5LCAD	0.768	2015
ZNET	0.915	2016

0.803, respectively. Therefore, the sensitivity of the model in this study was higher than that of the other three models (Figure 3).

3.2. Analysis of Extraction Results of Pulmonary Nodules. By comparing the image segmentation effects of the two existing algorithms, it was found that the segmentation of the EM algorithm model considered the similarity between image pixel features and well-preserved pulmonary nodules and blood vessels (Figure 4). In addition, from the DSC curves of the three segmentation methods, the EM algorithm model had the maximum DSC (Figure 5).

3.3. Comparison of Manifestations of Benign and Malignant Pulmonary Nodules. Figure 6 shows the images of some benign and malignant nodules. The images of the two groups were compared, and it was found that the edges of benign pulmonary nodules were mostly smooth and had no surrounding burrs or fewer burrs, while the edges of malignant pulmonary nodules were uneven and mostly had burrs, and the overall shape of nodules was irregular.

The imaging findings of the benign and malignant groups were compared. In the malignant group, the probabilities of the spiculation sign, lobulation sign, vacuole sign, vessel convergence sign, and pleural traction sign were 73.09%, 69.96%, 59.19%, 74.89%, and 17.49%, respectively. The probabilities of the spiculation sign (8.41%), lobulation sign (0), vacuole sign (3.74%), vessel convergence sign (11.21%), and pleural traction sign (4.67%) were higher than those of the benign group. The difference was statistically significant, $P < 0.05$. However, there was no statistically significant difference in the bronchial inflation sign between the two groups ($P > 0.05$). The details are shown in Table 2 and Figure 7.

4. Discussion

Lung cancer is a relatively common respiratory malignant tumor disease, and the most common clinical manifestations of this disease include expectoration, hemoptysis, fever, chest distress, and chest pain. However, as the above symptoms do not have classical specificity and most patients usually have no obvious clinical symptoms in the early stage, it is difficult to detect them in the early stage [21]. Lung cancer is classified into blame small cell lung cancer and small cell lung cancer and is classified into inchoate lung cancer, metaphase lung cancer, and terminal lung cancer according to local severity cent. Lung cancer is classified into four stages and nine small stages according to tumor size, lymph node metastasis, and distant metastasis [22].

Currently, the diagnostic methods for lung cancer include sputum cytology, thoracotomy exploration, X-ray examination, CT examination, and mediastinoscopy, which can distinguish pulmonary tuberculosis, pulmonary infection, and benign tumors [23]. Pulmonary nodules refer to pulmonary nodular lesions found in CT image examination. According to the size, shape, progression rate, and imaging characteristics of pulmonary nodules, the benign and malignant properties and etiology of pulmonary nodules can be predicted. Pulmonary nodules less than 10 mm have only a 1% possibility of malignancy, while the malignant degree of pulmonary nodules reaching 20 mm is greatly increased [24]. If pulmonary nodules are detected, attention should be given to the nature of the nodules, and it is necessary to actively look for the cause and perform a differential diagnosis. Regular review should be implemented for pulmonary nodules requiring continuous observation. Pulmonary nodules may be benign, such as pulmonary hamartoma, pulmonary infection, and pulmonary tuberculosis, or malignant, such as lung cancer and lung metastasis, depending on the external appearance and some characteristic values of the nodules. The early stage of lung cancer is often characterized by pulmonary nodules, so the detection of pulmonary nodules plays a crucial role in the diagnosis and treatment of lung cancer [25].

Computerized tomography (CT) is a disease detection instrument with relatively complete functions. It can measure the human body according to the difference in X-ray absorption and transmittance of different tissues of the human body and then use highly sensitive instruments to measure the human body. After the data are processed by the electronic computer, the cross section or three-dimensional image of the inspected part can be obtained [26]. CT plays an important role in assisting doctors in diagnosing diseases. In recent years, with the progress of the computer level, an increasing number of artificial intelligence algorithms have been developed, and they are applied in the medical field to help doctors diagnose diseases accurately and efficiently. Among them, the ES algorithm proposed by Dempster, Laird, and Rubin is an unsupervised learning algorithm. This algorithm finds the potential information in the data by iteration, which is conducive to solving the optimization problem of hidden variables. By iteration, it finds the maximum likelihood estimation of parameters from the probability model and then obtains the information of hidden variables [27]. Therefore, in this study, the ES algorithm was used to extract the features of pulmonary nodule images, and its extraction effect was tested. The test results showed that the detection sensitivity of the ETROCAD model proposed by scholars in 2011 was 0.929 and that of the M5LCAD model proposed in 2015 was 0.768. The detection sensitivity of the ZNET model proposed in 2016 was 0.915, and the calculated sensitivity of the detection model based on the ES algorithm was 0.955, which was higher than those of the above three detection models. The higher the sensitivity is, the smaller the number of missed pulmonary nodules. Therefore, the model based on the ES algorithm in this study showed certain advantages in the initial detection stage of pulmonary nodules. In the aspect of

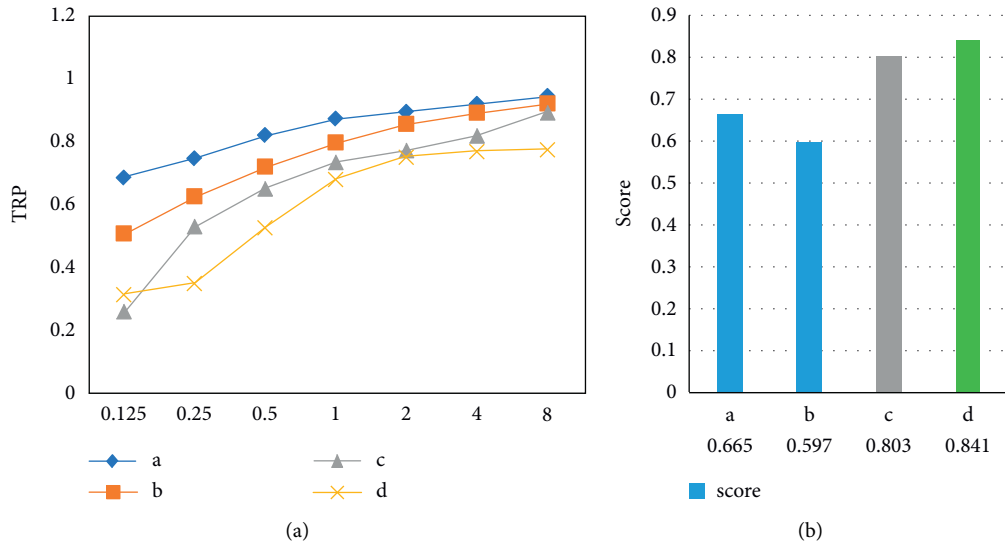


FIGURE 3: Comparison of ROC curve and ROC curve scores of four types of pulmonary nodule detection models. (a) ROC curve of the four types of models; (b) corresponding ROC curve score. a: ETROCAD model; b: M5LCAD model; c: ZNET model; d: model based on ES algorithm.

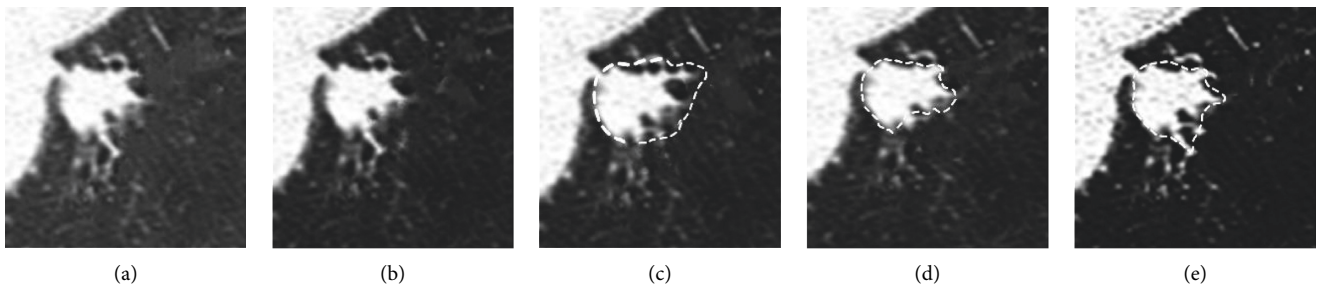


FIGURE 4: Comparison of segmentation effects of different segmentation methods. (a) Original nodule image; (b) gold standard image; (c) LBF model image; (d) ACM model image; (e) EM model image.

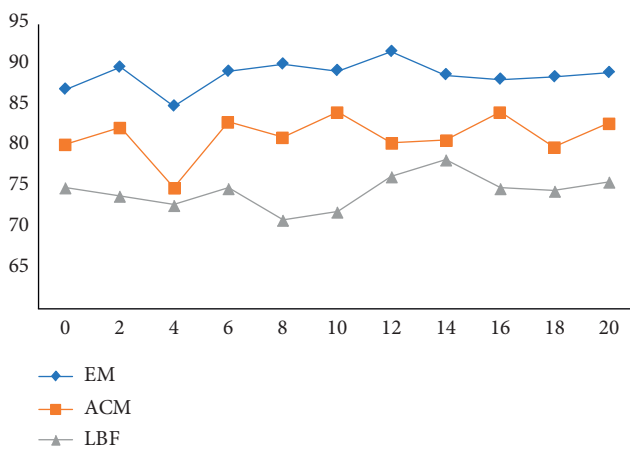


FIGURE 5: DSC curves of the three segmentation methods.

lung nodule image segmentation, the image segmentation effects of the LBF model and dACM model were compared. The LBF model algorithm was not very effective in segmenting pulmonary nodules with vascular adhesion, while the ACM model algorithm had some errors in separating the

edges of ground-glass nodules. The main reason was that these two methods were more concerned with the distance between pixels, while the information of pixels themselves was less. The segmentation of the EM algorithm model in this study considered the similarity between image pixel features and preserved lung nodules and blood vessels well. The DSC value can reflect the difference between the algorithm segmentation and the gold standard segmentation. The higher the DSC value is, the higher the overlap between the image segmented by the algorithm and the image segmented by the gold standard [28]. Compared with the LBF model and ACM model, the EM algorithm model had the highest DSC, which indicates that the image segmentation effect was the best. In addition, based on the extraction of the above imaging features of pulmonary nodules, a comparative analysis of the imaging manifestations of benign and malignant pulmonary nodules was performed. The comparative results showed that the probability of burr sign and lobulation sign in the malignant group was 73.09% and 69.96%, respectively. However, in the benign group, the probability of the burr sign was 8.41%, and the probability of the lobulation sign was 0. The difference was statistically

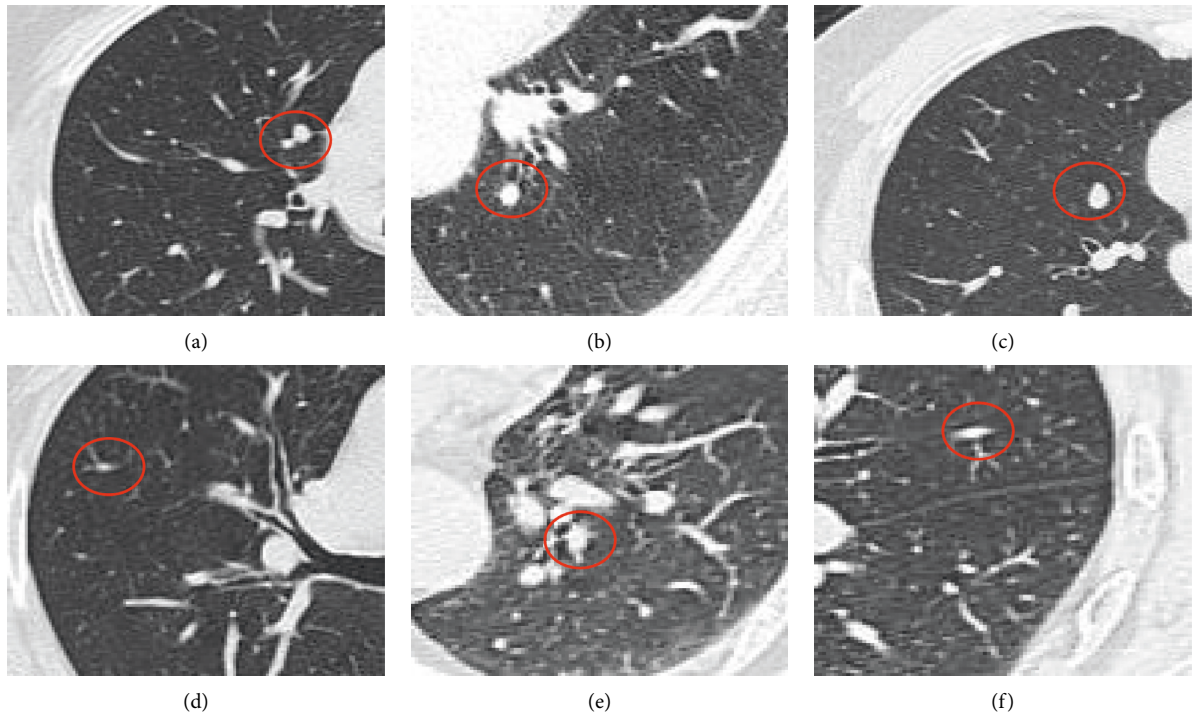


FIGURE 6: CT images of benign and malignant pulmonary nodules. The marked red areas in (a), (b), and (c) indicated benign nodules; the marked red areas in (d), (e), and (f) diagrams indicated malignant nodules.

TABLE 2: Comparison of benign and malignant pulmonary nodules.

Manifestations	Benign group (107)		Malignant group (223)		χ^2	P
	Exist	Proportion (%)	Exist	Proportion (%)		
Spiculation sign	9	8.41	163	73.09	17.325	$P < 0.001$
Lobulation sign	0	0	155	69.96	36.484	$P < 0.001$
Vacuole sign	4	3.74	132	59.19	19.502	$P < 0.001$
Air bronchus sign	14	11.21	31	13.90	0.124	0.089
Vessel convergence sign	5	4.67	167	74.89	39.790	$P < 0.001$
Pleural traction sign	0	0	39	17.49	4.639	0.041

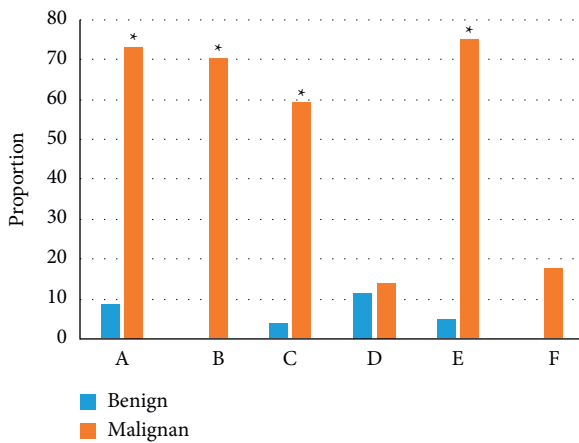


FIGURE 7: Proportion of benign and malignant pulmonary nodules. A, B, C, D, E, and F represent the burr sign, lobulation sign, vacuole sign, bronchial inflation sign, vascular set number sign, and pleural traction sign, respectively. *Compared with benign group, $P < 0.05$.

significant ($P < 0.05$). Compared with benign pulmonary nodules, the images of malignant pulmonary nodules often showed uneven edges and burrs. Among them, the burr sign refers to radial lines with different lengths and thicknesses distributed around the nodules. However, the burr sign is not unique to malignant nodules; it can also be seen in some benign nodules. Foliage refers to the uneven outline of nodules, showing a concave-convex shape composed of continuous arcs. The results showed that lobulation was unique to malignant nodules, but the research results of other related scholars showed that lobulation can also appear in a few benign nodules. The reason for this difference may be the limited experimental observation samples. The cavitation sign refers to a small (< 5 mm) and irregular transparent area in the nodule. In this study, the detection probability of the cavitation sign in the malignant nodule group was 59.19% and that in the benign nodule group was 3.74%, which was significantly higher than that in the benign nodule group. Therefore, cavitation signs can be used as one

of the diagnostic manifestations of lung cancer. The vascular bundle sign refers to the small blood vessels around the nodules that expand and are pulled to gather at the lesion and interrupt or pass through it at the lesion. The results showed that the probability of the vascular bunching sign in the malignant group was 74.89%, which was much higher than that in the benign group (4.67%), indicating that there were small blood vessels around most malignant nodules, which can be used as one of the manifestations to distinguish between benign and malignant nodules. Pleural traction refers to the linear or curtain shadow between the nodule and the adjacent pleura. The probability of pleural traction was 0 in the benign group and 17.49% in the malignant group, but this result was inconsistent with the existing research, which shows that some benign nodules also had pleural traction.

5. Conclusion

The imaging features of benign pulmonary nodules are usually smooth edges with no burrs or fewer burrs around them, while those of malignant pulmonary nodules are usually uneven edges with burrs, and there are small (<5 mm) and irregular bright areas inside the nodules, small blood vessels around the nodules or linear or curtain shadows between the nodules, and the adjacent pleura. The feature extraction and classification of pulmonary nodule images based on the ES algorithm had high sensitivity, and the image segmentation effect was good. Pulmonary nodule images based on the ES algorithm can be widely applied to the processing of clinical pulmonary nodule images, thus reducing the workload of doctors and improving the accuracy of diagnosis.

Data Availability

The data used to support the findings of this study are available from the corresponding author upon request.

Conflicts of Interest

The authors declare that there are no conflicts of interest.

References

- [1] M. B. Schabath and M. L. Cote, "Cancer progress and priorities: lung cancer," *Cancer Epidemiology, Biomarkers & Prevention*, vol. 28, no. 10, pp. 1563–1579, 2019.
- [2] P. Villalobos, "Lung cancer biomarkers," *Hematology-Oncology Clinics of North America*, vol. 31, no. 1, pp. 13–29, 2017.
- [3] R. Ruiz-Cordero and W. P. Devine, "Targeted therapy and checkpoint immunotherapy in lung cancer," *Surgical Pathology Clinics*, vol. 13, no. 1, pp. 17–33, 2020.
- [4] H. Hoy, T. Lynch, and M. Beck, "Surgical treatment of lung cancer," *Critical Care Nursing Clinics of North America*, vol. 31, no. 3, pp. 303–313, 2019.
- [5] F. Nasim, B. F. Sabath, and G. A. Eapen, "Lung cancer," *Medical Clinics of North America*, vol. 103, no. 3, pp. 463–473, 2019.
- [6] B. C. Bade and C. S. Dela Cruz, "Lung cancer 2020," *Clinics in Chest Medicine*, vol. 41, no. 1, pp. 1–24, 2020.
- [7] N. Duma, R. Santana-Davila, and J. R. Molina, "Non-small cell lung cancer: epidemiology, screening, diagnosis, and treatment," *Mayo Clinic Proceedings*, vol. 94, no. 8, pp. 1623–1640, 2019.
- [8] I. Toumazis, M. Bastani, S. S. Han, and S. K. Plevritis, "Risk-Based lung cancer screening: a systematic review," *Lung Cancer*, vol. 147, pp. 154–186, 2020.
- [9] Z. Wan, Y. Dong, Z. Yu, H. Lv, and Z. Lv, "Semi-supervised support vector machine for digital twins based brain image fusion," *Frontiers in Neuroscience*, vol. 15, Article ID 705323, 2021.
- [10] V. M. L. de Sousa and L. Carvalho, "Heterogeneity in lung cancer," *Pathobiology*, vol. 85, no. 1–2, pp. 96–107, 2018.
- [11] J. B. Alpert and J. P. Ko, "Management of incidental lung nodules," *Radiologic Clinics of North America*, vol. 56, no. 3, pp. 339–351, 2018.
- [12] J. P. Ko and L. Azour, "Management of incidental lung nodules," *Seminars in Ultrasound, CT and MRI*, vol. 39, no. 3, pp. 249–259, 2018.
- [13] P. J. Mazzone and L. Lam, "Evaluating the patient with a pulmonary nodule," *JAMA*, vol. 327, no. 3, pp. 264–273, 2022.
- [14] S. Ley and J. Ley-Zaporozhan, "Novelties in imaging in pulmonary fibrosis and nodules. A narrative review," *Pulmonology*, vol. 26, no. 1, pp. 39–44, 2020.
- [15] J. Ma, Y. Song, X. Tian, Y. Hua, R. Zhang, and J. Wu, "Survey on deep learning for pulmonary medical imaging," *Frontiers of Medicine*, vol. 14, no. 4, pp. 450–469, 2020.
- [16] M. Senent-Valero, J. Librero, and M. Pastor-Valero, "Solitary pulmonary nodule malignancy predictive models applicable to routine clinical practice: a systematic review," *Systematic Reviews*, vol. 10, no. 1, p. 308, 2021.
- [17] M. Spadafora, L. Evangelista, C. Gridelli, and A. Cuocolo, "Alternative imaging strategy of solitary pulmonary nodule by FDG PET/CT," *European Journal of Radiology*, vol. 90, pp. 188–191, 2017.
- [18] S. P. Kailasam and M. M. Sathik, "A novel hybrid feature extraction model for classification on pulmonary nodules," *Asian Pacific Journal of Cancer Prevention*, vol. 20, no. 2, pp. 457–468, 2019.
- [19] L. Sun, Z. Wang, H. Pu et al., "Attention-embedded complementary-stream CNN for false positive reduction in pulmonary nodule detection," *Computers in Biology and Medicine*, vol. 133, Article ID 104357, 2021.
- [20] W. Ye, W. Gu, X. Guo et al., "Detection of pulmonary ground-glass opacity based on deep learning computer artificial intelligence," *BioMedical Engineering Online*, vol. 18, no. 1, p. 6, 2019.
- [21] T. Brand and B. Haithcock, "Lung cancer and lung transplantation," *Thoracic Surgery Clinics*, vol. 28, no. 1, pp. 15–18, 2018.
- [22] C. Goebel, C. L. Loudon, R. Mckenna, O. Onugha, A. Wachtel, and T. Long, "Diagnosis of non-small cell lung cancer for early stage asymptomatic patients," *Cancer Genomics & Proteomics*, vol. 16, no. 4, pp. 229–244, 2019.
- [23] R. Pirker, "Conquering lung cancer: current status and prospects for the future," *Pulmonology*, vol. 26, no. 5, pp. 283–290, 2020.
- [24] A. Linehan and P. M. Forde, "Moving immunotherapy into early-stage lung cancer," *The Cancer Journal*, vol. 26, no. 6, pp. 543–547, 2020.
- [25] M. Wei and Y. Qiao, "[Progress of lung cancer screening with low dose helical computed tomography]," *Zhongguo Fei Ai Za Zhi*, vol. 23, no. 10, pp. 875–882, 2020.

- [26] C. K. Liam, P. Lee, C. J. Yu, C. Bai, and K. Yasufuku, "The diagnosis of lung cancer in the era of interventional pulmonology," *International Journal of Tuberculosis & Lung Disease*, vol. 25, no. 1, pp. 6–15, 2021.
- [27] S. Zhang, F. Sun, N. Wang et al., "Computer-aided diagnosis (CAD) of pulmonary nodule of thoracic CT image using transfer learning," *Journal of Digital Imaging*, vol. 32, no. 6, pp. 995–1007, 2019.
- [28] B. J. Bartholmai, C. W. Koo, G. B. Johnson et al., "Pulmonary nodule characterization, including computer analysis and quantitative features," *Journal of Thoracic Imaging*, vol. 30, no. 2, pp. 139–156, 2015.